HIGHWAY RESEARCH RECORD

Number 181

Embankments and Their Foundations

5 Reports

Subject Area

22 Highway Design
61 Exploration-Classification (Soils)
62 Foundations (Soils)
63 Mechanics (Earth Mass)
64 Soil Science

HIGHWAY RESEARCH BOARD
DIVISION OF ENGINEERING NATIONAL RESEARCH COUNCIL
NATIONAL ACADEMY OF SCIENCES—NATIONAL ACADEMY OF ENGINEERING

Washington, D.C., 1967 Publication 1512

Department of Soils, Geology and Foundations

Eldon J. Yoder, Chairman
Joint Highway Research Project
Purdue University, Lafayette, Indiana

Chester McDowell, Vice Chairman
Materials and Tests Soils Engineer
Texas Highway Department, Austin

HIGHWAY RESEARCH BOARD STAFF

J. W. Guinnee, Engineer of Soils, Geology and Foundations

DIVISION B

H. Bolton Seed, Chairman
Department of Civil Engineering
University of California, Berkeley

Carl L. Monismith, Vice Chairman
University of California, Berkeley

COMMITTEE ON EMBANKMENTS AND EARTH SLOPES
(As of December 31, 1966)

William P. Hofmann, Chairman
Director, Bureau of Soil Mechanics
New York State Department of Public Works
Albany

Frederick M. Boyce, Jr., Soils Engineer, Maine State Highway Commission, Bangor
Wilbur M. Haas, Department of Civil Engineering, Michigan Technological University, Houghton
Raymond C. Herner, Consulting Engineer, Indianapolis, Indiana
Henry W. Janes, Whitman, Requardt and Associates, Baltimore, Maryland
Martin S. Kapp, Soils and Foundation Engineer, The Port of New York Authority, New York, N. Y.
Philip Keene, Engineer of Soils and Foundations, Connecticut Highway Department, Wethersfield
Richard E. Landau, W. Hempstead, L. I., N. Y.
Ivan C. MacFarlane, Muskeg Subcommittee, National Research Council, Ottawa, Canada
Harry E. Marshall, Soils Engineer, Bureau of Location and Design, Ohio Department of Highways, Columbus
Rockwell Smith, Research Engineer—Roadway, Association of American Railroads, Chicago, Illinois
Olaf L. Stokstad, Design Development Engineer, Michigan Department of State Highways, Lansing
David J. Varnes, Chief, Engineering Geology Branch, U. S. Geological Survey, Denver, Colorado
William G. Weber, Jr., Senior Materials and Research Engineer, California Division of Highways, Sacramento

COMMITTEE ON MECHANICS OF EARTH MASSES AND LAYERED SYSTEMS

(As of December 31, 1966)

Robert L. Schiffman, Chairman
University of Illinois at Chicago Circle
Department of Materials Engineering
Chicago, Illinois

Richard G. Ahlvin, Chief, Flexible Pavement Branch, U. S. Army Waterways Experiment Station, Vicksburg, Mississippi

William Baron, Assistant Professor of Civil Engineering, Purdue University, Lafayette, Indiana

Donald M. Burmister, Professor Emeritus of Civil Engineering, Columbia University, New York, N. Y.

J. C. Christian, Assistant Professor of Civil Engineering, Massachusetts Institute of Technology, Cambridge

Lawrence A. DuBose, Testing Service Corporation, Wheaton, Illinois

Jacob Feld, Consulting Engineer, New York, N. Y.

A. A. Fungaroli, Associate Professor of Civil Engineering, Department of Civil Engineering, Drexel Institute of Technology, Philadelphia, Pennsylvania

Delon Hampton, Research Engineer, Soil Mechanics Section, IIT Research Institute, Chicago, Illinois

Milton E. Harr, Professor of Soil Mechanics, School of Civil Engineering, Purdue University, Lafayette, Indiana

R. L. Kondner, Department of Civil Engineering, University of Maryland, College Park

Charles C. Ladd, Associate Professor of Civil Engineering, Massachusetts Institute of Technology, Cambridge

Ulrich Luscher, Assistant Professor of Civil Engineering, Department of Civil Engineering, Massachusetts Institute of Technology, Cambridge

T. F. McMahon, U. S. Bureau of Public Roads, Washington, D. C.

Robert L. McNeill, Chief Engineer, Woodward-Clyde-Sherard & Associates, Oakland, California

Z. C. Moh, SEATO Graduate School of Engineering, Sanamma Road, Bangkok, Thailand

K. Nair, Materials Research and Development, Inc., Oakland, California

A. M. Richardson, Associate Professor of Civil Engineering, Department of Civil Engineering, University of Pittsburgh, Pittsburgh, Pennsylvania

F. E. Richart, Jr., Chairman, Department of Civil Engineering, University of Michigan, Ann Arbor

Bruce B. Schimming, Assistant Professor of Civil Engineering, Department of Civil Engineering, Notre Dame University, Notre Dame, Indiana

Werner E. Schmid, Department of Civil Engineering, Princeton University, Princeton, N. J.

F. H. Scrivner, Research Engineer, Texas Transportation Institute, Texas A and M University, College Station

Eugene L. Skok, Jr., Department of Civil Engineering, University of Minnesota, Minneapolis

Aleksandar S. Vesic, Professor of Civil Engineering, Duke University, Durham, North Carolina

H. E. Wahls, Associate Professor of Civil Engineering, Department of Civil Engineering, North Carolina State University, Raleigh

William G. Weber, Jr., Senior Materials and Research Engineer, California Division of Highways, Sacramento

Russell A. Westmann, Dept. of Engineering, University of California, Los Angeles

DIVISION C

O. L. Lund, Chairman
Assistant Engineer of Materials and Tests
Nebraska Department of Roads, Lincoln

L. F. Erickson, Vice Chairman
Materials and Research Engineer
Idaho Department of Highways, Boise

COMMITTEE ON FROST ACTION
(As of December 31, 1966)

L. F. Erickson, Chairman
Materials and Research Engineer
Idaho Department of Highways, Boise

Hamilton Gray, Chairman, Department of Civil Engineering, Ohio State University, Columbus
L. E. Gregg, L. E. Gregg and Associates, Consulting Engineers, Lexington, Kentucky
Wilbur M. Haas, Department of Civil Engineering, Michigan Technological University, Houghton
Frank B. Hennion, Assistant Chief, Civil Engineering Branch, Engineering Division, Military Construction, Office, Chief of Engineers, Department of the Army, Washington, D.C.
Alfreds R. Jumikis, Professor of Civil Engineering, College of Engineering, Rutgers, The State University, New Brunswick, New Jersey
Chester W. Kaplar, U. S. Army Cold Regions Research & Engineering Laboratory, Hanover, New Hampshire
Miles S. Kersten, Professor of Civil Engineering, University of Minnesota, Minneapolis
R. I. Kingham, Staff Engineer, The Asphalt Institute, University of Maryland, College Park
Clyde N. Laughter, Chief Soils Engineer, State Highway Commission of Wisconsin, Madison
O. L. Lund, Assistant Materials and Testing Engineer, Nebraska Department of Roads, Lincoln
A. E. Matthews, Engineer of Soils, Office of Testing and Research, Michigan Department of State Highways, Lansing
George W. McAlpin, Deputy Chief Engineer (Research), Technical Services Subdivision, New York State Department of Public Works, Albany
Eugene B. McDonald, Materials Engineer, South Dakota Department of Highways, Pierre
Paul S. Otis, Materials and Research Engineer, New Hampshire Department of Public Works and Highways, Concord
R. G. Packard, Senior Paving Engineer, Design Section, Engineering Services, Portland Cement Association, Chicago, Illinois
Edward Penner, Division of Building Research, National Research Council of Canada, Ottawa, Ontario, Canada
Harold R. Peyton, Principal Investigator, Arctic Environmental Engineering Laboratory, University of Alaska, College
C. K. Preus, Materials and Research Engineer, Minnesota Department of Highways, St. Paul
Willis H. Taylor, Jr., Assistant Chief Construction Engineer, Louisiana Department of Highways, Baton Rouge
K. B. Woods, Goss Professor of Engineering, Purdue University, Lafayette, Indiana

Foreword

The papers in this RECORD are in the area of what can be termed "earth engineering," i. e., the art of the utilization of earth—soil and rock—for the construction of engineering works. Earth engineering can be subdivided into two closely related branches: foundation engineering and earthwork engineering. The former is the art of the efficient utilization of the earth for the support of engineering works; the latter is the art of the efficient utilization of earth as a material for the construction of such works as embankments, earth dams, dikes, cuts, and canals.

Few engineers realize the magnitude of the expenditures for earthwork in relation to the highway construction dollar. In one Northeastern state, the total 1966 construction expenditure for earthwork and subbase items alone amounted to $136, 000, 000; of this $25, 000, 000 was expended for the subbase items.

Obviously, the earth engineering field accounts for a significant proportion of the nationwide highway construction expenditure. This fact emphasizes that earth engineering operations, in both the design and construction phases, deserve the same attention and thoroughness that is employed in the design and construction of the other components of the highway.

The effects of freezing and thawing on pavements, subbases and subgrades greatly influence the design, construction, performance and cost of highways in the northern United States and Canada. This influence ranges from pavement thickness design considerations to the problems and economics of earthwork construction during the winter season. The paper by Rutka and Matich and that by Straub and Williams furnish interesting and valuable data in this area.

Perloff, Baladi and Harr present information extremely useful in the design of embankments, particularly in computations for settlement prediction purposes.

Nielson and Cardenas offer an interesting concept for the detailed consideration of a solution to the problem of settlement of pavement at bridge abutments caused by post construction consolidation of the approach embankment.

Benson presents concepts useful in the design of retaining walls, particularly from the standpoint of rapidly and conveniently ascertaining the effect of variations in the characteristics of the retained earth material.

—Wm. P. Hofmann

Contents

Unusual Case of Embankment Failure

A. RUTKA, Materials and Testing Engineer, Department of Highways, Ontario; and M. A. J. MATICH, President, Geocon Ltd., Toronto, Ontario

The paper describes a study of an unusual failure which occurred in a short section of a winter-placed rock fill embankment constructed over swampy terrain composed of muskeg followed by soft to firm sensitive clay overlying a highly irregular bedrock surface. The embankment was built by the partial excavation and displacement method. The failure occurred suddenly, without warning, about three months after construction.

The study included a detailed subsurface investigation and examination of climatological information, settlement data and construction records. It established that the section of the embankment which collapsed was originally "floating" in the clay and supported at either end on bedrock. The spacing between the supports on bedrock was found to be only about 6 times the overall depth of the fill. The evidence indicated that the rock fill must have been frozen as placed, so that the part above swamp water level would have remained frozen until thawing in the spring. It is concluded that the collapse of the roadway at failure, and the resulting downward displacement of about 12 feet which occurred, was due to a rare combination of circumstances. It is believed that flat horizontal arching between bedrock supports had developed in the section of frozen rock fill and that thawing in the spring led to collapse of the arching and consequent failure of the roadway. This explanation is consistent with the geometry and delayed nature of the failure and other evidence obtained.

A brief discussion of published precedent relating to implications of the phenomenon of arching in granular materials in other civil engineering works is given. Methods of dealing with soil and bedrock conditions which might be potentially troublesome through arching in winter-placed rock fills constructed over soft ground are also discussed.

•IN the spring of 1964, a section of rock fill embankment near Parry Sound, Ontario, failed suddenly. It had been completed more than three months earlier, having been constructed entirely during the winter, mostly at below freezing temperatures. The embankment was built across a muskeg swamp underlain by soft to firm sensitive clay which in turn was underlain by bedrock with a highly irregular profile. Construction generally was by the method of partial excavation and displacement in which complete displacement of the clay was generally achieved. However, over a short section underlain by a considerable depth of clay, the embankment "floated" in the clay and was supported by bedrock at either end. This section was involved in the failure.

The sudden delayed nature and the geometry of the failure were unusual. Analysis of all evidence gathered during the post-failure investigation led to the conclusion that the failure was due to an unusual combination of circumstances relating to weather, subsurface conditions, and geometry of the fill. It is believed that the fill was frozen as placed, and therefore that it had a higher strength and void ratio than it would have

Paper sponsored by Committee on Embankments and Earth Slopes and presented at the 46th Annual Meeting.

had subsequently upon thawing. Thawing of the fill is thus considered to have influenced the timing of the failure. Because the failure occurred suddenly and without warning, it is also believed that arching between bedrock supports occurred in the winter-placed fill, and that the arching was destroyed by the effects of spring thaw. The breakdown of the arching is believed to have suddenly thrown additional load onto the clay beneath the embankment, in the process inducing the resultant large initial downward plunge of about 12 ft. Although this explanation appears to give the best fit to the available evidence, it is admittedly based partly on intuition and is thus subject to debate. Nevertheless, the authors feel that combinations of soil, bedrock and weather conditions such as prevailed at the subject site warrant special attention in areas such as the Canadian North where construction of rock fill road embankments during winter is commonplace.

SOIL CONDITIONS

Before construction there was about 8 ft of muskeg along the embankment alignment. Beneath this there was a soft to firm sensitive silty clay. The clay is underlain by a relatively thin stratum of sand and gravel, then bedrock, or by bedrock directly. Bedrock is hard, sound granitic rock. Its elevation varies considerably. A stratigraphic profile along the embankment centerline is shown in Figure 1.

The clay has liquid and plastic limits of about 65 and 20, respectively, with a moisture content of about 60 percent. It is essentially normally loaded and has an undrained shear strength, as measured by vane apparatus, varying from about 100 lb/sq ft at the surface of the stratum, to about 800 lb/sq ft at a depth of 50 ft below clay surface level. The sensitivity varied from 3 to 6.

DESCRIPTION OF EMBANKMENT

The embankment, which is 44 ft wide at road level, was constructed of granitic rock fill quarried from nearby road cuts. Rock sizes were variable and, in extreme cases, up to 8 ft in maximum dimension. The overall embankment length is about 500 ft between bedrock outcrops on either side of a long narrow valley. The roadway at both outcrops is in cut. On the south side of the valley the bedrock face forming the valley wall is very steep. The road climbs upward over this steep face and crosses it at an angle of about 45 deg. A small stream, bordered by swamp growth, meanders along the valley. This stream, which was carried through the fill by a 7-ft diameter culvert, maintains local water level in the valley normally to within 1 or 2 ft of ground level depending on time of year and the presence or absence of beaver dams. The site and the embankment after repairs are shown in Figure 2. This figure also shows that the roadway is slightly curved in plan. Figure 3 shows a longitudinal section through the embankment and subsoil.

Construction was carried out on a one-shift-per-day basis. It involved advance excavation of muskeg along the embankment to full width. This was followed by end-

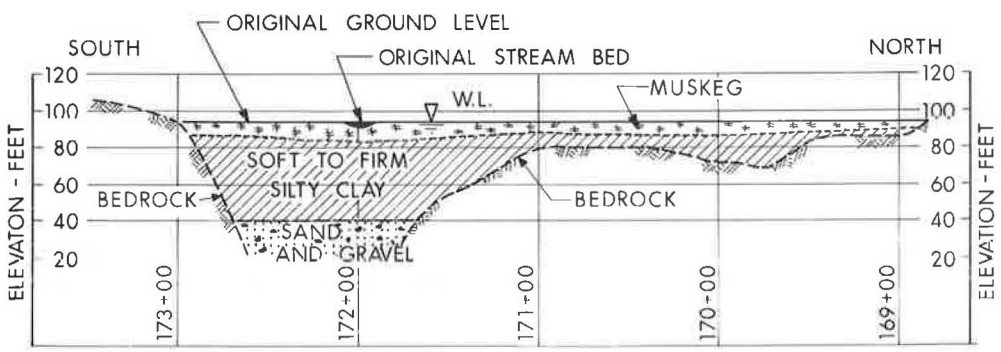

Figure 1. Soil stratigraphy along roadway centerline.

Figure 2. Site and embankment after repairs.

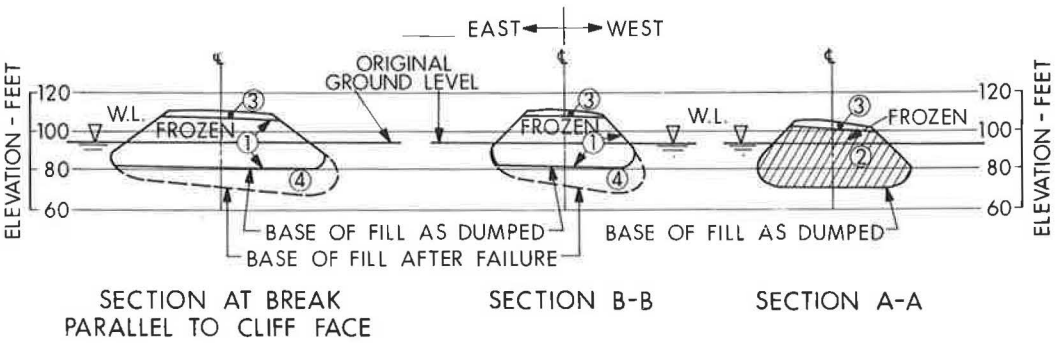

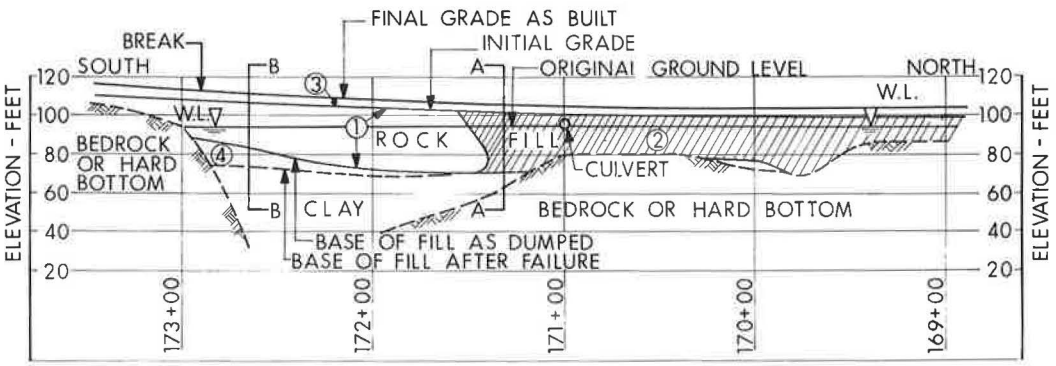

Figure 3. Longitudinal section through embankment and subsoil.

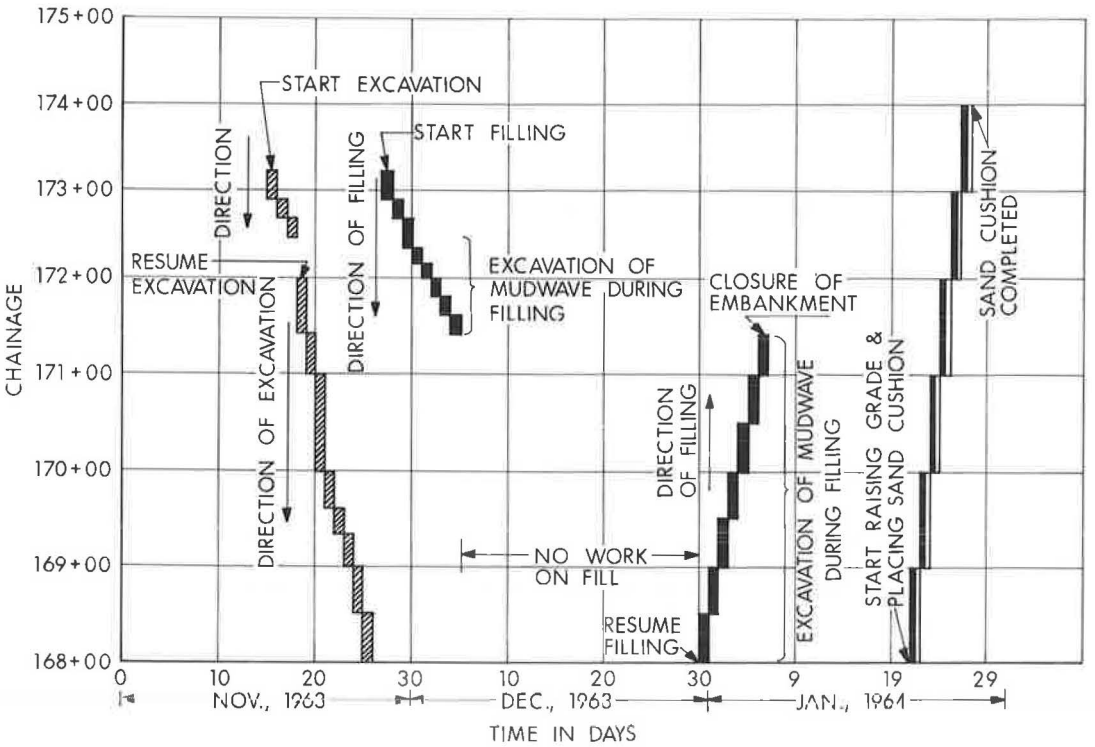

Figure 4. Embankment construction schedule.

dumping of rock fill in a single lift to the original design grade shown in Figure 3. Mudwaves, produced in front of the fill as it advanced, were progressively removed by dragline working from the fill already completed. The filling operations to original design grade were carried out first from one side of the valley, and then the other, until the two sections were joined at about chainage 171+50. Care was taken to ensure that a good connection was made. About two weeks after the two sections were joined, grade was raised by 4 ft using rock fill and a sand cushion. This grade raising was carried out without inducing visible movement or settlement. The sequence of construction is shown by the circled numbers, 1 to 3 inclusive, in Figure 3 and by the schedule shown in Figure 4. As can be seen, the construction period was between mid-November 1963, and the end of January 1964. With reference to Figure 3, the fill above water level is shown as being frozen; the hatching of the rock fill zone, designated by circled number 2, is merely to distinguish this zone from zones 1 and 3.

From the results of exploratory drilling carried out after completion of repairs, observed vertical movements, and inferred below-ground movements, the embankment cross sections before and after failure have been drawn up as shown in Figure 3—the areas designated by the circled number 4 indicating the inferred amount of downward movement at initial failure. This figure indicates that complete sinkage had for all practical purposes been achieved down-chainage from about 171+00. Only partial displacement of the clay had been effected, as expected, between about chainages 171+00 and 173+00, which resulted in a "floating" fill in this section.

Between end of construction and time of failure the embankment was used as a haul road and subject to loads from heavy equipment. Inspections and movement readings were made at about weekly intervals during this period. Total settlements of a few inches only were observed for the section of fill floating in the clay. No visible signs of abrupt movement of the roadway vertically or laterally were noticed in the interval between end of construction and failure.

CLIMATOLOGICAL DATA

Daily air temperatures and precipitation data for Parry Sound, Ontario, about 7 mi from the site, are shown in Figure 5 for November 1963 to May 1964. These show that construction was almost entirely during below freezing temperatures, and that temperatures were almost always above freezing in the month preceding failure. Snow and freezing rain were recorded on site during placement of rock fill. Further, there were periods of sunny weather and rain for three weeks prior to failure.

During the winter, up to 6 in. of ice was present on the water in the trench excavated in advance through the muskeg. However, this was removed ahead of dumping of rock fill. The trench was continuously full of water during construction. Because of snow cover and natural insulating effects of the muskeg, the amount of frost penetration into the natural swamp cover adjacent to the embankment was generally slight and less than 1 ft.

DESCRIPTION OF FAILURE

The failure, perhaps better described as a collapse of the roadway, occurred very suddenly, a car having passed over the road 15 minutes before. It occurred on May 3, 1964, more than 3 months after completion of construction. At failure the roadway did not tilt laterally; in other words, there was essentially no rotation of the fill about its long axis (Fig. 6). The movement was largely a vertical drop pivoting around a point at about chainage 171+50, with the maximum vertical movement of about 12 ft occurring along the contact between the embankment and the crest of the rock cliff forming the south valley wall. A reconstructed section after failure showing the form of downward movement is illustrated in Figure 7, from which it may be seen that a hoizontal movement of about 3 ft maximum also occurred in a northwesterly direction. Significantly, however, the rock cliff also slopes steeply downward in the same direction.

Immediately after failure the roadway was brought up to grade. This operation was just completed on May 11, 1964, when a further sudden downward movement of about 5 ft took place near chainage 173+00. As before, the movement was a maximum at this point and tapered off to zero near chainage 171+50. At this stage the roadway was brought up to grade again and then raised by about 10 ft so as to surcharge the affected area. Just as this operation was being completed on June 21, 1964, a further subsidence took place with a maximum downward movement of 13 to 14 ft occurring near station 173+00. Subsequently, the surcharge was moved onto the muskeg to the west of the embankment to form a 5-ft high, 80-ft wide berm. The roadway was then brought up to design grade and has been stable since. In the following two years about 6 in. of gradual settlement has taken place and this has manifested itself in a diagonal crack extending across the roadway at about chainage 173+25. The repairs to this crack are shown in Figure 2.

From a study of all pertinent evidence a number of factors were considered particularly significant, as follows:

1. Failure occurred suddenly, not during construction as might be expected, nor during grade raising in the winter, but more than three months later in the spring.
2. The failure occurred in a period of alternating warm rain and sunny weather shortly after conditions for spring thaw were definitely established.
3. Air temperatures during construction were almost always below freezing, and below-freezing temperatures predominated for two months after completion.
4. The rock fill was produced at a slow rate from nearby shallow cuts on the highway and not as a high-rate production operation from a special quarry. Considering the generally below-freezing temperatures which prevailed during placement, the rock fill and the fill used for grade raising must therefore have been frozen when placed. Inasmuch as snow and freezing rain occurred during construction, entrapment of some snow and ice within the fill was unavoidable.
5. There was no evidence of abrupt movement anywhere on the embankment during raising of grade above original design elevation, or between end of construction and time of failure. This is in contrast to the immediate progressive downward movement

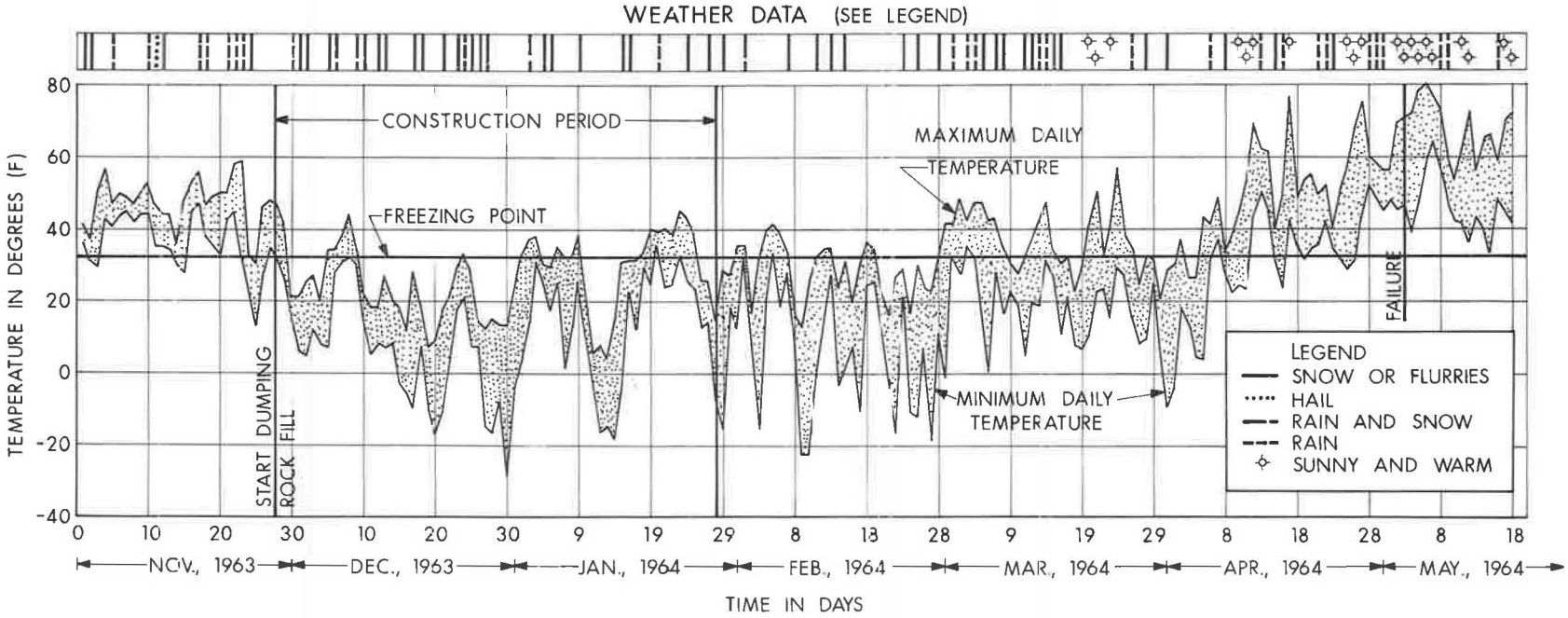

Figure 5. Climatological data for site area.

Figure 6. Collapsed section immediately after failure looking north.

of the roadway surface which occurred the first two times that grade was raised during repairs to the section involved in the initial failure of May 3, 1964.

6. A settlement of only a few inches occurred in the three months between end of construction and the initial failure.

7. At about chainage 173+00 the amount of rock fill above water level, and correspondingly the depth of rock fill remaining frozen after placement, was considerably greater than elsewhere because the roadway grade rises toward the south and crosses the rock cliff at an angle.

8. The visible break in the embankment at failure was almost vertical (Fig. 6). It occurred along the line of contact between the rock fill and the steep bedrock cliff in the area where the majority of the embankment cross section remained frozen after placement.

9. Figure 6 also shows that there was essentially no rotation of the embankment at failure, the movement being a vertical drop, giving the impression that the fill had "slipped off the rock cliff." There was some heaving of the muskeg immediately adjacent to the west side of the fill, probably as a result of a sideways deflection of the embankment by the bedrock cliff which slopes steeply downward to the northwest.

10. The section of embankment involved in the failure was originally "floating" in the underlying clay, and was also supported on an exposed rock cliff at one end and an underground bedrock pinnacle at the other. In addition, the length of embankment between supports on bedrock was short in relation to the depth and width of the rock fill—the length was only about 6 times the depth.

ANALYSIS OF FAILURE

It is believed that, for all practical purposes, the rock fill was completely frozen as placed and that the part above swamp water level would have remained at below-freezing temperatures until thawed out in the spring. The fill extending below water level would, however, thaw out immediately. The rock fill as dumped was not fully saturated, of course. However, it is believed that there was sufficient moisture present in the form of ice and snow to act as a skeletal cement between rock particles.

This lattice of ice would give the fill a temporary cohesion and therefore a higher strength than in the unfrozen state. A more significant effect of end-dumping of the fill under winter conditions in this instance is that the resulting void ratio would be higher as placed than after thawing. It is not possible to assess accurately the influence of either of these two factors in the present case. However, evidence of the type discussed later supports the fact that the fill as placed must have been stronger and greater in bulk volume than it would have been after thawing and wetting in the spring.

It is well known that frozen soil, even if only partially saturated, has a higher strength than the same material when thawed. For example, strengths of a variety of soil types at below-freezing temperatures are given in the U. S. Navy publication, "Arctic Engineering" (1), and references quoted therein. There is precedent also for considerable reduction in volume of winter-placed rock fills after thawing; e.g., Holestol et al (2) and Bernell (3). The latter reference describes a project in Sweden on which construction of a test rock fill, about 25 ft high, was carried out in a single lift. Construction was during the winter under temperatures similar to those given in Figure 5 with no special precautions to remove ice and snow trapped in the fill. Observations showed that the settlement during the thawing period amounted to about 20 percent of the height of the fill, and additional settlement after sluicing amounted to about 5 percent. Bernell also suggests that in analyzing stability of rock fills placed under winter conditions, an angle of internal friction of 40 deg be used, as compared to a value of 45 deg for similar fill, placed and compacted normally.

It is considered that the pronounced reduction in volume associated with thawing of winter-placed rock fill was of special significance in explaining the failure. Under normal conditions, any such reduction in volume of the fill upon thawing would have been evidenced merely as settlement of the fill surface, inasmuch as the fill would be essentially influenced by its self-weight only. However, in the present instance, it is believed that the effect was to cause collapse of arching which had developed within the fill in the section located between the closely spaced abutments of bedrock. This breakdown of arching is thought to explain the sudden nature of the failure, the lack of warning, and the large initial downward plunge of the fill.

The phenomenon of arching in granular material has long been recognized, and there are numerous references to it in the literature. The essential features of arching in soils have been demonstrated by Terzaghi (4) and Terzaghi and Peck (5), and a discussion of the theories of arching are given by Terzaghi (6) in which he states that "arching is one of the most universal phenomena encountered in soils both in the field and in the laboratory." These references and others describe practical implications of arching in the design of storage silos, tunnels, shafts, bulkheads, etc. Tschebotarioff (7) has shown theoretically that a relatively flat, horizontal arch in hard, tightly wedged, cohesionless material can support its own weight by friction at unyielding abutments. Coates (8) has analyzed a boulder arch in a similar manner. Jennings et al (9) describe the influence of arching in the formation of sinkholes in Transvaal, South Africa. Apparently, at one stage in the formation of such sinkholes which are reported up to 300 ft in diameter, an arch at ground surface is developed over an air-filled cavity in limestone rock. A common agency causing collapse of such arches is said to be water in the arched material leading to loss of strength or washing out of critical binding or keying material. The collapse of a three-story mine crusher plant into one such sinkhole is described (9). The building had apparently shown only small movements, and the collapse occurred suddenly with practically no warning. Baumann (10) mentions arching of a high lift of rock fill when dumped across a V-shaped gap in the construction of Cogswell rock fill dam, and the pronounced settlement of this section when subsequently subjected to heavy rainfall and sluicing. Krynine and Judd (11) illustrate examples of arching, including arching across the width of a roadway embankment. Oszter (12) describes problems in bulk handling of coarse ore rock due to arching across the discharge openings of hoppers.

Despite the considerable volume of published experience relating to arching, to the authors' knowledge, arching within end-dumped rock fills in the direction parallel to the long axis of a "floating" embankment has not been recognized as a factor which should be considered in the design of such fills.

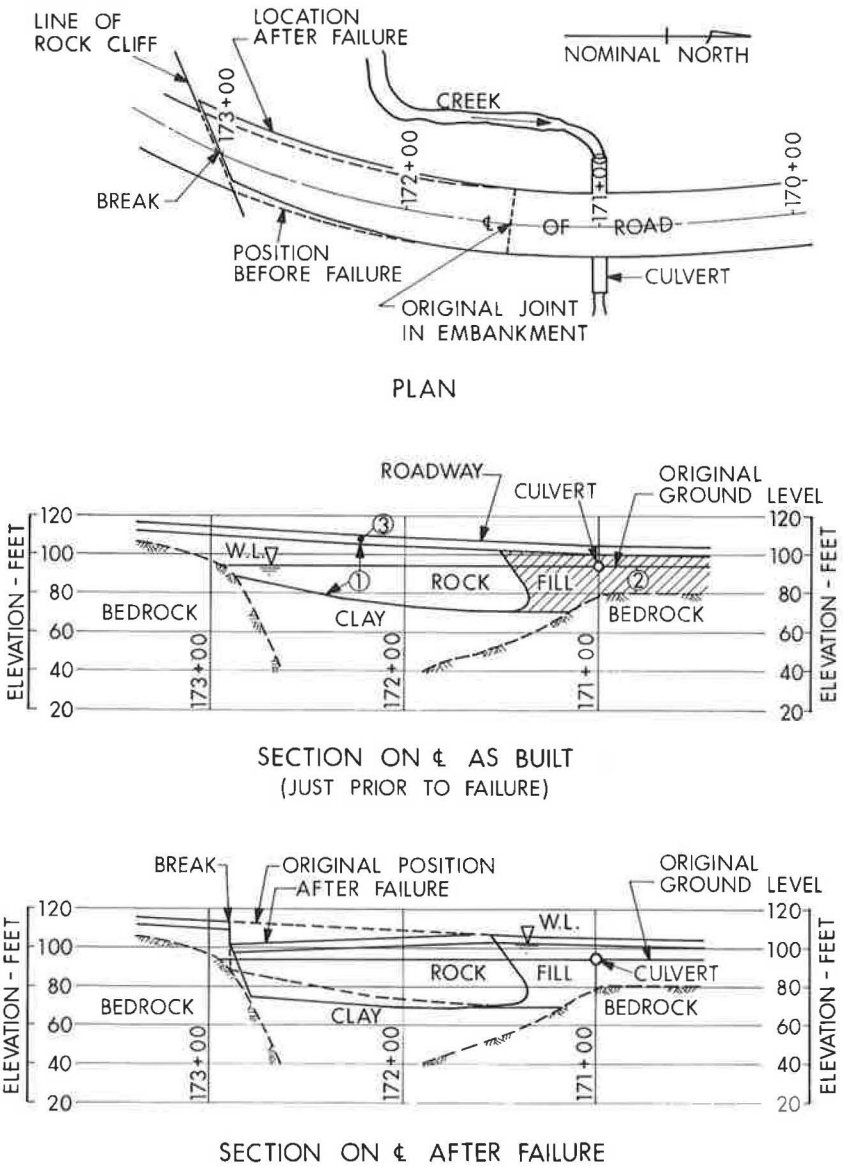

Figure 7. Inferred cross sections before and after failure.

However, a close parallel is mentioned by Tschebotarioff (7) in connection with horizontal arching which is thought to have occurred in sand backfill between a rock fill dyke and closely spaced battered anchor piles. The dyke and batter piles were elements of an anchored sheet pile bulkhead, at Pier C, Long Beach, California. The sand backfill was underlain by about 5 ft of soft silty clay which consolidated under the weight of the sand. In this connection it is mentioned also that layered soil systems can cause considerable difficulties especially if soft clay underlies sand or rock fill.

It is believed that the following sequence of events led to the failure which took place.

1. During dumping of the fill, penetration into the clay immediately adjacent to the rock cliff in the vicinity of chainage 173+00 was less than elsewhere, probably because of the influence of the cliff. Sinkage to bedrock or hard bottom was generally achieved to the north of about station 171+00 (Fig. 3).

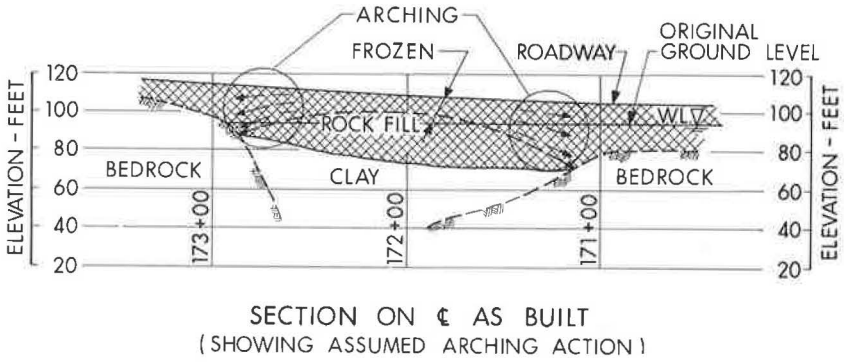

Figure 8. Assumed arching action of section.

2. The rock fill was considered to have been frozen as placed and to have remained frozen above water level until spring. In addition, in the week between closure of the north and south sections of the fill and grade raising, air temperatures fell as low as 52 F below freezing point. The 4-ft surcharge of rock fill used to raise the grade must have also been frozen during placement. This surcharge probably did not induce further immediate sinkage of the embankment because of the added strength imparted by freezing to the fill above water level and because some arching between bedrock supports had already developed.

3. After closure and grade raising, some comparatively minor subsidence of the "floating" fill occurred due to consolidation and/or progressive displacement of the underlying clay. In the process of this deformation, horizontal arching within the rock fill was developed resulting in a transfer of some of the embankment weight to the bedrock abutments at about chainages 171+00 and 173+00. The frozen fill would be involved in the arching and would in effect provide the "keystone" to the arch. The arching action (Fig. 8) would remain intact as long as the fill remained frozen (i.e., at least until the first week in April 1964).

For the ratio of length to depth of rock fill involved in this case, flat horizontal arching is possible according to the theoretical treatment given by Tschebotarioff (7) and Coates (8), as mentioned earlier.

4. Once thawing started, it would progress downward from the surface of the embankment and inward from the exposed sides. Eventually, a situation would be reached where the arching action would be destroyed due to reduction in strength and volume of the rock fill resulting from thawing and wetting, and the restraint against slipping of the south end of the embankment off the bedrock cliff would be removed. Therefore, the fill would collapse, suddenly throwing excess weight (including weight of the fill used to raise grade) onto the underlying clay, thereby inducing sinkage into the clay. The fill surface would, therefore, be expected to drop most in the vicinity of chainage 173+00 with the amount of movement tapering off to essentially zero at about chainage 171+50. This is consistent with the geometry of the initial failure.

5. In contrast to the performance of the embankment during raising of grade in the winter, the addition of further unfrozen fill in an attempt to restore grade caused further immediate sinkage to occur twice before stability was finally achieved.

CONCLUSIONS

It is concluded that the failure was due to an unusual combination of circumstances arising out of winter construction of a "floating" end-dumped rock fill embankment and to the particular geometry of the embankment in relation to the bedrock profile. This combination is believed to have resulted in the development of flat, horizontal arching within the fill and a delayed, sudden failure due to collapse of the arching during spring thaw. Although winter construction of rock fill embankments over swampy terrain is common, in Northern Canada at least, the occurrence of conditions favorable to the formation of arching in winter fills is probably rare. Nevertheless, it should be

possible to recognize potentially dangerous situations during design on the basis of the results of a routine soil investigation. These situations would occur as a rule where the distance between points of support on bedrock or other hard bottom is short in relation to the overall depth of the fill. Possible difficulties due to arching could be avoided in a number of different ways, such as complete excavation or remolding of the clay where practical, changing the geometry of the fill, introducing a bridged opening in the fill, or applying a suitable surcharge during dumping so that there would be no question of possible major collapse after construction even if arching did occur.

Several other lessons are to be learned from this case history of a winter-placed "floating" rock fill embankment. First, the question of raising grade of such fills shortly after completion must be given special attention. Second, special attention should be given to effecting as much fill penetration as possible adjacent to steep faces forming the transition points between swamp deposits and bedrock outcrops.

ACKNOWLEDGMENTS

The authors are indebted to H. W. Adcock, Assistant Deputy Minister (Engineering), Ontario Department of Highways, for permission to publish this paper.

REFERENCES

1. United States Navy, Bureau of Yards and Docks. Arctic Engineering. Navdocks TP-PW-11, 1955.
2. Holestol, Kjaernasli, and Torblaa. Compression of Tunnel Spoil at Venemo Dam. Proc., Sixth Internat. Conf. on Soil Mech. and Found. Eng., Vol. II, 1965.
3. Bernell, C. E. Placement of Rock Fill Under Winter Conditions. Proc., Eighth Internat. Cong. on Large Dams, 1964.
4. Terzaghi, K. Stress Distribution in Dry and in Saturated Sand Above a Yielding Trap-Door. Proc., First Internat. Conf. on Soil Mech. and Found. Eng., Vol. I, 1936.
5. Terzaghi, K., and Peck, R. B. Soil Mechanics in Engineering Practice. John Wiley & Sons, 1948.
6. Terzaghi, K. Theoretical Soil Mechanics. John Wiley & Sons, 1948.
7. Tschebotarioff, G. P. Soil Mechanics, Foundations and Earth Structures. McGraw-Hill Book Co., 1956.
8. Coates, D. F. Rock Mechanics Principles. Dept. of Mines and Tech. Surveys, Canada, Mines Branch Monograph 874, 1965.
9. Jennings, Brink, Louw, and Gowan. Sinkholes and Subsidences in the Transvaal Dolomite of South Africa. Proc., Sixth Conf. on Soil Mech. and Found. Eng., Vol. I, 1965.
10. Baumann, P. Rockfill Dams: Cogswell and San Gabriel. Trans. ASCE, Vol. 125, Part II, 1960.
11. Krynine, D. P., and Judd, W. R. Principles of Engineering Geology and Geotechnics. McGraw-Hill Book Co., 1957.
12. Oszter, Z. F. Comments on Specific Feeder Applications. Canadian Mining and Metallurgical Bull., March 1966.

Stress Distribution Within and Under Long Elastic Embankments

W. H. PERLOFF, Associate Professor of Soil Mechanics,
G. Y. BALADI, Graduate Research Assistant, and
M. E. HARR, Professor of Soil Mechanics, School of Civil Engineering,
Purdue University

The distribution of stresses within and under long elastic embankments continuous with the underlying material is presented. The magnitude and distribution of stress in the foundation material in the vicinity of the embankment is significantly different from that predicted by the usual assumption of stress proportional to embankment height applied normal to the foundation. Influence charts for a variety of embankment shapes are given.

•THE distribution of stresses within and and under earth embankments, due to the embankment weight, is of interest to civil engineers in a variety of applications. Consideration of deformations within embankments, analysis of stability, consolidation of underlying compressible materials, all require determination of the distribution of these stresses.

At the present time there is no means available by which a closed-form solution for such stresses can be obtained. Consequently, various approximations of the real problem have been made with the objective of obtaining at least an estimate of the stresses. The first such effort was made by Carothers (3). He analyzed the stresses within a homogeneous, isotropic elastic half-space resulting from a "long embankment" loading. It was assumed that the load was applied normal to the boundary with a magnitude proportional to the height of the embankment. These results were presented in tabular form by Jurgenson (13). Osterberg (18) superimposed solutions given by Newmark (16, 17) to develop an influence chart for the determination of the magnitude of vertical stresses induced in an elastic half-space by a long embankment loading with a variety of cross sections. Again, the magnitude of the pressure was assumed to be proportional to the embankment height and applied normal to the surface of the foundation material. This "normal loading approximation" to the actual embankment loading is illustrated in Figure 1a.

Terzaghi (20) described an effort to evaluate the shear stresses transmitted to the foundation material by an embankment made by Rendulic (19). It was assumed that the embankment material was on the verge of failure and thus the shearing resistance of the embankment was fully mobilized in order to maintain equilibrium. Consequently, Terzaghi (20) suggested that the magnitude of the computed shear stress at the base was likely to be lower than the actual in situ stresses.

Trollope (22), and Davis and Taylor (6) considered the state of stress within a granular embankment resting on a foundation which yielded an arbitrary amount. No attempt was made to compute the amount of foundation movement which would be created by the embankment.

Finn (8) suggested the use of the Schwarz-Christoffel transformation to map the embankment surface into a straight line, thereby utilizing the distribution of stresses within

---

Paper sponsored by Committee on Mechanics of Earth Masses and Layered Systems and presented at the 46th Annual Meeting.

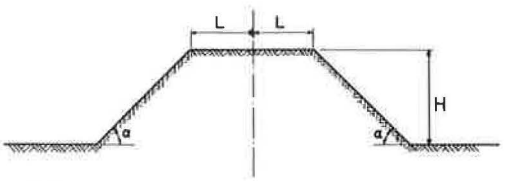

(a) Long Symmetric Elastic Embankment Continuous With Foundation

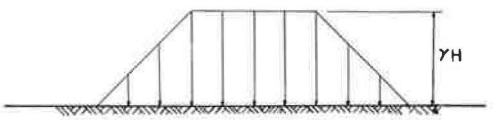

(b) Normal Loading Approximation

Figure 1. Problem considered.

a semi-infinite elastic medium. However, he did not carry out the suggested procedure.

Numerical methods have been used to obtain, for particular cases, solutions for the stress distribution in an elastic embankment resting on elastic or rigid foundations. Zienkiewicz (24) used a finite difference approach to analyze the stress distribution within a triangular gravity dam resting on an elastic foundation. This was extended by Zienkiewicz and Gerstner (27) to the case in which the foundation modulus differed from that of the dam. Dingwall and Scrivner (7) applied the method of finite differences to the solution of an embankment on a rigid foundation. Carlton (2) used a similar method to study an elastic embankment continuous with an elastic foundation.

The finite element method of numerical analysis has been applied by Zienkiewicz and Cheung (25, 26) in the study of stresses within buttress dams resting on elastic foundations. Clough and Chopra (5) and Finn (9), respectively, have also applied the finite element method to the study of a triangular dam on a rigid foundation and a rock slope continuous with its elastic foundation.

Brown (1) and Goodman and Brown (10) investigated the case of a long elastic slope constructed incrementally; it is not clear to what degree their results are influenced by the fact that compatibility is not satisfied by their solution method.

In each of the cases approached by numerical methods, the solution was either restricted to a single embankment cross section or a complete stress picture was not obtained. Thus, despite numerous attempts to determine the distribution of stresses within and under an embankment, no closed-form solution is presently available. It is the objective of this paper to present such a solution.

PROBLEM CONSIDERED

The problem considered herein is the determination of the distribution of stresses within and under an embankment resulting from the self-weight of the embankment. The embankment is shown schematically in Figure 1b. It is assumed that the embankment and the foundation material with which it is continuous are composed of homogeneous, isotropic, linear elastic material. Further, the embankment is assumed to be sufficiently long so that plane strain conditions apply. The shape of the symmetric cross section is defined by the slope angle α and the ratio of the half-width of the top of the embankment, L, to the embankment height, H.

The solution is obtained by transforming the region of the embankment where the solution is unknown, into a half-space where the solution can be found. Application of the Cauchy integral formula to the boundary conditions permits determination of the stresses. An outline of the method is given in Appendix A.

RESULTS AND DISCUSSION

Vertical Normal Stress

A typical result is illustrated in Figure 2. This figure shows contours of the vertical normal stress in dimensionless form $\sigma_y/\gamma H$, for an embankment with $\alpha = 45^0$, $L/H = 3$, and Poisson's ratio, $\mu = 0.3$. The contour lines show only the effect of the embankment weight. Thus, at depths below the base of the embankment ($y/H = 0$) the material is assumed weightless. The effect of the medium weight can be superimposed upon these values to give the total stress acting at a point. The two dashed lines in Figure 2 show

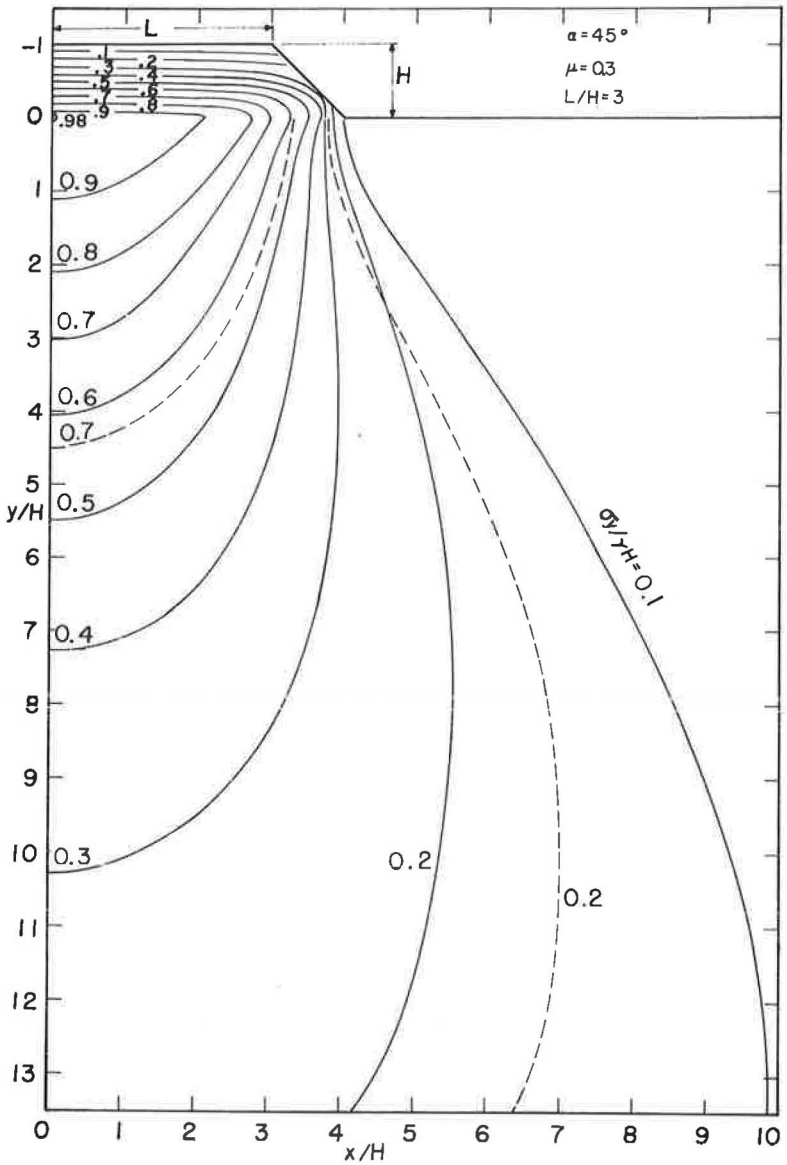

Figure 2. Contours of vertical stress.

stress contours, in terms of $\sigma_y/\gamma H$, for the usual normal loading approximation corresponding to this embankment. These indicate that the vertical normal stresses produced in the foundation material below the elastic embankment are generally smaller than computed for the normal loading approximation.

The stress distribution due to the normal loading approximation is independent of Poisson's ratio; the stresses due to the elastic embankment are dependent upon μ. However, the vertical stresses are insensitive to its magnitude; changing μ from 0.3 to 0.5 changes the vertical stress at a point by less than five percent.

The effect of embankment shape on the vertical stress along vertical sections through the centerline of the embankment and the toe of the slope is illustrated in Figure 3, for $\alpha = 45^0$ and $\mu = 0.3$. The figure is a composite diagram showing the embankment schematically, and the magnitude of the vertical stress at each section as a function of depth.

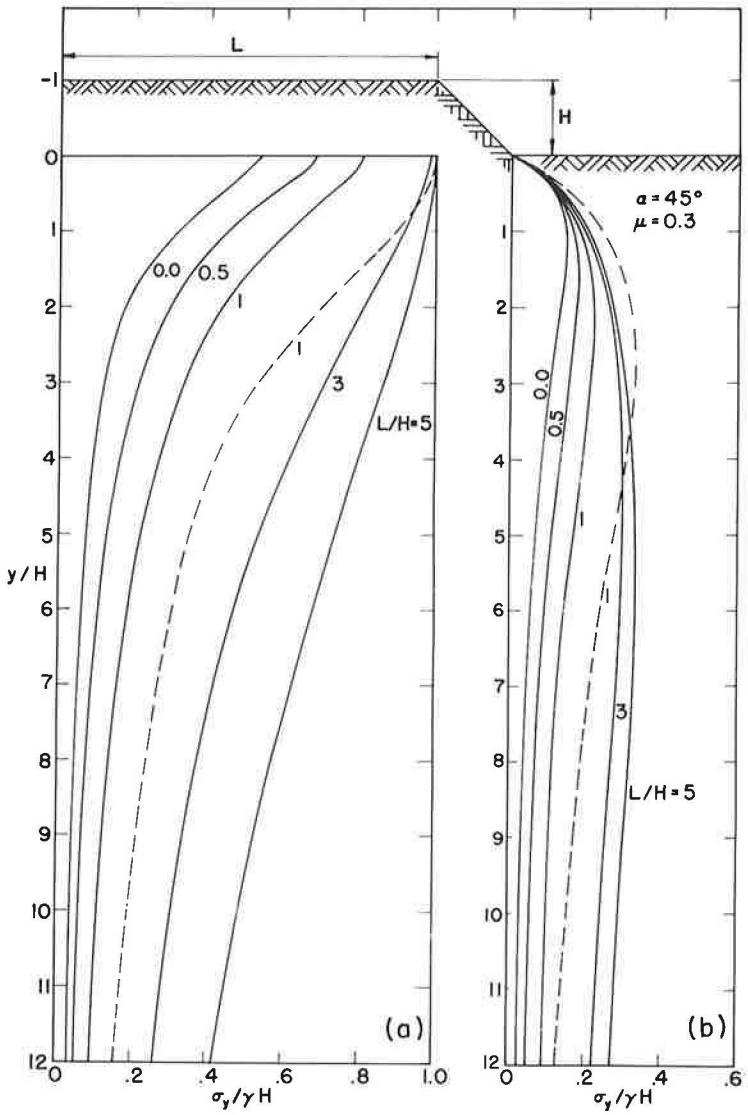

Figure 3. Distribution of vertical stress along vertical sections for varying L/H ratios: (a) at centerline and (b) at toe of slope.

Clearly, the L/H ratio has a pronounced effect on the distribution of vertical stress. As L/H decreases, the stress decreases. Furthermore, a smaller L/H ratio produces a more rapid dissipation of stress with depth.

The dashed lines show the vertical normal stress for the normal loading approximation equivalent in shape to the embankment for which L/H = 1. As indicated in Figure 2, the vertical stress for the corresponding elastic embankment is smaller.

Figure 4 shows the distribution of vertical normal stress along the base of the embankment for $\mu = 0.3$, four values of α, and several embankment shapes shown schematically in the figure. The curved solid lines represent the distribution of stress against the base; dashed lines show the distribution of stress assumed in the usual normal loading approximation. The stress distribution is much more uniform under the elastic embankment than is ordinarily assumed. The difference becomes especially apparent as the L/H ratio of the steeper embankments decreases. Moreover, the

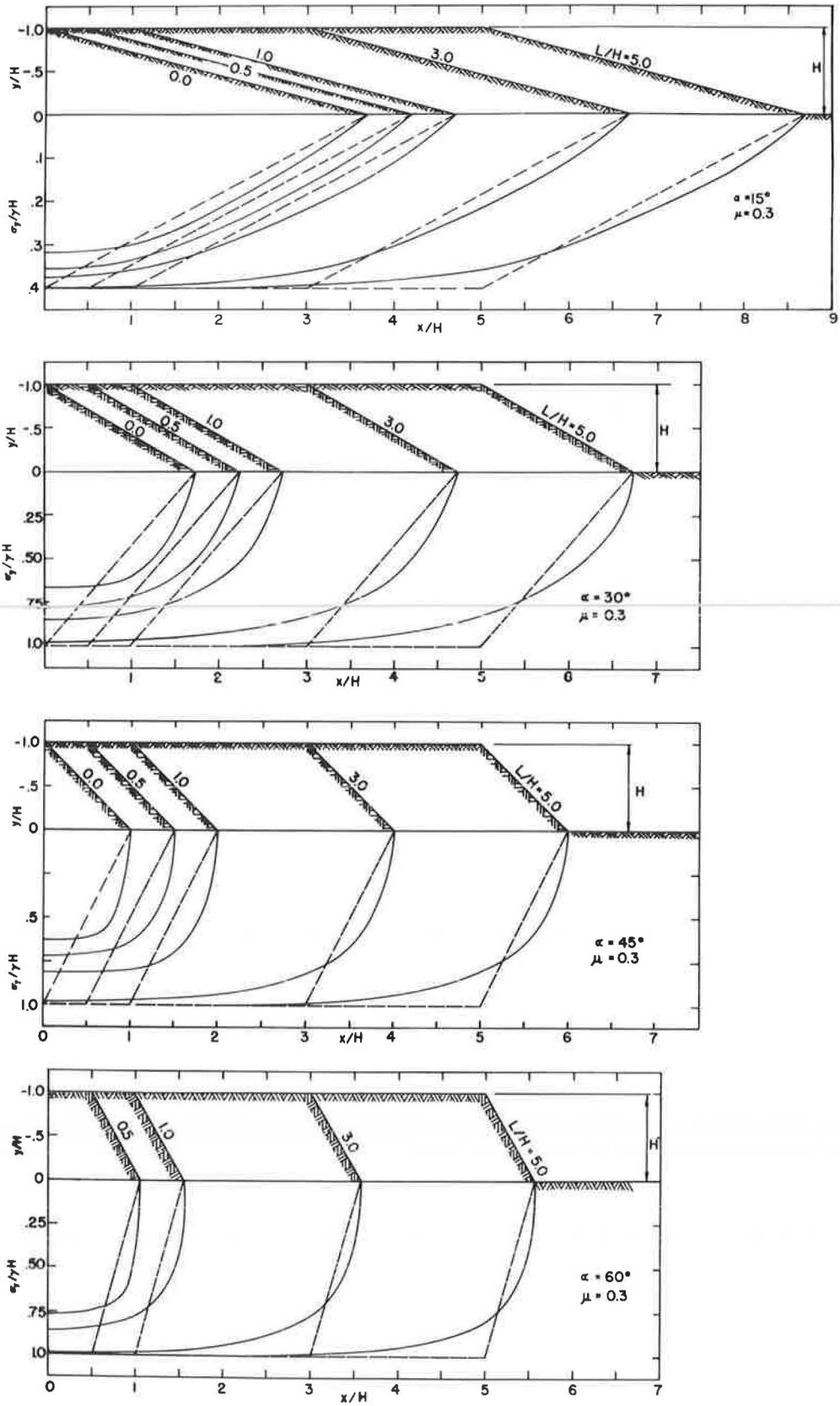

Figure 4. Distribution of vertical normal stress , $\sigma_y/\gamma H$, on the base of the embankment for varying α, and L/H ratios.

magnitude of the stress under the central zone of the elastic embankment is less than that shown by the dashed curves. Again the effect is enhanced for narrow, steep embankments (for $\alpha = 45^0$ and L/H = 0 the vertical stress is only 65 percent of that usually assumed).

To satisfy equilibrium, the areas under corresponding dashed and solid curves must be the same. Hence the difference between these curves becomes less pronounced, at least near the central portion of the embankment, as L/H increases. However, near the outer edge of the embankment, the stresses are still significantly larger on a proportional basis than indicated by the normal loading approximation. Thus, for embankments with moderate L/H ratios, the normal loading approximation leads to larger estimates of differential settlement, assuming one-dimensional compression, than would be computed by the method presented herein.

Horizontal Normal Stress

Contours of horizontal normal stress, $\sigma_x/\gamma H$, for $\alpha = 45^0$, L/H = 3 and $\mu = 0.3$ are shown in Figure 5. The dashed lines are contours determined from the usual normal loading approximation. The stresses shown are those due to the embankment only. The figure shows that the maximum horizontal stress occurs within the body of the embankment and decreases with increasing depth. In the foundation material in the vicinity of the elastic embankment, $\sigma_x/\gamma H$ is less than half of that usually assumed.

The effect of embankment shape on the horizontal stress along vertical sections through the centerline of the embankment and the toe of the slope is illustrated in Figure 6 for $\alpha = 45^0$ and $\mu = 0.3$. As the embankment becomes narrower (L/H ≤ 1), the stress is actually negative at some points below the centerline. That is, the embankment causes a reduction in horizontal stress at these points.

The dashed line shows the stresses determined from the normal loading approximation for L/H = 1. The stress is larger than that due to the elastic embankment at all depths. In fact, in the vicinity of the embankment it is more than five times as large under the centerline and twice as large under the toe. In contrast to the elastic embankment,

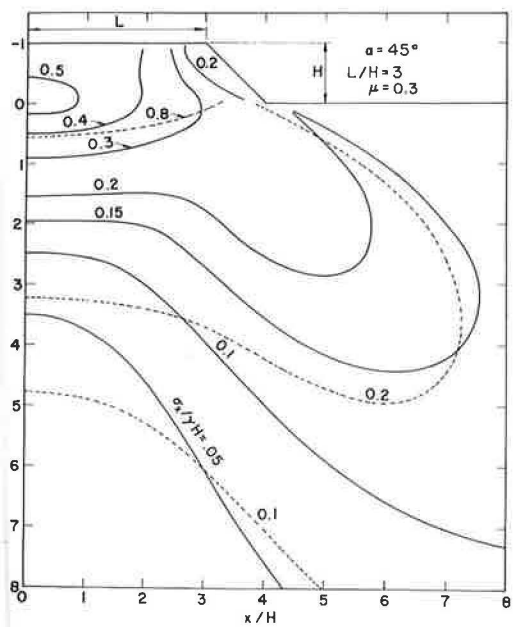

Figure 5. Contours for horizontal stress.

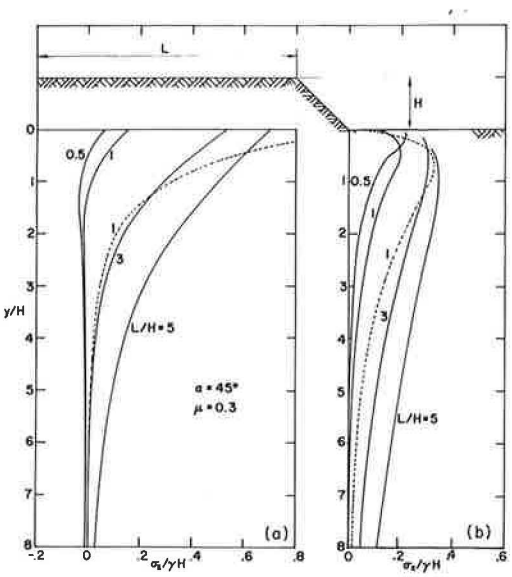

Figure 6. Distribution of horizontal stress along vertical sections for varying L/H ratios: (a) at centerline (b) at toe of slope.

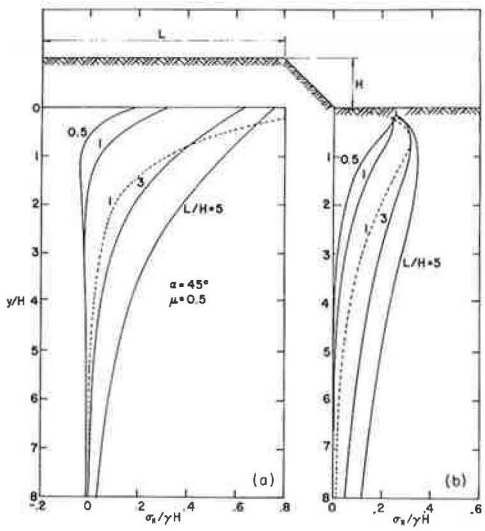

Figure 7. Distribution of horizontal stress along vertical sections for varying L/H ratios: (a) at centerline and (b) at toe of slope.

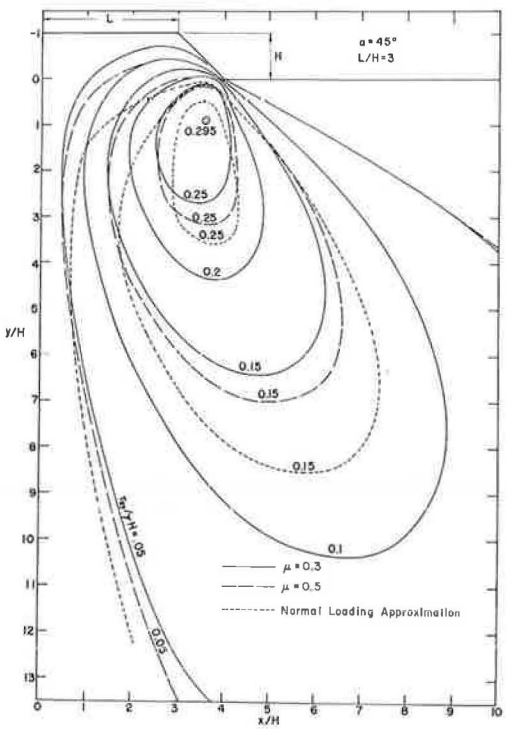

Figure 8. Contours of shear stress, τ_{xy}.

the normal loading approximation does not produce negative horizontal stress at any depth. The reason for this difference becomes apparent when the shear stresses transmitted by the embankment to the foundation material are considered.

The effect of Poisson's ratio on the horizontal stress is illustrated in Figure 7. This figure shows the horizontal stress along vertical sections through the centerline and toe of the embankment for $\alpha = 45^0$ and $\mu = 0.5$. The dashed line shows the stress due to the normal loading approximation for L/H = 1. Comparison with Figure 6 indicates that a change in Poisson's ratio from 0.3 to 0.5 changes the stress at shallow depths below the central portion of the embankment by as much as a factor of three. The difference decreases as the L/H ratio increases. The influence of μ is less pronounced below the toe than below the centerline.

Horizontal and Vertical Shear Stress

Contours of horizontal and vertical shear stress, $\tau_{xy}/\gamma H$, are shown in Figure 8, for $\alpha = 45^0$ and L/H = 3. The solid contours are for Poisson's ratio of 0.3. The long dashed contours are for $\mu = 0.5$, and short dashed lines are for the normal loading approximation. The figure indicates the existence of horizontal shear stresses within the body of the embankment, increasing to a value in excess of 0.2 γH at the base near the toe of the slope. However, the maximum value of horizontal shear stress (approximately 0.3 γH) occurs below the base of the embankment.

Like the horizontal normal stress, the shear stress, τ_{xy}, is affected markedly by the magnitude of Poisson's ratio. However, the effect observed depends upon the position of the point considered, relative to the base of the embankment. In the zone below the embankment to a depth of y/H equal approximately two or three, the shear stresses in the incompressible material ($\mu = 0.5$) are less than for the case in which $\mu = 0.3$. At greater depths the reverse is true. The shear stress determined from the normal loading approximation is less than that for either μ above a depth factor of approximately three to five, and more at greater depths. The magnitude of this effect depends upon the horizontal location considered, as shown in the figure.

The normal loading approximation assumes that there is no shear stress at the

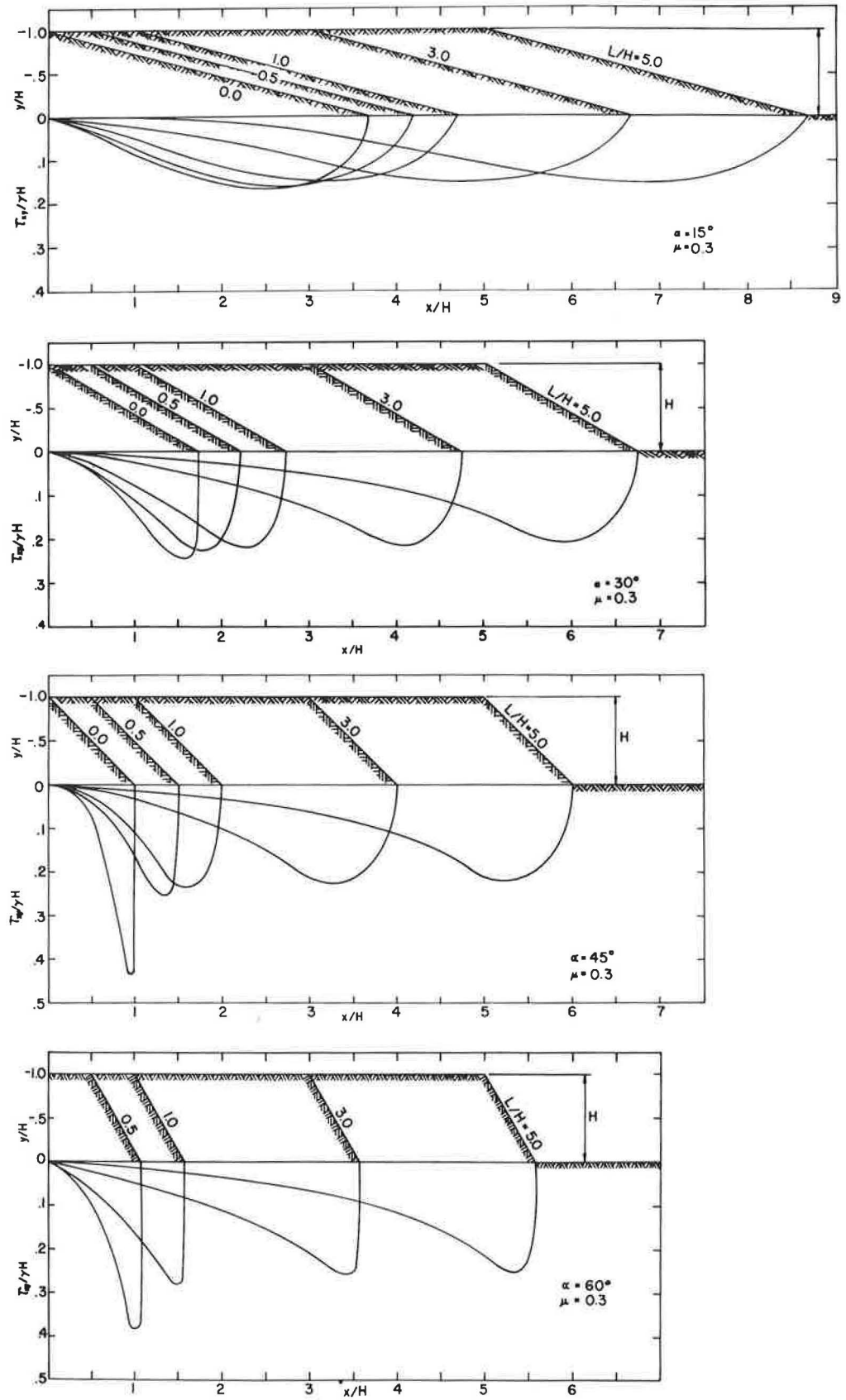

Figure 9. Distribution of shear stress, $\tau_{xy}/\gamma H$ on base of embankment for varying α, and L/H ratios.

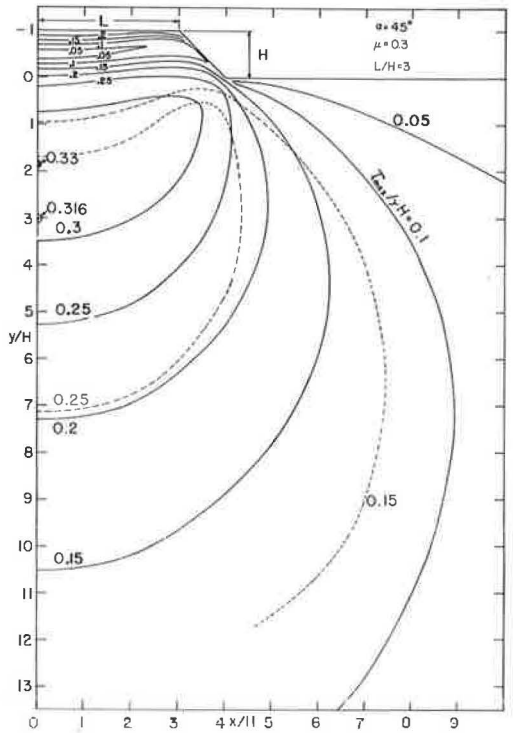

Figure 10. Contours for maximum shear, $\tau_{max}/\gamma H$.

base of the embankment. Figures 8 and 9 indicate that, for the elastic embankment, this assumption is not reasonable. Figure 9 shows the horizontal shear stress, $\tau_{xy}/\gamma H$, at the base of the embankment for $\mu = 0.3$, four values of α, and a variety of embankment shapes shown schematically in the figure. The horizontal shear stress is zero at the centerline, as required by symmetry, and reaches a maximum near the toe of the slope. The magnitude of the maximum and its location depend upon α and the embankment shape. As L/H decreases for a given α, the maximum $\tau_{xy}/\gamma H$ increases and moves closer to the toe of the slope. The magnitude of the increase is slight for $\alpha = 15^0$, but becomes more significant as α increases. Note that a maximum $\tau_{xy}/\gamma H$ in excess of 0.4 implies that the horizontal shear stress at the base of a 40-ft high embankment may be greater than one ton per square foot (unless the shear strength of the material is such that failure is induced).

To assist the designer in evaluating the significance of these results to his particular problem, influence diagrams for vertical normal, horizontal normal and shear stress distribution for a variety of cases are presented in Appendix B.

Maximum Shear Stress

It is often useful to consider whether the maximum (i.e., principal) shear stress, $\tau_{max}/\gamma H$, at any depth beneath the embankment exceeds the available shear strength.

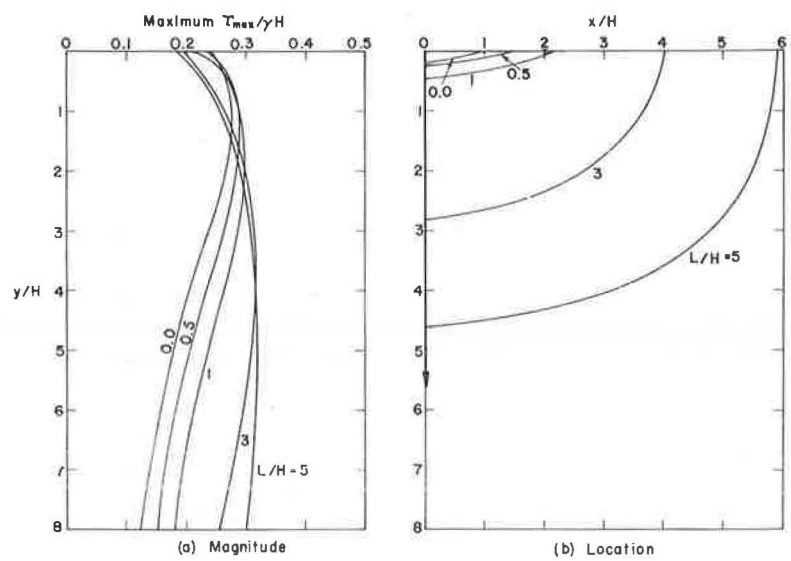

Figure 11. Magnitude and location of maximum ($\tau_{max}/\gamma H$) as a function of depth for $\mu = 0.3$, $\alpha = 15°$.

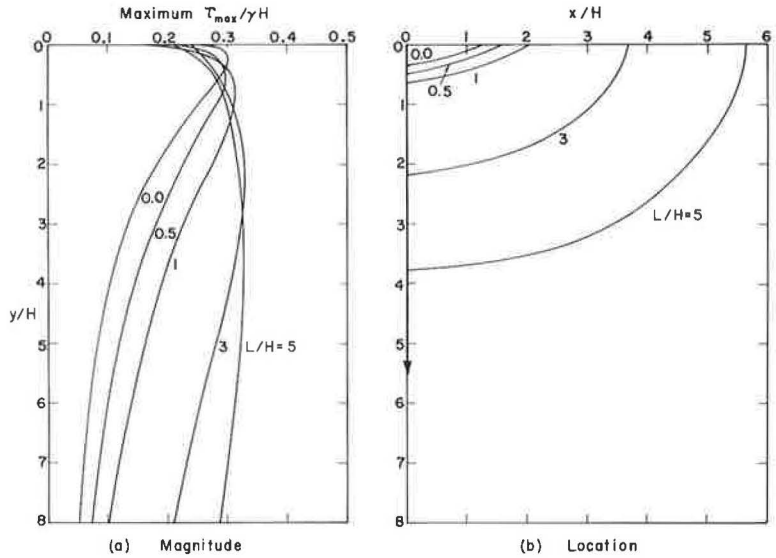

Figure 12. Magnitude and location of maximum ($\tau_{max}/\gamma H$) as a function of depth for $\mu = 0.3$, $\alpha = 30°$.

Thus, it is desirable to know the magnitude and distribution of maximum shear stresses due to the embankment. Contours of $\tau_{max}/\gamma H$ are shown in Figure 10 for the embankment section of Figures 2, 5 and 8. Note that the magnitude of τ_{max} transmitted from the embankment to the foundation material is approximately 0.25 γH at the base of the embankment in the vicinity of the toe. However, the largest shear stress, 0.33 γH, occurs beneath the centerline at y/H = 1.8. It is also interesting to observe that within the embankment, the maximum shear stresses are larger near the top than in the mid-depth region, and that they increase again as depth increases. This is believed due to

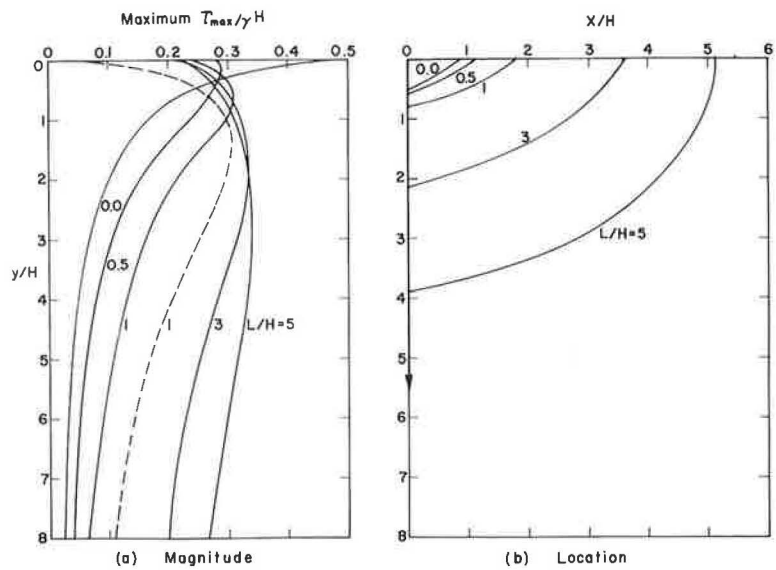

Figure 13. Magnitude and location of maximum ($\tau_{max}/\gamma H$) as a function of depth for $\mu = 0.3$, $\alpha = 45°$.

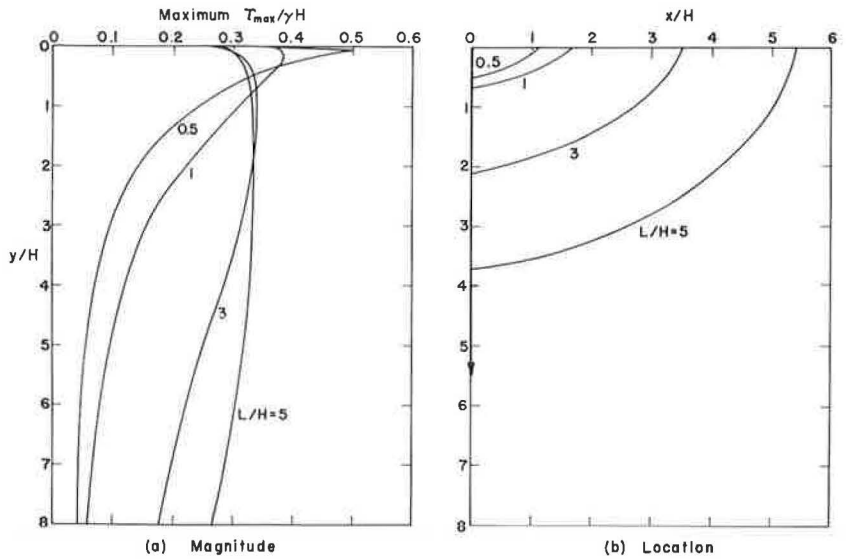

Figure 14. Magnitude and location of maximum ($\tau_{max}/\gamma H$) as a function of depth for $\mu = 0.3$, $\alpha = 60°$.

the relatively large horizontal stresses which are induced by the deformation mode of the embankment (cf. Fig. 5).

Two contours of $\tau_{max}/\gamma H$ for the normal loading approximation corresponding to the embankment considered are shown in Figure 10 as dashed lines. They indicate a shear stress less than that produced by the elastic embankment in a shallow zone below the embankment, but larger shear stresses at depth.

Data for a variety of embankment shapes, with $\mu = 0.3$, and $\alpha = 15$, 30, 45, 60 and 75^0 are shown in Figures 11 to 15, respectively. In these figures, the maximum value of τ_{max} at a particular depth is plotted as a function of depth for various L/H ratios.

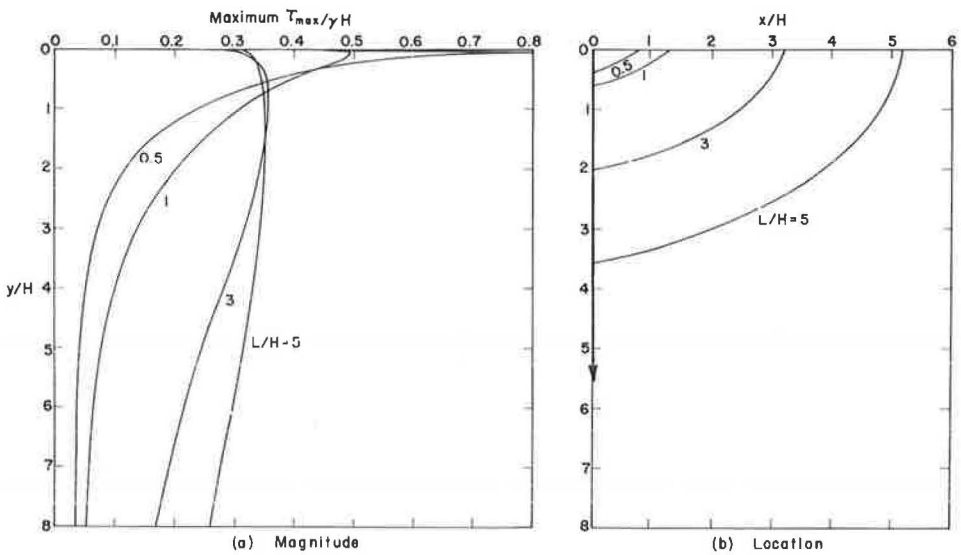

Figure 15. Magnitude and location of maximum ($\tau_{max}/\gamma H$) as a function of depth for $\mu = 0.3$, $\alpha = 75°$.

The horizontal location of the point at which this maximum value occurs is also shown. Figure 11 shows that as the L/H ratio increases for $\alpha = 15^0$, peak τ_{max} increases in magnitude and acts at an increasing depth below the embankment. The horizontal location of the maximum shear stress at a particular depth moves from a position near the toe of the slope immediately beneath the embankment to the centerline of the embankment at a depth which depends upon the L/H ratio.

A similar trend is shown in Figure 12 for $\alpha = 30^0$. However, in Figure 13 ($\alpha = 45^0$), the largest shear stress occurs near the toe of the slope for L/H = 0.0. Although the smallest L/H ratio shown in Figures 14 and 15 is 0.5, the development of large shear stress near the toe of narrow steep embankments is clearly indicated.

The dashed line in Figure 13 shows the magnitude of the maximum τ_{max} as a function of depth for the normal loading approximation corresponding to the 45^0 embankment for which L/H = 1. It is evident that the peak magnitudes are nearly the same for the two cases, but it occurs at approximately twice the depth in the case of the normal loading approximation. A similar effect is evident in Figure 10 for L/H = 3. Thus the influence of the elastic embankment is more pronounced nearer the surface where softer soils might be expected. As a result, it may be that current estimates of stability, potential creep and other shear stress related phenomena, for soils at shallow depths beneath embankments, are unconservative.

Relationship of Results to In Situ Stresses

It is not immediately clear what relationship these results have to stresses which actually exist in the field. In the case of a built-up embankment, it is likely that the embankment material will exhibit significantly different mechanical properties from the foundation material. For a cut-down slope, the assumption of homogeneity in the two zones may be more nearly justified. The non-linearity in the mechanical response of most natural materials will undoubtedly also influence the results. However, the feature which may be most significant, at least in the case of built-up embankments, is the fact that they are constructed in layers rather than instantaneously. Thus when the topmost lift is placed on an earth embankment, the upper material does not undergo strain due to elastic deformation of the embankment resulting from the stresses imposed by the entire mass. Rather, the strains are due only to the increment of stress imposed by this layer. The degree to which the results would be changed is not clear. However, it is believed that the results presented herein provide a more realistic estimate of stress conditions than that computed from the normal loading approximation.

Effect of Results on Stress Path Determination

Lambe (14) has suggested that the "stress path" method for prediction of vertical settlements of cohesive soils is superior to conventional analyses in cases where compression is clearly not one-dimensional. This approach involves three basic steps (Lambe, 14):

1. Estimation of the effective stress path of an "average" element in the compressible layer, for the field loading.
2. Performance of a laboratory compression test which duplicates, insofar as practicable, the field effective stress path.
3. Computation of settlement by multiplying the thickness of the layer considered by the axial (vertical) strain from the laboratory test.

Because the strains in the laboratory sample depend upon the applied stresses, the method requires a means of correctly assessing the in situ stresses.

A comparison of the total stress paths for several points under the centerline of an elastic embankment ($\alpha = 30^0$, $L/H_{final} = 0.5$, $\mu = 0.3$), with those computed using the normal loading approximation, is shown in Figure 16. The dashed "initial stress" line shows the state of stress in an elastic half-space, for which $\mu = 0.3$, before construction of the embankment. The three points shown on the line correspond to the stress states depths of 0.5, 1.0 and 2.0 times the final height of the embankment, H_{final}. The

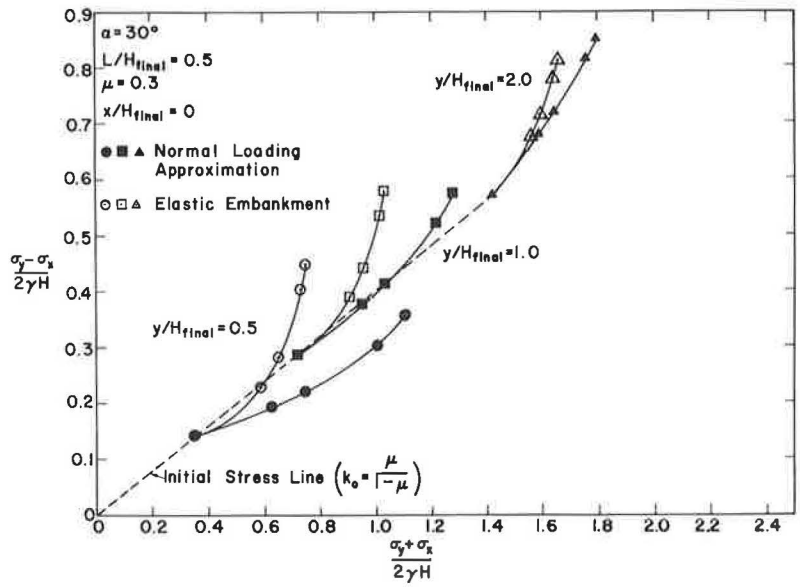

Figure 16. Stress path for three points under the centerline during embankment construction.

open points show the stress paths during "construction" of an elastic embankment continuous with the foundation material. The solid points show the stresses for corresponding embankment heights, determined by the conventional method. Several features of this comparison are especially noteworthy.

1. At relatively shallow depths ($y/H = 0.5$) the conventional method leads to a total stress path which lies entirely below the K_o line. That is, one would predict relatively small shear settlements. However, on the basis of the elastic embankment analysis, the estimated shear induced settlement would likely be larger, and compression settlement would be less.
2. At greater depth ($y/H_{final} = 2.0$) both methods lead to stress paths which lie above the K_o line. The two paths are closer, and the shear stress under the elastic embankment is actually less than that due to the normal loading approximation.
3. At intermediate depths ($y/H_{final} = 1.0$) the normal loading approximation remains relatively close to the K_o line. The stress path due to the elastic embankment is still considerably steeper.

Because of the influence of the applied stress path on the measured laboratory settlements, and therefore on the computed field settlements, it would seem essential to estimate accurately the predictive capability of the method to the field stresses. In the case considered, the stresses produced by the elastic embankment are significantly different from those due to the normal loading approximation, at least at shallow depths. The effect of this difference on the results predicted by the stress path method is not obvious, however this question would appear to deserve further attention.

CONCLUSIONS

The analysis presented herein permits determination of the stresses within and under long elastic embankments which are continuous with the underlying foundation material. The results indicate that the horizontal distribution of vertical stress is more nearly uniform than is usually assumed. Thus, differential settlements computed using the normal loading approximation will be larger than those determined using the stress distributions presented herein.

The horizontal vertical shear stresses created in the foundation material by the embankment are found to be significantly higher at shallow depths for the elastic embankment than for the normal loading approximation.

The influence diagrams presented provide the designer with what is believed to a more realistic estimate of the vertical stresses than that usually employed.

ACKNOWLEDGMENTS

The research described herein was supported in part by the Ohio Department of Highways in conjunction with the U.S. Bureau of Public Roads, and in part by the Joint Highway Research Project, Purdue University, in conjunction with the U.S. Bureau of Public Roads. The assistance of W. L. DeGroff, R. Hockema, and R. Corbett in the preparation of the drawings is gratefully acknowledged.

REFERENCES

1. Brown, C. B. Incremental Analysis of Gravitational Stresses in Embankments and Their Effect Upon the Failure of Earth Structures. PhD dissertation, Univ. of Minnesota, 1962.
2. Carlton, T. A., Jr. The Distribution of Gravity Stresses in a Symmetrical Trapezoidal Embankment and Its Foundation. PhD thesis, Univ. of Texas, 1962.
3. Carothers, S. D. Direct Determination of Stresses. Proc. The Royal Society of London, Series A., Vol. XCVII, p. 110, 1920.
4. Churchill, R. V. Introduction to Complex Variables and Applications. McGraw-Hill Book Co., New York, 1948.
5. Clough, R., and Chopra, A. K. Earthquake Stress Analysis in Earth Dams. Jour. Eng. Mech. Div., Proc. ASCE, Vol. 92, No. EU2, April 1966.
6. Davis, E. H., and Taylor, H. The Movement of Bridge Approaches and Abutments on Soft Foundation Soils. Paper No. 37, Proc. Australian Research Board, Part 2, Vol. 1, 1962.
7. Dingwall, J. C., and Scrivner, F. H. Application of the Elastic Theory to Highway Embankments by Use of Difference Equations. HRB Proc., Vol. 33, p. 474, 1954.
8. Finn, W. D. L. Stresses in Soil Masses Under Various Boundary Conditions. PhD thesis, Univ. of Washington, 1960.
9. Finn, W. D. L. Static and Dynamic Stresses in Slopes. Proc. First Congress of the International Society of Rock Mechanics, Vol. II, p. 167, 1966.
10. Goodman, L. E., and Brown, C. B. Dead Load Stresses and Instability of Slopes. Jour. Soil Mech. and Found. Div., Proc. ASCE, Vol. 89, No. SM3, May 1963.
11. Henderson, F. M. Elliptic Functions with Complex Arguments. Univ. of Michigan Press, Ann Arbor, 1960.
12. Hildebrand, F. B. Introduction to Numerical Analysis. McGraw-Hill Book Co., New York, 1956.
13. Jurgenson, L. The Application of Theories of Elasticity and Plasticity to Foundation Problems. Jour. Boston Soc. of Civil Engineers, July 1937.
14. Lambe, T. W. Methods of Estimating Settlement. Proc. ASCE Conf. on Design of Foundations for Control of Settlement, p. 47, 1964.
15. Muskhelishvili, N. I. Some Basic Problems of the Mathematical Theory of Elasticity. P. Noordhoff, Groningen, 1953.
16. Newmark, N. M. Stress Distribution in Soils. Proc. Purdue Conf. on Soil Mechanics and Its Applications, p. 295, 1940.
17. Newmark, N. M. Influence Charts for Computation of Elastic Stresses in Foundations. Univ. of Illinois Eng. Exp. Sta., Bull. No. 338, 1942.
18. Osterberg, J. O. Influence Value for Vertical Stresses in a Semi-Infinite Mass Due to an Embankment Loading. Proc. 4th Internat. Conf. on Soil Mech. and Found. Eng., Vol. I, p. 393, 1957.
19. Rendulic, L. Der Erddruck im Strassenbau und Bruckenbau. Forschungsbarb. Strassenwesen, Bd. 10, Volk u. Reich Verlag, Berlin, 1938.
20. Terzaghi K. Theoretical Soil Mechanics. John Wiley, New York, 1943.

21. Timoshenko, S., and Goodier, J. N. Theory of Elasticity. McGraw-Hill Book Co., New York, 1951.
22. Trollope, D. H. The Systematic Arching Theory Applied to Stability Analysis of Embankments. Proc. 4th Internat. Conf. on Soil Mech. and Found. Eng., Vol. 2, p. 382, 1957.
23. Wylie, C. R., Jr. Advanced Engineering Mathematics, Third Ed. McGraw-Hill Book Co., New York, 1966.
24. Zienkiewicz, O. C. Stress Distribution in Gravity Dams. Jour. Inst. of Civil Engineers, Vol. 27, p. 247, January 1947.
25. Zienkiewicz, O. C., and Cheung, Y. K. Buttress Dams on Complex Rock Foundations. Water Power, Vol. 16, No. 5, p. 193, May 1964.
26. Zienkiewicz, O. C., and Cheung, Y. K. Stresses in Buttress Dams. Water Power, Vol. 17, No. 2, p. 69, Feb. 1965.
27. Zienkiewicz, O. C., and Gerstner, R. W. Foundation Elasticity Effects in Gravity Dams. Proc. Inst. of Civil Engineers, Vol. 19, p. 209, 1961.

Appendix A

SOLUTION OF THE PROBLEM

The method of solution is a modification of the Muskhelishvili (15) method. A brief outline of the solution is given below. A more complete discussion of the details will be presented in a forthcoming paper.

For the plane strain problem, the stresses can be defined in terms of an Airy stress function, $U(x, y)$ as:

$$\left.\begin{aligned} \sigma_x &= \frac{\partial^2 U(x,y)}{\partial y^2} + \frac{\mu}{1-\mu}\gamma y \\ \sigma_y &= \frac{\partial^2 U(x,y)}{\partial x^2} + \gamma y \\ \tau_{xy} &= -\frac{\partial^2 U(x,y)}{\partial x \partial y} \end{aligned}\right\} \qquad (1)$$

where σ_x, σ_y, τ_{xy} are the horizontal normal, vertical normal and shear stress, respectively, γ is the unit weight of the material, μ is the Poisson's ratio. For a case in which weight is the only body force acting, the requirements of equilibrium and compatibility will be satisfied if (Timoshenko and Goodier, 21):

$$\nabla^4 U(x, y) = 0 \qquad (2)$$

where ∇^2 is the Laplacian operator.

When the boundary conditions of the specific problem are also satisfied, the unique solution has been obtained.

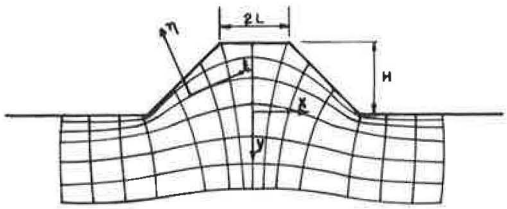

(a) Geometrical Transformation

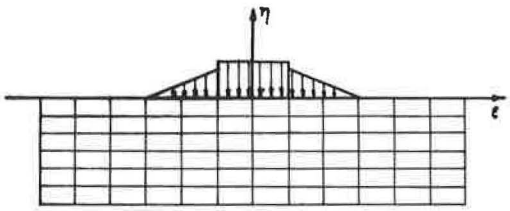

(b) Transformation of "Fictitious Stresses" on Boundary-Real Part

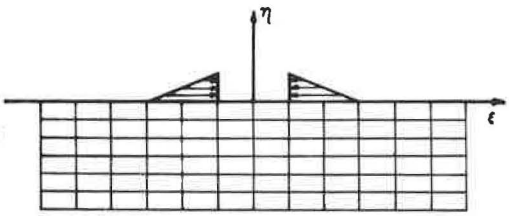

(c) Transformation of "Fictitious Stresses" on Boundary-Imag. Part

Figure 17. Graphical representation of transformation procedure.

In considering the boundary conditions associated with the embankment, it is convenient to represent the Airy stress function in complex form. Referring to the plane in which the embankment section is shown in Figure 17a, as the z-plane, a point within the medium can be represented by the complex number, $z = x + iy$. Assuming that the stress function is analytic within the medium, the function can be written as

$$U(x, y) = \text{Re}\ [\bar{z}\phi(z) + \chi(z)] \qquad (3)$$

where $\bar{z} = x - iy$, ϕ and χ are single-valued analytic functions throughout the z-plane. The functions ϕ and χ are determined from the conditions that the normal and tangential stresses on the boundary are equal to zero. Substituting Eq. 3 into Eq. 1, and expressing the stresses in terms of the boundary tractions leads to

$$N + iT = \phi'(z) + \overline{\phi'(z)} - e^{2i\theta}\left[\bar{z}\phi''(z) + \chi'(z) + \frac{\gamma y}{2}\left(\frac{1 - 2\mu}{1 - \mu}\right)\right] + \frac{\gamma y}{2}\left(\frac{1}{1 - \mu}\right) \qquad (4)$$

where a bar indicates the complex conjugate of the quantity, θ is the angle between the slope and the x-axis measured in a clockwise direction, μ is Poisson's ratio, N and T are the normal and tangential components, respectively, of the boundary traction.

Evaluation of the stresses is then accomplished by a two-step transformation. First, the boundary of the z-plane is transformed into the straight-line boundary of an auxiliary plane, the t-plane, $t = \xi + i\eta$, by the application of the Schwarz-Christoffel transformation (Churchill, 4):

$$z = f(t) = R \int_{\lambda = 0}^{t} \left(\frac{1 - \beta^2 \lambda^2}{1 - \lambda^2}\right)^{\frac{1}{n}} d\lambda + S \qquad (5)$$

where R and S are constants, β is the modulus, λ is a dummy variable and $n = \pi/\alpha$. Note that when $n = 2$, corresponding to a slope angle of 90^0, the integral expression in Eq. 5 is an elliptic integral of the second kind, for which tables or charts (Henderson, 11) are available. For those cases where n is larger than 2, the integral can be evaluated numerically on the computer. In this analysis, Eq. 5 was evaluated for all values of n on the IBM 7094 digital computer by a Simpson's rule integration (Hildebrand, 12).

Because Eq. 5 represents a conformal transformation, straight lines, ξ = constant and η = constant in the t-plane, correspond to orthogonal curvilinear coordinates in the z-plane. This is illustrated in Figure 17a. Thus, the boundary conditions in terms of $\phi(z)$ and $\chi(z)$ can be written as functions of $\phi[f(t)] = \phi(t)$ and $\chi[f(t)] = \chi(t)$. Then the boundary tractions become

$$N + iT = 0 = \Phi(t) + \overline{\Phi(t)} + \frac{\gamma}{2(1-\mu)} \operatorname{Im}[f(t)] + \frac{f'(t)}{\overline{f'(t)}} \left[\overline{f(t)} \frac{\Phi'(t)}{f'(t)} + \Psi(t) + \frac{\gamma}{2} \left(\frac{1-2\mu}{1-\mu} \right) \operatorname{Im}[f(t)] \right] \quad (6)$$

where $\Phi(t) = \phi'(t)$, $\Psi(t) = \chi'(t)$ and $f'(t)$ is the integrand of Eq. 5. Recognizing $\eta = 0$ and $t = \xi$ in Eq. 6, and rearranging leads to

$$\Phi(\xi) + \overline{\Phi(\xi)} + \frac{f'(\xi)}{\overline{f'(\xi)}} \left[\overline{f(\xi)} \frac{\Phi'(\xi)}{f'(\xi)} + \Psi(\xi) \right] = \frac{\gamma}{2(1-\mu)} \left[1 + (1-2\mu) \frac{f'(\xi)}{\overline{f'(\xi)}} \right] \operatorname{Im}[f(\xi)] \quad (7)$$

In this form, Eq. 7 expresses the effect in the t-plane of the geometric shape of the embankment. This effect can be visualized as a "fictitious loading" applied to the boundary of the t-plane. The real and imaginary parts of this "fictitious boundary loading" are shown in Figures 17b and 17c, respectively.

Having expressed the desired functions of the boundary, it is necessary to determine them inside the boundary. This is accomplished by the application of the Cauchy integral formula. This formula states that for a given function $g(\xi)$ along a closed contour, C, which satisfies certain conditions, the value of the function at an interior point, t, is (Wylie, 23)

$$g(t) = \frac{1}{2\pi i} \int_C \frac{g(\xi)}{\xi - t} \, d\xi \quad (8)$$

If the point t is exterior to the closed contour, then the integral expression equals zero. By this means, the desired functions can be evaluated inside the boundary. Knowing $\Phi(t)$ and $\Psi(t)$, and substituting Eq. 3 into Eq. 1, leads to the determination of the stresses:

$$\left.\begin{aligned} \sigma_x &= 2 \operatorname{Re} \Phi(t) - \operatorname{Re}\left[\overline{f(t)} \frac{\Phi'(t)}{f'(t)} + \Psi(t) \right] + \left(\frac{\mu}{1-\mu} \right) \gamma \operatorname{Im}[f(t)] \\ \sigma_y &= 2 \operatorname{Re} \Phi(t) + \operatorname{Re}\left[\overline{f(t)} \frac{\Phi'(t)}{f'(t)} + \Psi(t) \right] + \gamma \operatorname{Im}[f(t)] \\ \tau_{xy} &= \operatorname{Im}\left[\overline{f(t)} \frac{\Phi'(t)}{f'(t)} + \Psi(t) \right] \end{aligned}\right\} \quad (9)$$

Appendix B

This Appendix contains influence diagrams for vertical normal stress and horizontal normal stress along vertical sections for $\mu = 0.3$, $\alpha = 15$, 30, 45, 60 and 75^0, and various embankment shapes. Influence diagrams for horizontal and vertical shear stress for $\alpha = 45^0$, $\mu = 0.3$ and various embankment shapes are also given.

The diagrams indicate the stress due to the embankment weight alone. Stresses due to the weight of material underlying the embankment must be superimposed to obtain the total stress. The stresses are expressed in dimensionless form as $\sigma_y/\gamma H$, $\sigma_x/\gamma H$ or $\tau_{xy}/\gamma H$. The coordinates are also in dimensionless form. For convenience in the semi-logarithmic plot, the depth is measured from the top of the embankment, and designated $\bar{y}/H$. This is in contrast to the discussion in the body of the paper where the vertical distances are measured from the base of the embankment and designated y/H.

Each of the four diagrams in a given figure refers to a particular vertical section, shown schematically on the diagram. The upper left diagram indicates stresses along a vertical section midway between the centerline and the toe of the slope; the lower left diagram indicates stresses along a vertical section through the toe of the slope; the lower right diagram indicates stresses along a vertical section located a distance from centerline equal to 1.5 times the distance from the centerline to the toe of the slope.

The influence diagrams are reproduced as Figures 18 through 28 on the following pages.

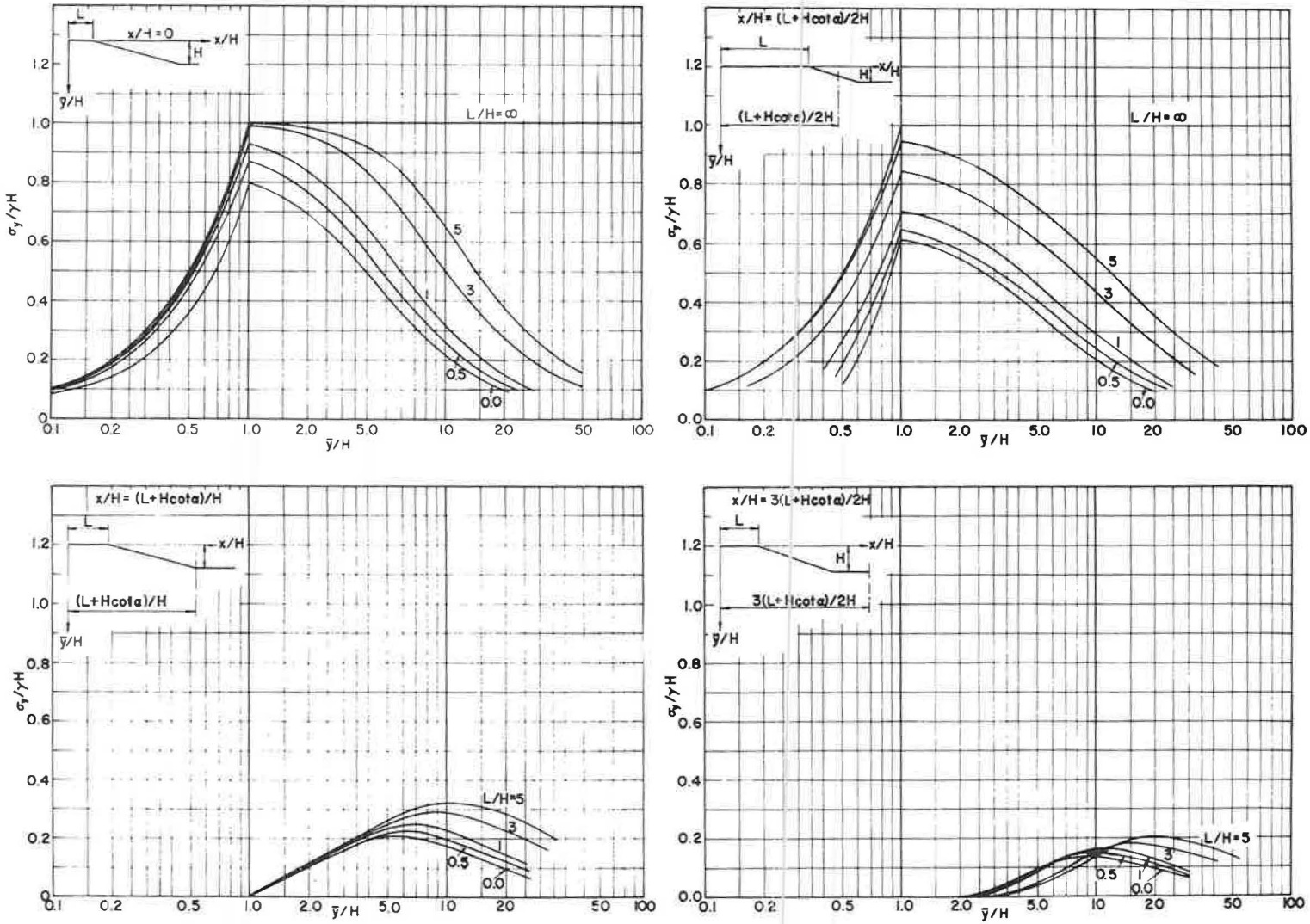

Figure 18. Influence diagrams for vertical normal stress along selected vertical sections for $\alpha = 15^{\circ}$, $\mu = 0.3$.

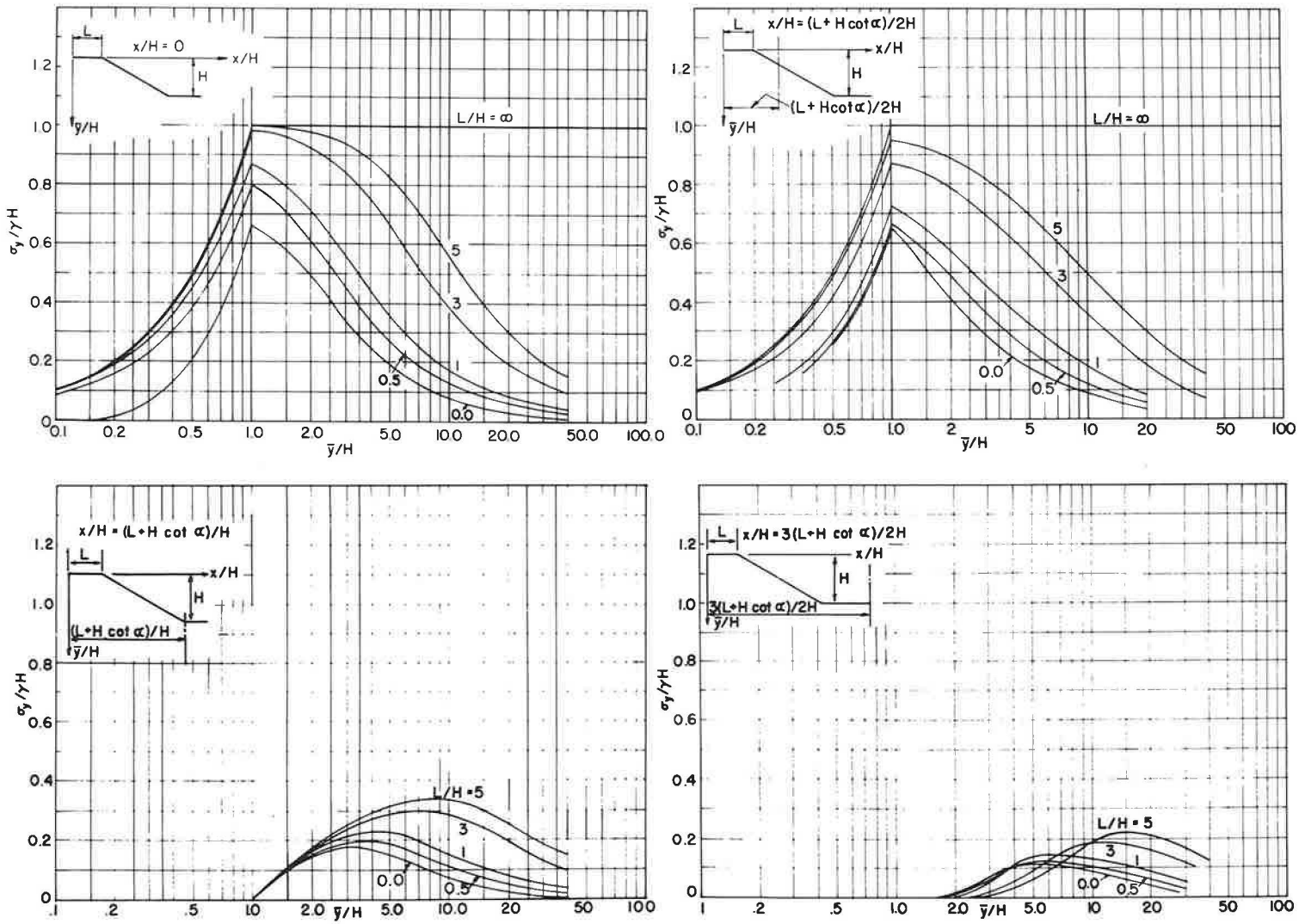

Figure 19. Influence diagrams for vertical normal stress along selected vertical sections for $\alpha = 30°$, $\mu = 0.3$.

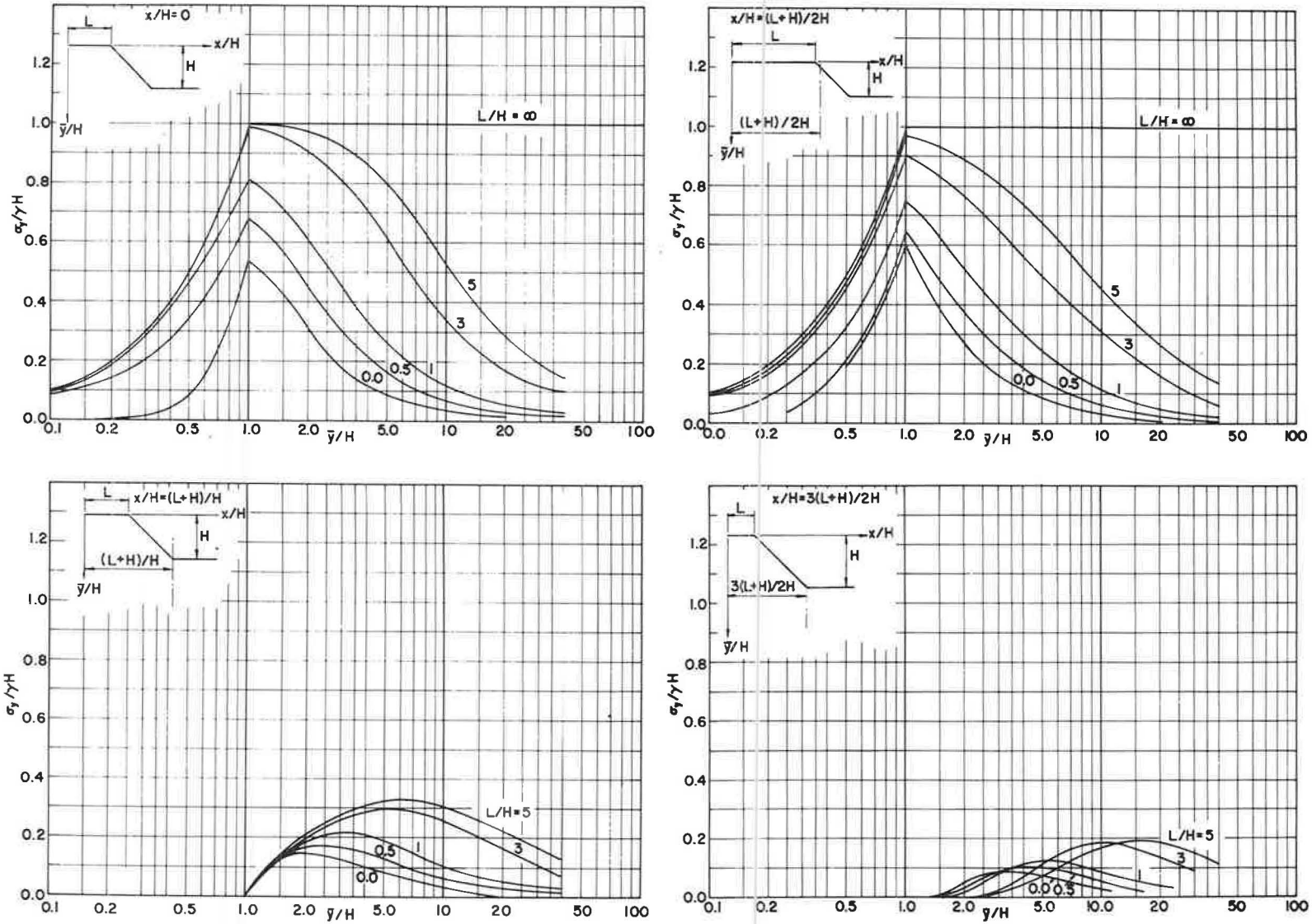

Figure 20. Influence diagrams for vertical normal stress along selected vertical sections for $\alpha = 45°$, $\mu = 0.3$.

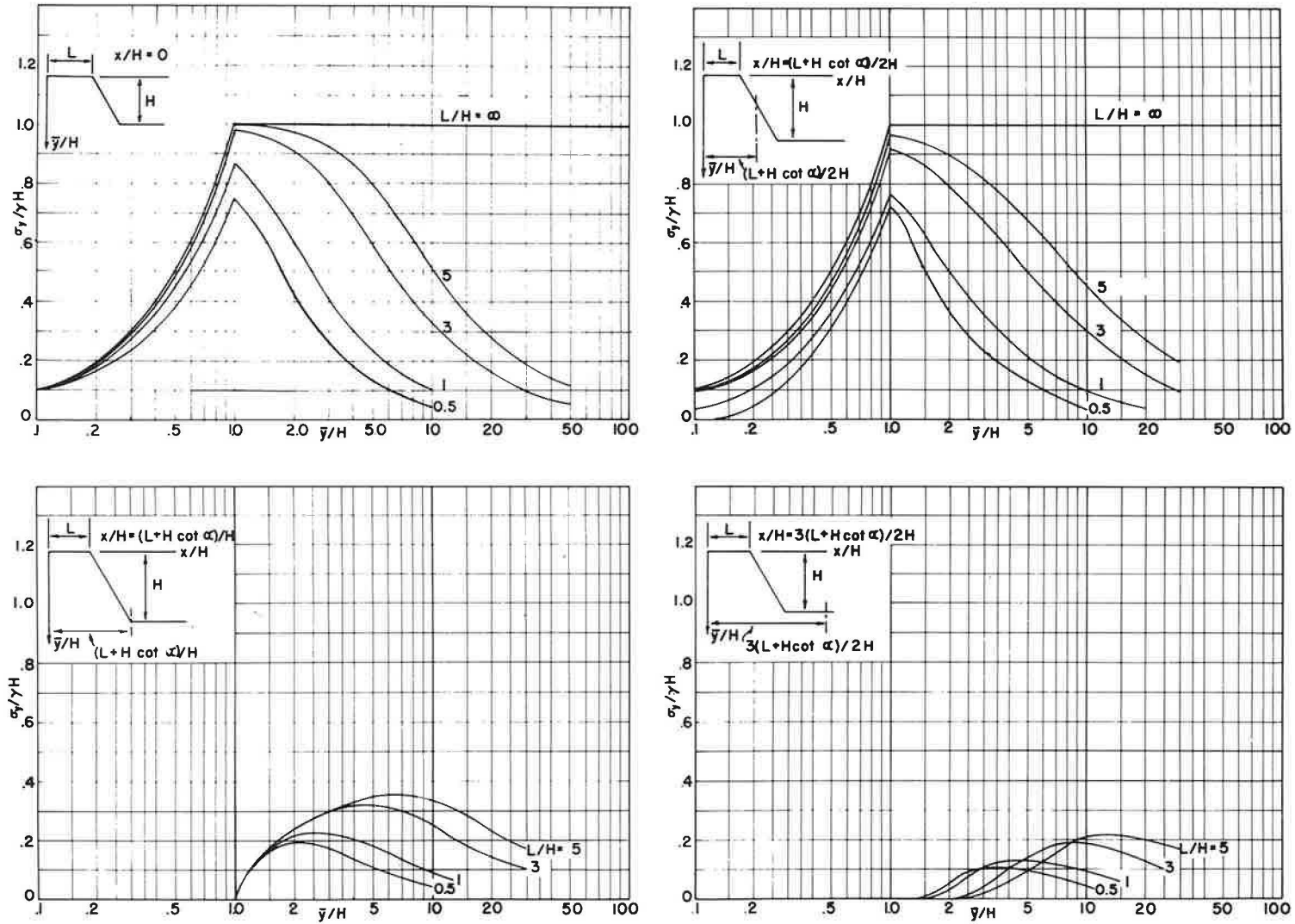

Figure 21. Influence diagrams for vertical normal stress along selected vertical sections for $\alpha = 60°$, $\mu = 0.3$.

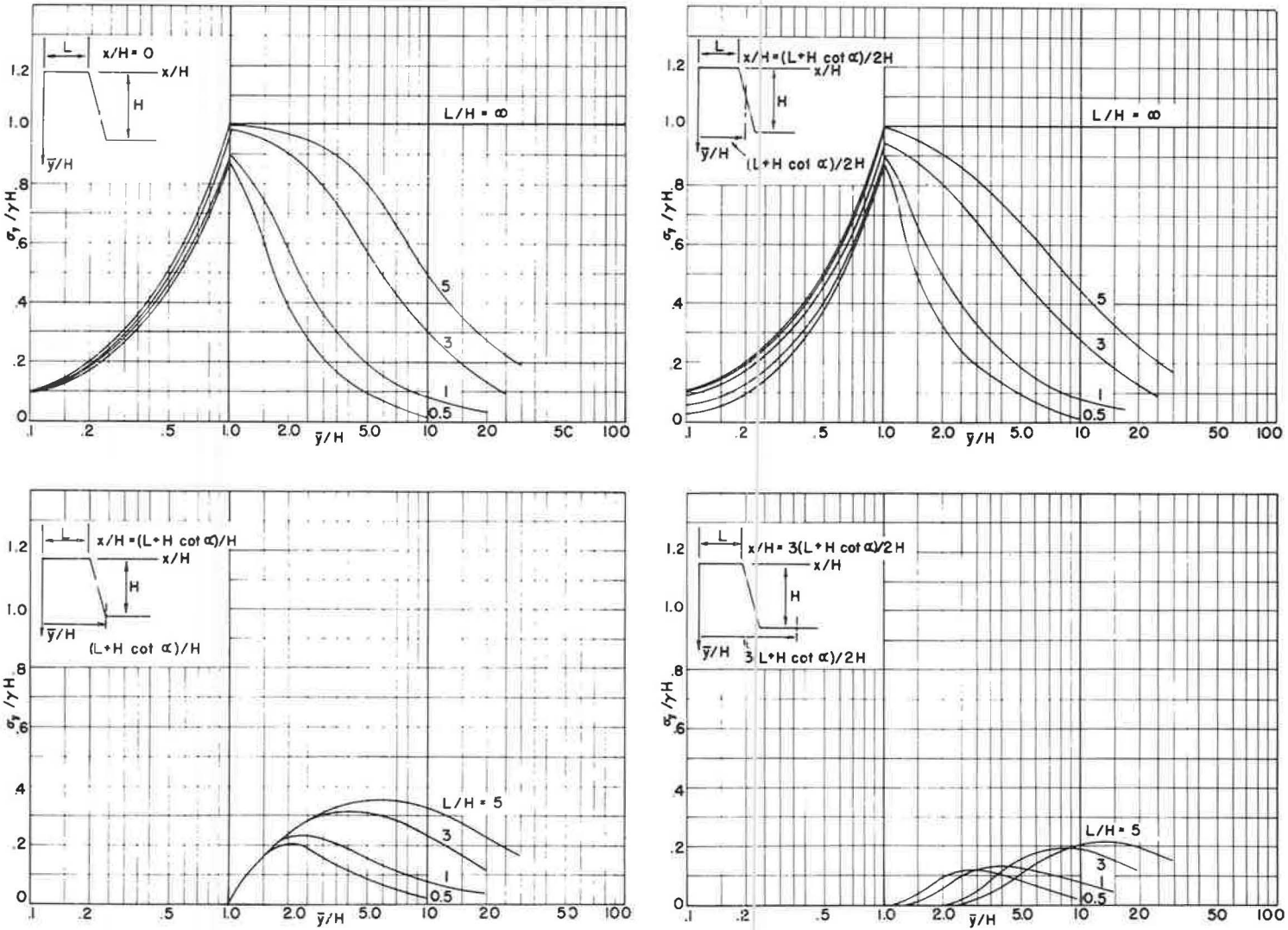

Figure 22. Influence diagrams for vertical normal stress along selected vertical sections for $\alpha = 75°$, $\mu = 0.3$.

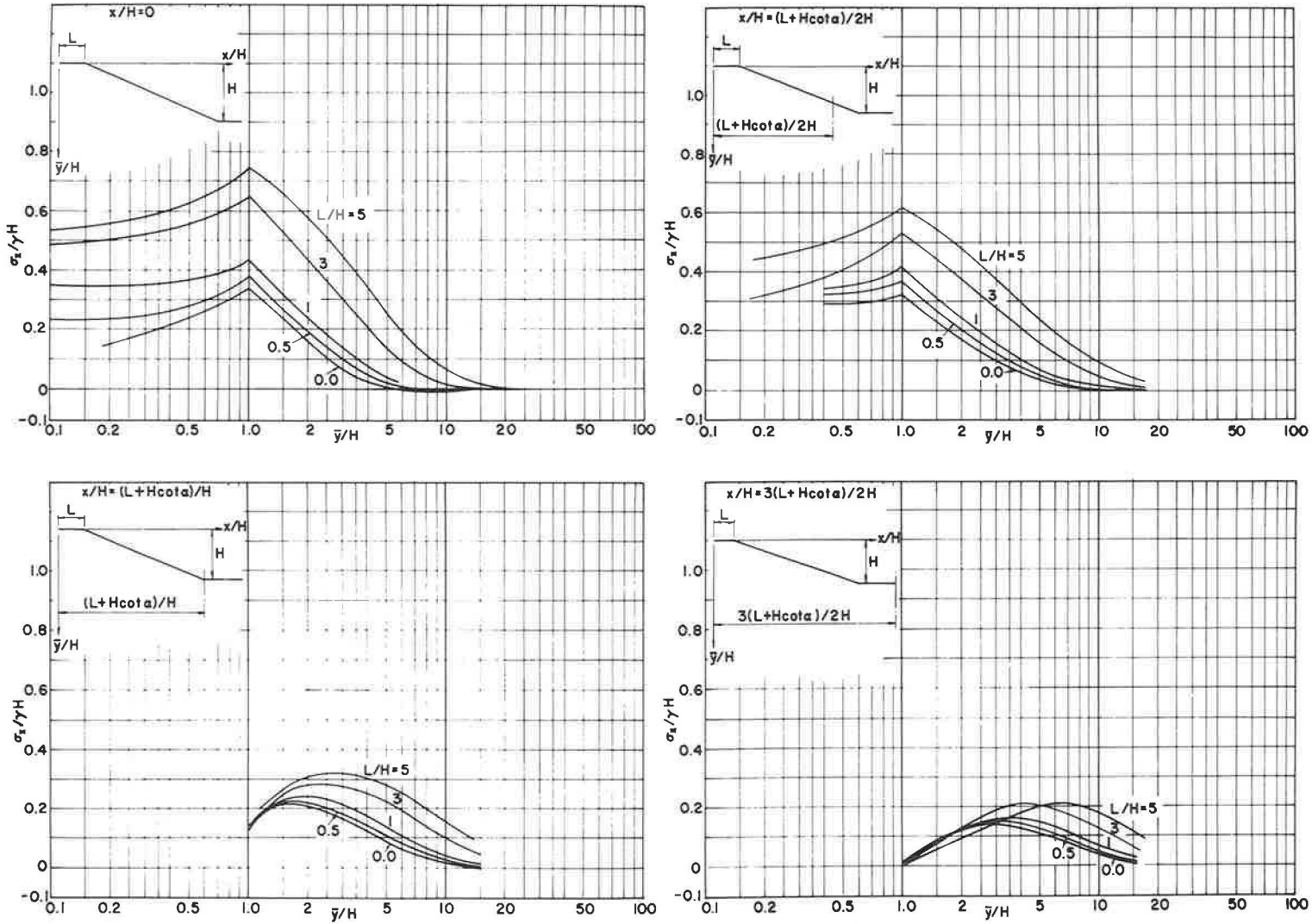

Figure 23. Influence diagrams for horizontal normal stress along selected vertical sections for $\alpha = 15°$, $\mu = 0.3$.

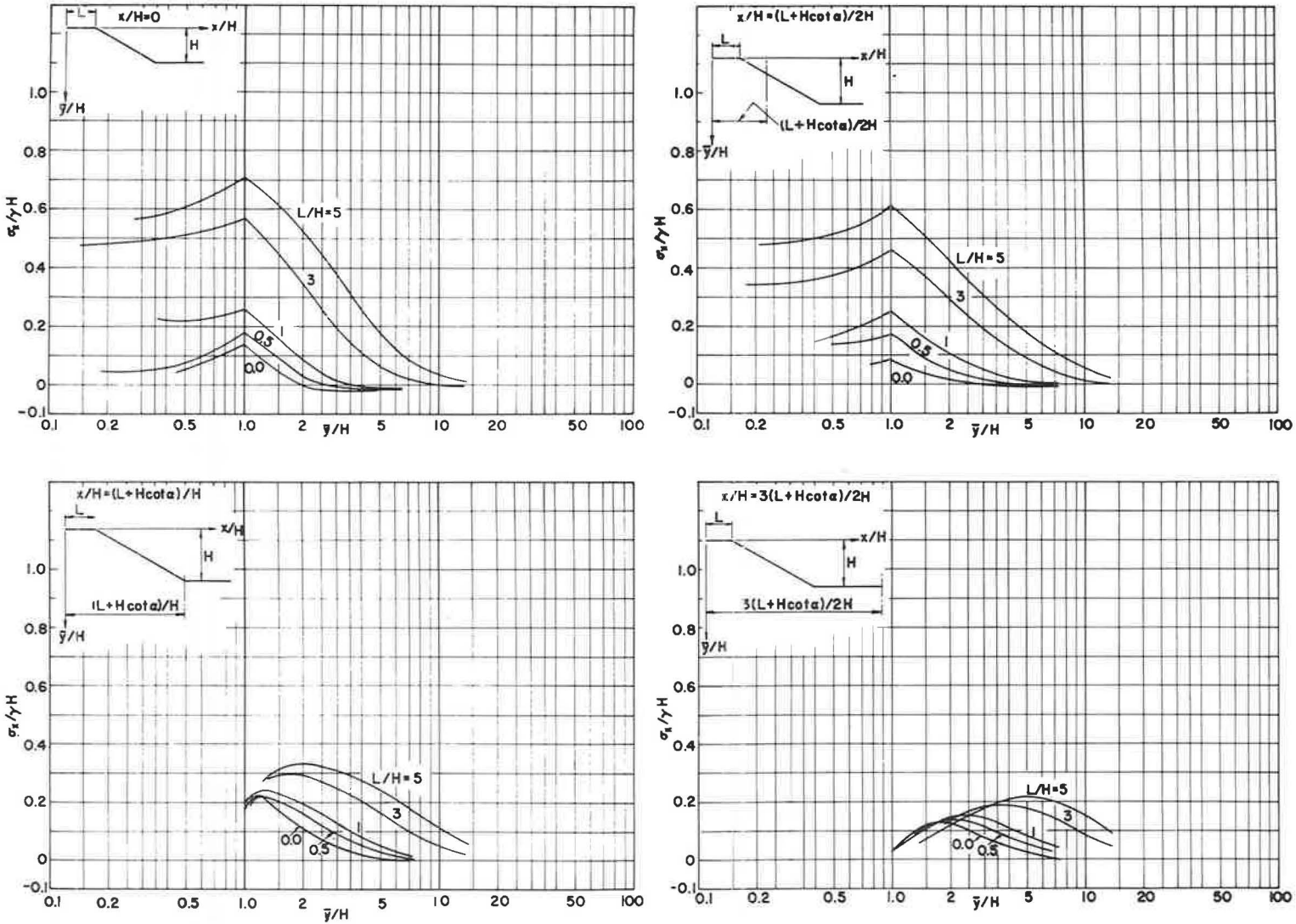

Figure 24. Influence diagrams for horizontal normal stress along selected vertical sections for $\alpha = 30°$, $\mu = 0.3$.

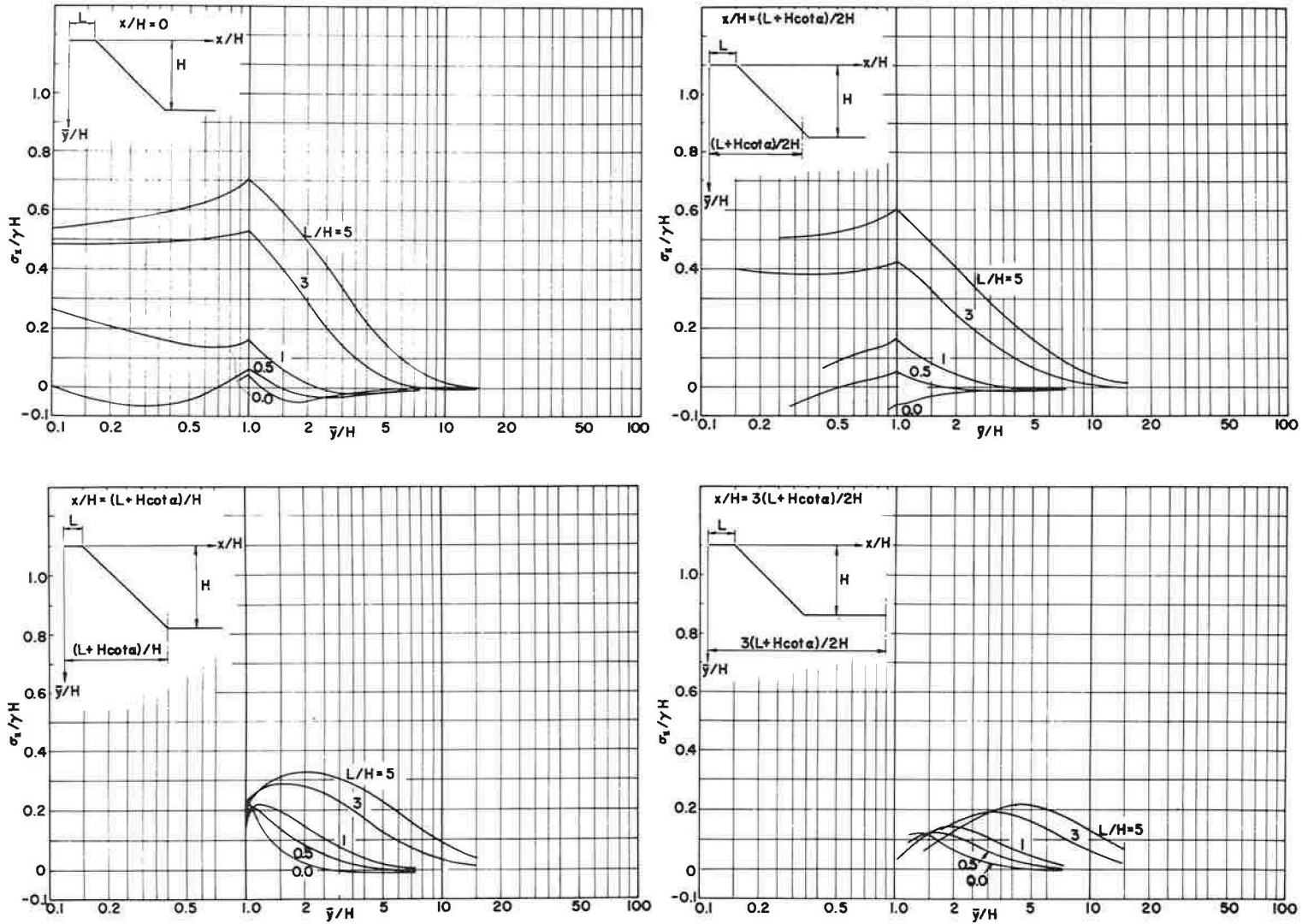

Figure 25. Influence diagrams for horizontal normal stress along selected vertical sections for $\alpha = 45°$, $\mu = 0.3$.

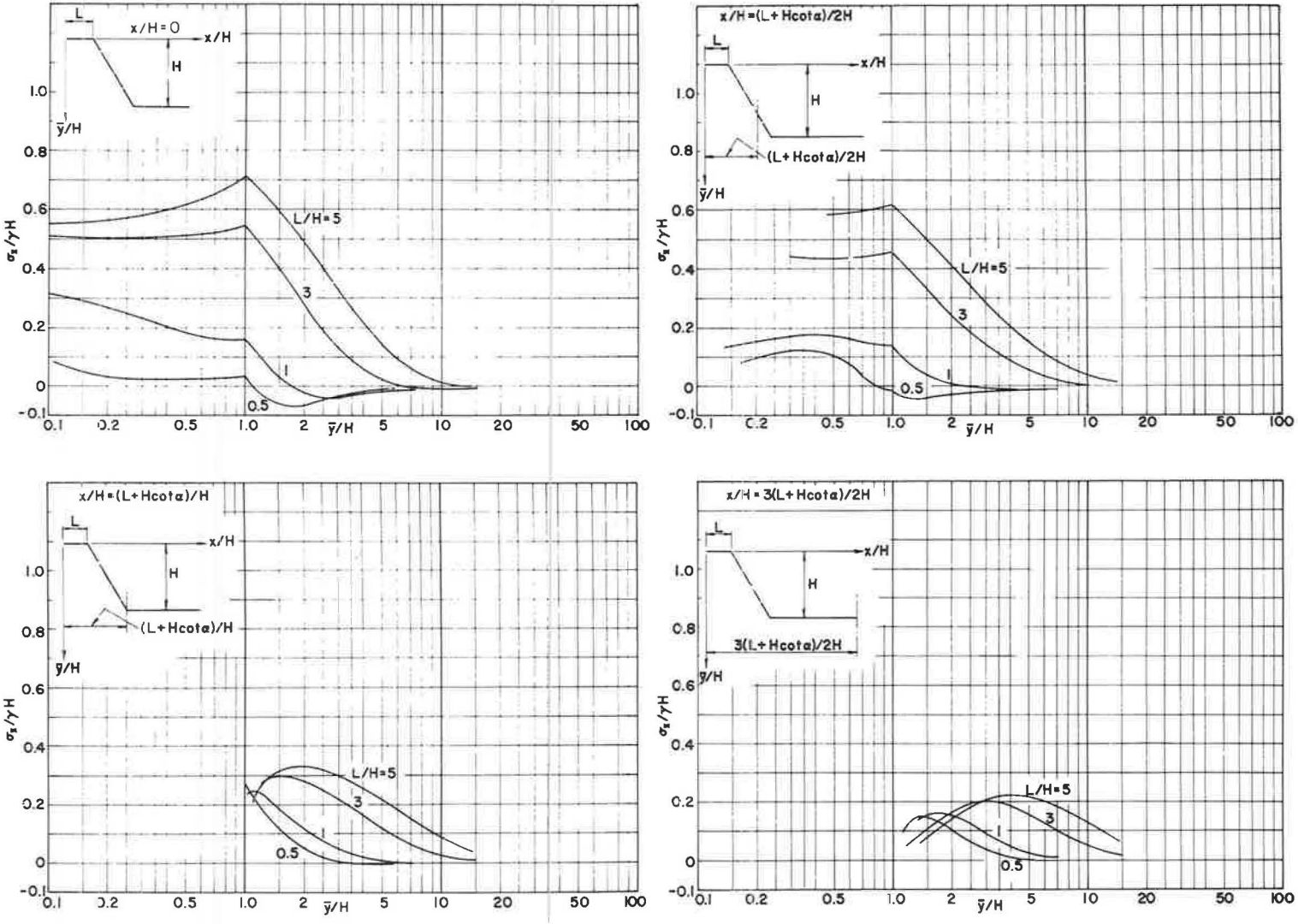

Figure 26. Influence diagrams for horizontal normal stress along selected vertical sections for $\alpha = 60°$, $\mu = 0.3$.

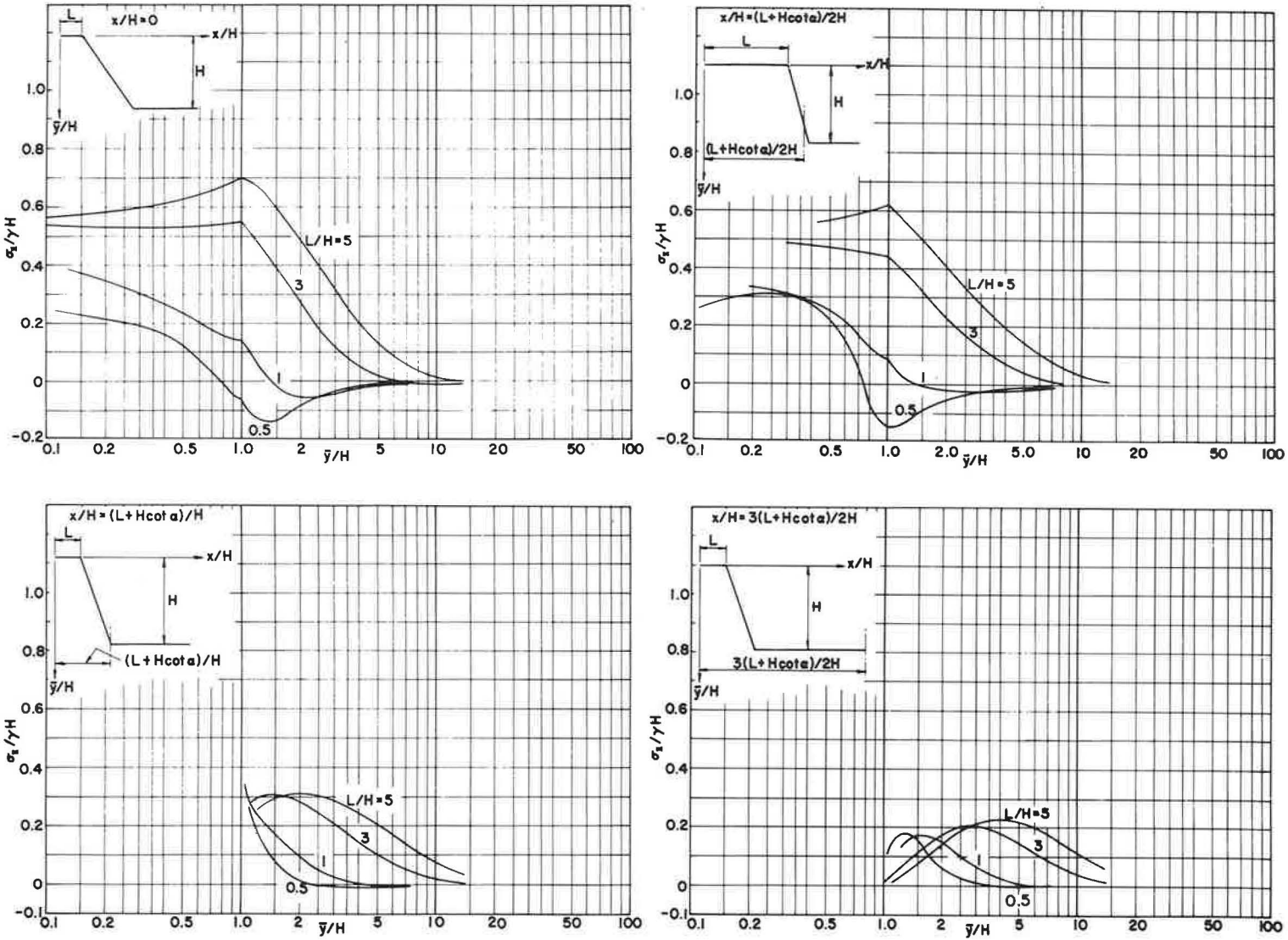

Figure 27. Influence diagrams for horizontal normal stress along selected vertical sections for $\alpha = 75°$, $\mu = 0.3$.

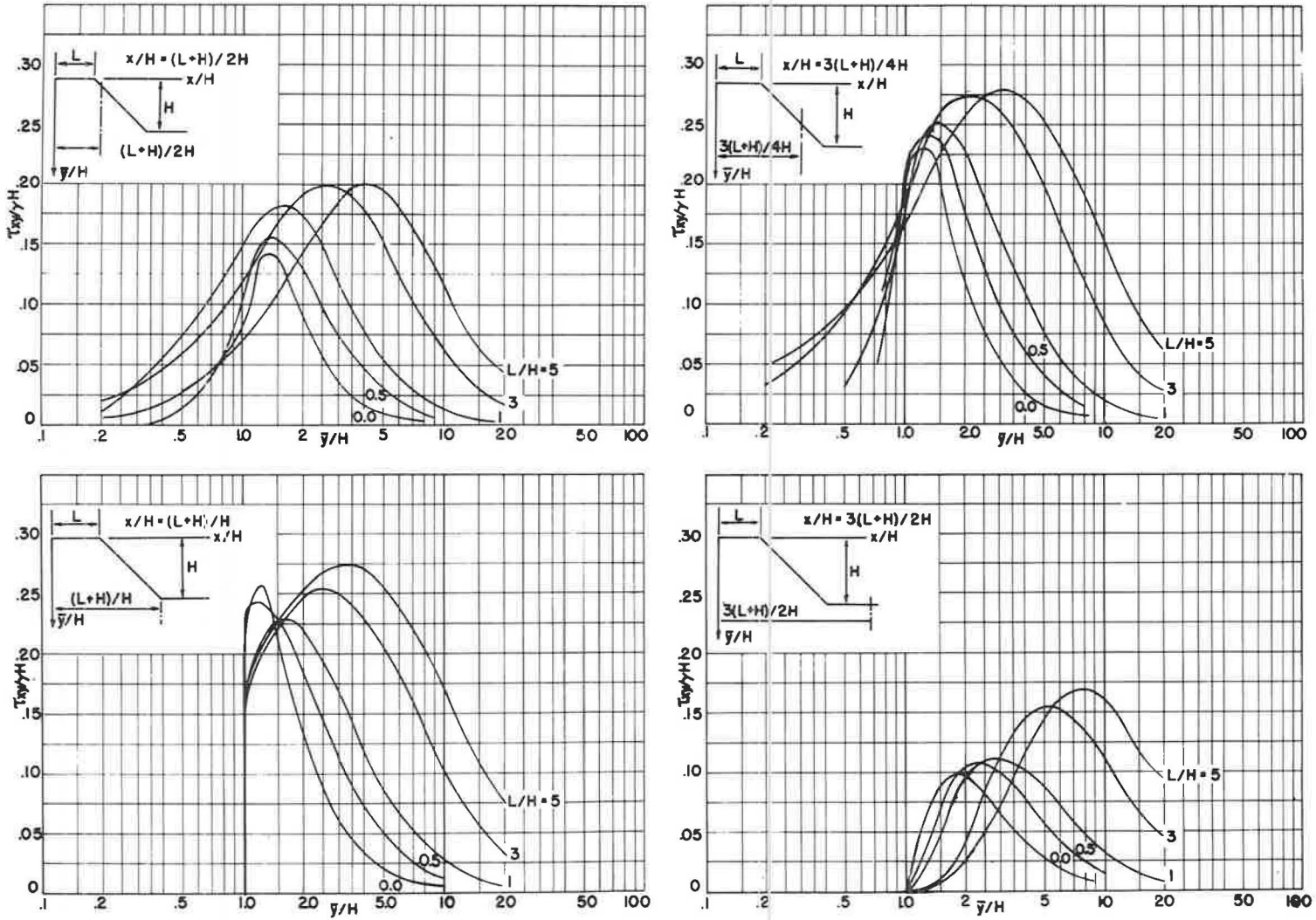

Figure 28. Influence diagrams for shear stress along selected vertical sections for $\alpha = 45°$, $\mu = 0.3$.

Influence of Soil Properties on Volumetric Change Under Dynamic Loading

F. DWAYNE NIELSON, Assistant Professor, Civil Engineering, New Mexico State University; and
JESUS A. CARDENAS, Professor, Ingenieria Civil, Universidad de Chihuahua, Mexico

The purpose of the present study is to evaluate soils adjacent to bridge abutments. It has been observed that some cracks have appeared precisely in the joint between bridge abutments and the pavement. Assuming that this type of failure is not due to settlement of underlying soils but is attributed to a microseismic vibratory phenomena caused by the vehicular traffic vibration, an experimental study was performed (a) to evaluate the effect of soil properties on the behavior of soils under dynamic loading, (b) to determine the type of soil that will develop the minimum volumetric change when subjected to vibration, and (c) to try to correlate their properties in an index of the susceptibility of soils to volumetric changes.

For the purpose of this study the index is called "vibration index." This index was determined by measuring the volumetric changes which occurred when a soil sample in a compaction mold was vibrated on a vibratory table. A high vibration index is associated with large volumetric changes.

Impact tests were also performed on different samples prepared in the laboratory and an "energy index" was determined relating the volumetric change to the impact energy per blow during the test. Again, a high energy index is indicative of greater susceptibility to volumetric changes under dynamic loading.

•THE purpose of the present study is to evaluate soils adjacent to bridge abutments. It has been observed that in some highways a transverse crack appears precisely in the joint between the rigid bridge abutment and the flexible pavement. Sometimes the crack is not developed but a noticeable bump is present. Failures of this type have appeared on roads a short time after they were opened to traffic. Figure 1 shows a typical crack.

With the assumption that this failure is not due to settlement of underlying soils, but due to a volumetric change within the soil mass caused by a microseismic vibratory phenomena associated with vehicular traffic vibration, a study to evaluate soils adjacent to bridge abutments is presented. For this work an experimental program was undertaken to correlate such soil properties as void ratio, moisture content, gradation, plasticity, cohesion, compression index and friction angle to an index that will serve as a measure of the susceptibility of soils to volumetric changes when subjected to vibrations. For the purpose of this work two indexes were encountered and used: the "vibration index" as determined by a vibration test on soil samples and the "energy index" as determined by impact tests. Both indexes are defined in the next section. The main objective will be to relate these indexes to the different soil properties to determine a type of soil that will undergo minimum volumetric change under dynamic loading.

Paper sponsored by Committee on Embankments and Earth Slopes and presented at the 46th Annual Meeting.

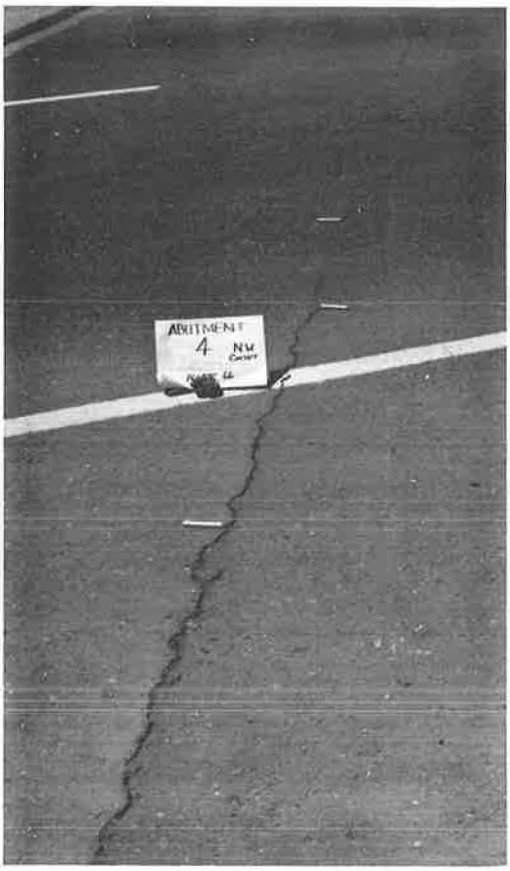

Figure 1. Typical crack in pavement next to bridge abutments.

Natural soils as well as specially prepared laboratory mixes were tested. Among the natural soils is the fine sand which is very common in southern New Mexico. Samples from the actual bridge abutments (six of them) were also studied. Eight mixes with different gradations were prepared for this study. The grain size curves for these materials are shown in Figure 2. To accomplish this evaluation of soils, an experimental program was developed in the laboratory to determine the various properties of the soils involved. The following tests were run: vibration, impact, triaxial, consolidation, compaction (standard and modified), Atterberg limits and grain size analysis.

EXPERIMENTAL PROGRAM

Vibration Test

The soil samples are compacted (according to the purpose of the test) in a standard $\frac{1}{30}$-cu ft Proctor mold. Moisture content determinations and weights were measured to determine the initial void ratio. This mold with the soil sample is attached to the vibratory table and a vertical load is applied as shown in Figure 3. The soil sample is vibrated through 30 cycles. This vibrating table is motor driven in the horizontal plane by an eccentric drive. One cycle will be used here as one complete revolution of the eccentric in one minute during which the frequency of vibrations goes from 14 to 60 cycles per sec as a maximum and then returns to 14 cycles per sec. During each cycle the amplitude of vibrations is kept constant. In this first study it was maintained at 0.025 in. which is large enough to induce vibration pressures to cause volumetric

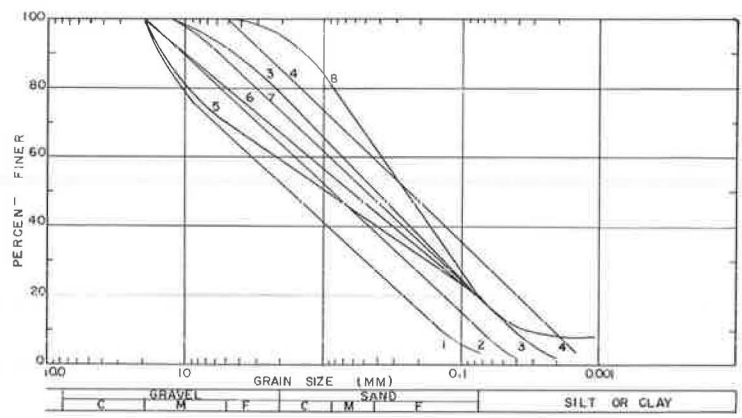

Figure 2. Grain size curves.

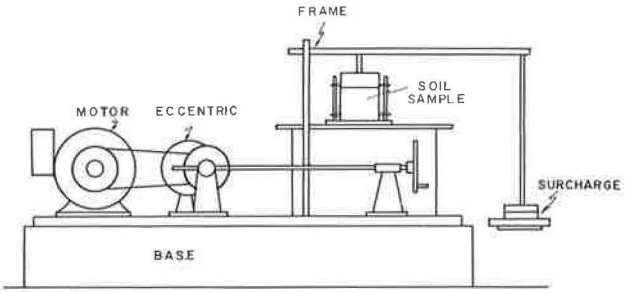

Figure 3. Vibrating table.

changes. The frequency values are within the range observed by Nijboer and Van der Poel (1). Also, the vertical pressures applied at the soil surface were 2.79, 11.15, and 16.24 psi, which are within the range of the pressures caused by vehicular loading as measured by Sowers and Vesic (2). The following sequence of cycles was used: 1, 2, 3, 4, 5, 6, 8, 10, 12, 14, 16, 18, 20, 25, and 30. After this the vertical deformation was measured at three different points on the surface of the sample. With these readings the change in void ratio was computed. When data from a vibration test are plotted on arithmetic paper with number of cycles versus void ratio, a curve as shown in Figure 4 is obtained. Changing the plotting to a log-log paper with log of number of cycles versus log of void ratio the curve is transformed into a straight line. The absolute value of the slope of this line is called "vibration index." A flat line does not show much variation in void ratio (volumetric change), and a steeper line shows a large volumetric change. Therefore, the vibration index will be used to evaluate the susceptibility of soils to volumetric changes under vibration. The use of the vibration index will eliminate the necessity of determining the energy applied by vehicular traffic. If the vibration index is high, the soil is expected to show larger volume changes.

Regarding the use of a Proctor mold for this test, and the vibratory table, the explanation is as follows: in almost every vibration test the vibrator is applied at the soil surface, but the effect of vibrations depends not only on soil properties but also on the size and weight of the vibrator. In this case the use of the mold is intended to isolate the soil properties in such a way that the volumetric change be only a function of soil properties.

Impact Test

This test consists of compacting a soil sample in a mold and then applying various amounts of impact energy by allowing a given weight to fall a given distance onto the sample; these blows cause a change in volume that is computed by measuring the vertical deformations produced by the blows. The blow sequence used in this test was 5, 10, 15, 20, 25, 35, 45, 55, 75, 100 and 150, which applies approximately 120,000 foot-pounds per cubic foot of energy to the soil. Also, the data from an impact test when plotted on log-log paper with log of impact energy versus log of void ratio show a straight-line correlation. The absolute value of the slope of this line is called the "energy index" (see Fig. 4). This energy index will also be used to evaluate the susceptibility of soils to volumetric change under dynamic or traffic loading. It will be observed also that the higher the energy index the larger the volumetric change expected.

With respect to the mold used for this impact test, three types were studied: Proctor, CBR, and Marshall. The Proctor and CBR molds were disregarded because the impact energy applied did not cause an even volumetric change. The top soil showed greater deformations than the bottom soil due to the presence of the fixed bottom plate of these molds which introduced undesirable friction. To avoid this the Marshall mold, 2 in. in diameter and $2\frac{1}{2}$ in. in depth with the free base, was selected. Also, the Marshall hammer weighing 10 lb and with an 18-in. free fall distance was used to apply the impact energy.

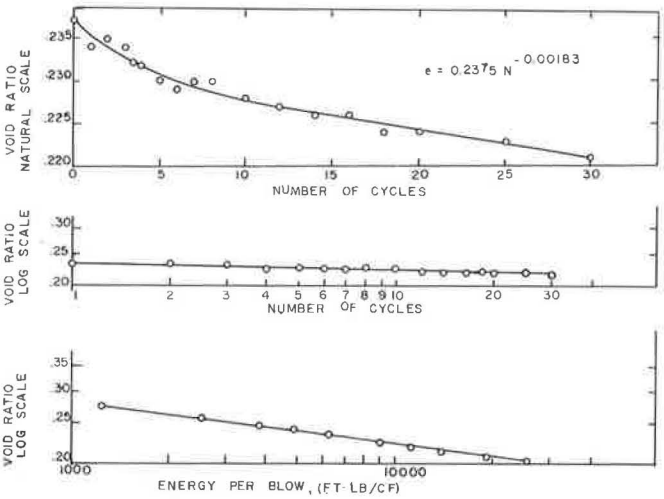

Figure 4. Definition of vibration index and energy index.

Before running the impact test, the optimum moisture content as determined by the AASHO T-180 compaction test was obtained. The amount of soil and its moisture content required to fill the Marshall mold at the maximum dry density was carefully determined. The soil sample was placed in the mold and was compacted applying static pressure until the desired volume corresponding to the maximum dry density was obtained. Then, impact energy was applied to the surface of the specimen, and dial readings were taken to compute the change in void ratio. Finally, soil samples from three different places were taken to check moisture content.

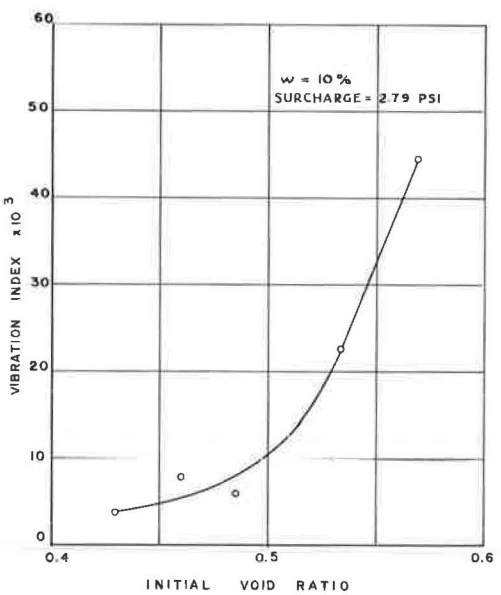

Figure 5. Effect of initial void ratio on vibration index.

Triaxial Test

Ordinary quick triaxial tests were performed on each specimen. The values of the chamber pressures were 0, 15, 30, and 45 psi. The samples were compacted in the Harvard miniature compaction apparatus at the optimum moisture content. The values of cohesion and the friction angle were measured at the same densities as the vibration and impact tests.

Consolidation Test

Samples were tested in a consolidometer at optimum moisture content and for various densities. A range of pressures from 0.25 to 8.0 kg per sq cm were applied. The time allowed to increase the loads depends on the soil type. Values of the compression index for every sample were obtained in this way. Also, the samples were saturated throughout the tests.

DETERMINATIONS

Effect of Initial Void Ratio

To determine the influence of initial void ratio on the vibration index, several

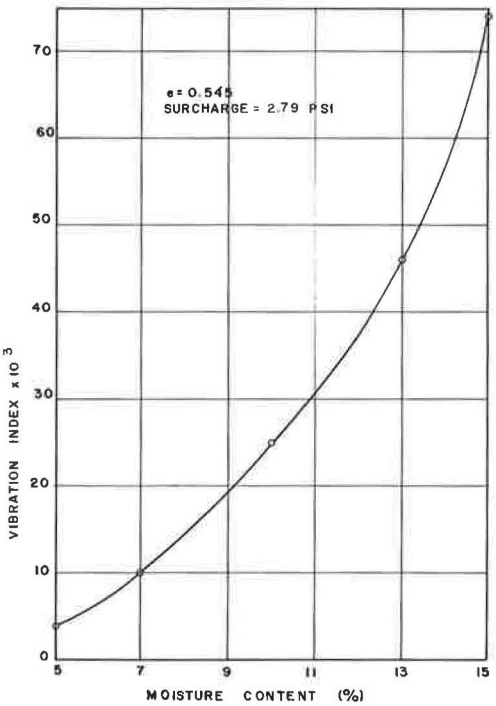

Figure 6. Effect of moisture content on vibration index.

samples of the same soil were tested. The material used was the so-called fine sand with 10 percent moisture content. The change in void ratio was accomplished by compacting the soils with different number of blows. Figure 5 shows the results. It is seen that when the initial void ratio of the soil is high, the corresponding vibration index is also high, which means that in a loose state soils are much more susceptible to volumetric changes under vibration than those soils which are compacted to lower void ratios. This large volumetric change is possible due to a further accommodation of the soil particles which try to fill the great number of voids in the soil. Therefore, the best material to resist volumetric changes under vibration are those which are compacted initially with high densities, that is, with low initial void ratios.

A surcharge of 2.79 psi was used in this test because in sandy soils with less than 7 percent of material finer than 0.074 mm, a large volumetric change was observed. The change in void ratio with higher pressures was appreciably less. From this fact it can be derived that the sandy subgrade soils, in spite of withstanding lighter pressures due to traffic loads, undergo large deformations under vibration, causing the undesirable effects on highways near the bridges.

Effect of Water Content

Several tests were run on the fine sand, changing moisture content from 5 to 15 percent. The void ratio remained constant and equal to 0.545. Also the same surcharge

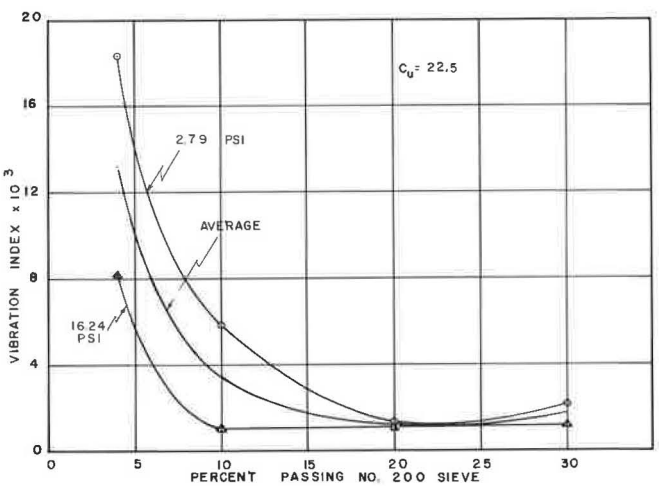

Figure 7. Effect of amount of material passing No. 200 sieve on vibration index.

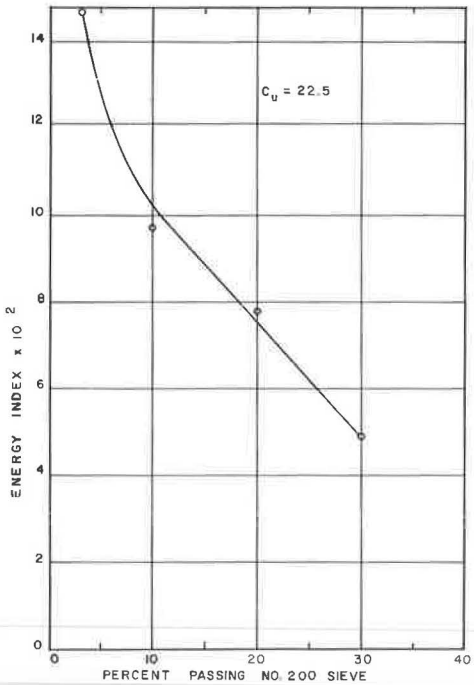

Figure 8. Effect of amount of material passing No. 200 sieve on energy index.

of 2.79 psi was used. Figure 6 shows the effect of water content on the vibration index. It is seen that the increase in water content develops remarkable volumetric changes in the soil. It was also seen that at water contents higher than the optimum for the sample, water appeared on the top and bottom of the sample and consequently developed some pore pressures within the soil and very high vibration indexes.

Effect of Material Finer Than 200 Sieve

To evaluate the influence of the amount of fines in a soil when subjected to vibration, various samples were prepared varying the amount of material less than 0.074 mm from 4 to 30 percent. These mixes were called gradation numbers 1, 2, 3 and 4; the coefficient of uniformity, C_u, was kept constant and equal to 22.5, which means a well-graded soil. It was observed (Fig. 7) that as the percent of minus 200 material increases the vibration index decreases. These facts were observed with all surcharges. An average vibration index was taken as the arithmetic mean of the vibration index for every surcharge at the same soil densities. Above 20 percent the change in vibration index is very small. It seems that there is an optimum amount of minus 0.074-mm material required to reduce these volumetric changes—approximately 20 percent in this case.

Figure 8 shows the relationship found between the energy index and the percent passing 200 sieve. It also shows the decrease in energy index when the percent passing 200 sieve increases.

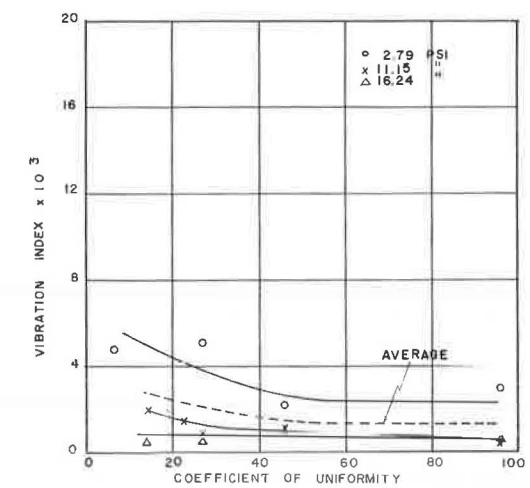

Figure 9. Effect of uniformity coefficient on vibration index.

Effect of Coefficient of Uniformity

To determine the effect of this coefficient another set of samples (gradation numbers 5, 6, 7 and 8) was prepared. In this case the amount of fines used was 20 percent for all gradations. Figure 9 shows the results of this test series. It is seen that at values of the coefficient of uniformity greater than 30 the change in vibration index was almost negligible, but as the coefficient decreases the susceptibility of soil to volumetric changes increases. This effect was more pronounced in the impact test, whose results are shown in Figure 10.

Effect of Plasticity

Atterberg limits were run on the fraction passing No. 40 sieve of each sample. The purpose of these tests was to determine a correlation of such common tests

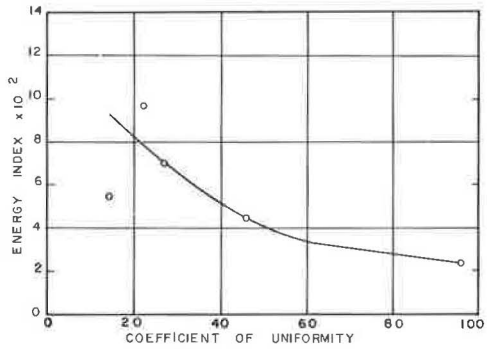

Figure 10. Effect of uniformity coefficient on energy index.

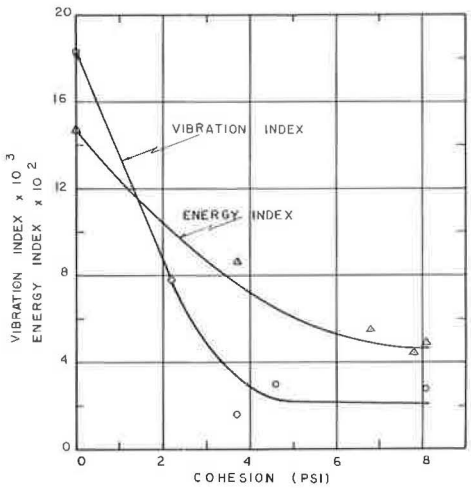

Figure 12. Effect of cohesion on vibration and energy indexes.

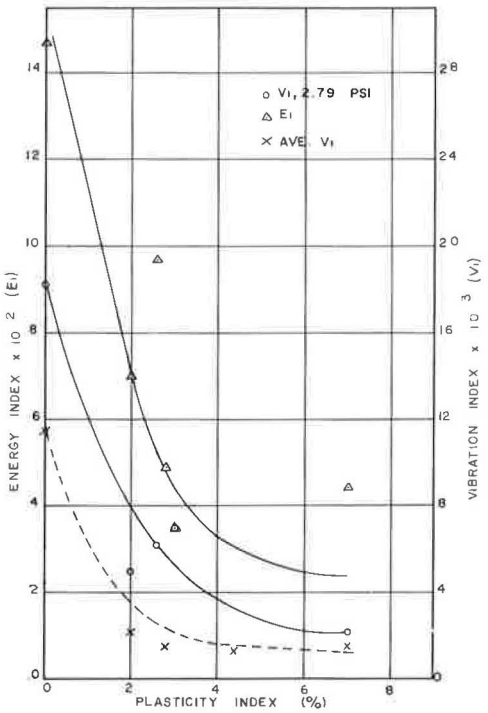

Figure 11. Effect of plasticity index on vibration and energy indexes.

with the vibration index and energy index. The results are shown in Figure 11. For nonplastic soils the indexes were higher than for those soils showing some plasticity. This correlation shows that noncohesive soils deform to a considerably higher degree than cohesive soils when subjected to vibrations.

Effect of Cohesion and Friction Angle

Quick triaxial shear tests were performed on each sample to determine the shearing strength parameters, cohesion and friction angle. Figure 12 shows the results when cohesion is plotted versus vibration index and energy index. It is observed that the more cohesion the soil possesses the lower will be the volumetric change due to dynamic loading. Above 5-psi cohesion, the indexes remained essentially constant. Therefore, soils showing such cohesion values will not undergo large deformations. Figure 13 also shows that soils with lower friction angle (cohesive soils) do not undergo large volumetric changes. The higher values of the indexes corresponding to soils with large friction angles are due mainly to the lack of cohesion in this type of soil and not to this high value of the friction angle.

Effect of Difference in Standard and Modified Maximum Dry Densities

One of the objectives of this study was to correlate the results of common tests performed in soils laboratories to the vibration and energy indexes. An attempt was made to correlate the difference in dry densities of soils as determined by the AASHO T-180 and AASHO T-99 compaction tests to the indexes which measure the susceptibility of soils to volumetric changes under dynamic loading. The relationship is shown in

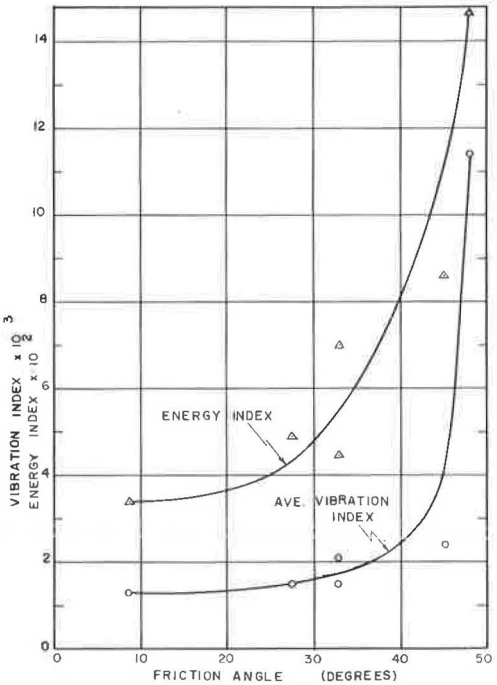

Figure 13. Effect of friction angle on vibration and energy indexes.

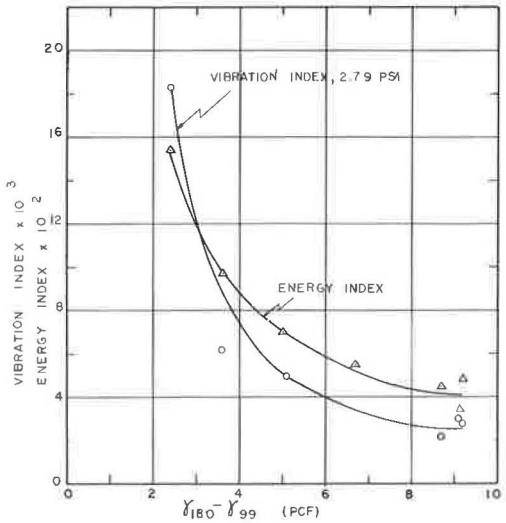

Figure 14. Relationship between difference in dry densities (AASHO T-180 and T-99) and vibration and energy indexes.

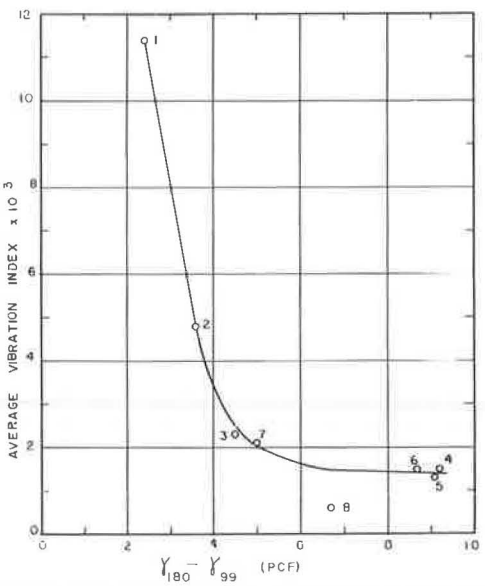

Figure 15. Relationship between difference in dry densities (AASHO T-180 and T-99) and average vibration index.

Figures 14 and 15. These figures show that if the two types of compaction tests are performed on a soil and if the difference in dry densities is determined, this difference will give an indication of the susceptibility of soils to deformation under dynamic loading. When this difference is less than 5 pcf the expected deformation will be large, and if these differences are greater than 5 pcf the deformation will be reduced.

Effect of Compression Index

The values of compression index as determined by consolidation tests are plotted versus vibration index and energy index in Figure 16. As the amount of fines increases the soil has a larger compression index, which is due to the amount of clay particles present, so the soil behaves more and more like a cohesive soil, therefore having a larger compression index. It is observed in this graph again that cohesionless soils with low compression index develop larger volumetric changes.

Figure 17 shows the relationship between the vibration index and the energy index.

Comparison With Field Abutments

Table 1 gives the soil characteristics of six field abutments as determined in

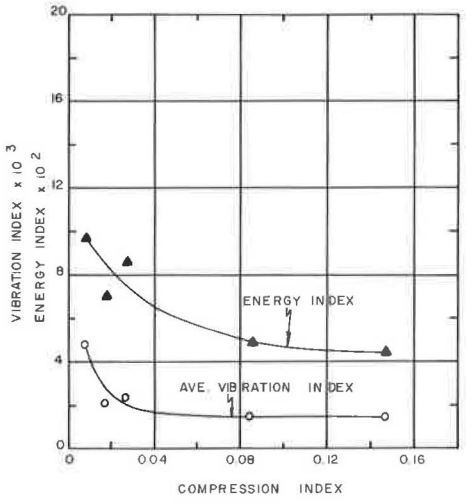

Figure 16. Relationship between compression index and vibration and energy indexes.

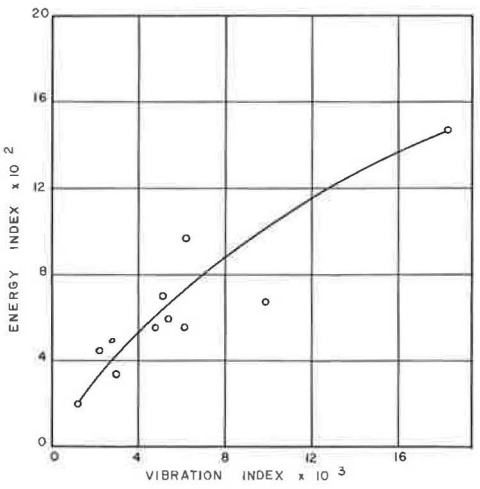

Figure 17. Relationship between vibration index and energy index.

the laboratory. It is seen that cracking has appeared near the abutments with higher indexes (except V_I for No. 3). So it seems that soils with a vibration index greater than 4.8×10^3 will undergo considerable volumetric changes as is actually shown in the field. Also, in soils whose energy index is greater than 5.4×10^2 cracking has occurred.

Concerning the difference in densities, it is seen that differences greater than approximately 5 will develop soils with small volumetric change; abutments No. 2 and No. 3 are within this range. At present these abutments do not show any evidence of failure; also they have a higher percent of material passing 200 sieve than the others which show cracking.

In general the values of cohesion, friction angle and plasticity index show the tendency disclosed from laboratory results regarding these properties.

SUMMARY AND CONCLUSIONS

In the preceding section a comparison was made between the findings obtained in the laboratory and the actual conditions of the field abutments. The behavior of these abutments could be predicted, based on the correlations determined for the different soil properties, without the necessity of performing the more complex tests to determine the susceptibility of soils to volumetric change under dynamic loading. Routine laboratory tests will give this information. It is advisable to run more tests and make correlations to check the tendency shown in this first part of the study. Change in vibration amplitude should be studied also.

TABLE 1

CHARACTERISTICS OF FIELD ABUTMENTS

Abutment No.	$V_I \times 10^3$	$E_I \times 10^2$	γ_{180}	γ_{99}	$\gamma_{180} - \gamma_{99}$	C_u	-200 Sieve	C	ϕ	PI	Field Conditions
1	4.8	5.4	123.7	120.6	3.1	6.4	18	6.7	33.0	4.2	Cracked
2	1.2	2.0	128.0	122.4	5.6	4.3	16	4.2	37.7	2.9	Not cracked
3	5.2	1.3	125.5	120.6	4.9	7.8	15	7.5	36.0	1.6	Not cracked
4	5.4	6.0	127.3	123.2	4.1	4.8	7	4.7	37.6	N. P.	Cracked
5	6.1	5.6	123.7	122.2	1.5	5.0	13	2.3	39.6	N. P.	Cracked
6	9.9	6.8	119.7	115.8	3.9	3.5	3	0.4	39.8	N. P.	Cracked

Considering these results the following conclusions can be made to evaluate soils next to bridge abutments.

1. Soils should be compacted at the highest density possible to achieve the minimum void ratio. A minimum value of 95 to 100 percent AASHO T-180 is suggested.
2. Carefully control the optimum water content for maximum densities and try to keep a low moisture content in the embankment after construction is complete.
3. Use selected soils as backfill with the following properties: (a) 20 to 25 percent of the material should pass through the 200 sieve; (b) high uniform coefficient should be above 40 or 50; and (c) soils whose difference in densities as determined by the AASHO T-180 and AASHO T-99 are small (below 4 pcf) should be avoided.

ACKNOWLEDGMENTS

This study was sponsored by the New Mexico State Highway Department in cooperation with the U. S. Bureau of Public Roads and was conducted by the Engineering Experiment Station at New Mexico State University.

The authors wish to thank Charles Behounek, Don Bell, and Rudolph Orosco for helping in laboratory work.

REFERENCES

1. Van der Poel, C. Dynamic Testing of Road Constructions, Jour. Appl. Chem., Vol. 1, No. 7, pp. 281-290, July 1954.
2. Sowers, G. F., and Vesic, A. B. Vertical Stresses in Subgrades Beneath Statically Loaded Flexible Pavements. HRB Bull. 342, pp. 90-123, 1962.
3. Nielson, F. D. Soil Vibration Study, Impact Tests, Progress Report, Phase I. Engineering Experiment Station, New Mexico State Univ., Feb. 1966.
4. Linger, D. A. Effect of Vibration on Soil Properties, Progress Report. Engineering Experiment Station, New Mexico State Univ., July 1961.
5. Barkan, D. D. Dynamics of Bases and Foundations. McGraw-Hill Book Company, 1962.

Appendix

FIELD DATA OF HIGHWAY ABUTMENTS
(Obtained from District No. 1 of New Mexico State Highway Department)

Interstate Highway 25 Between Ft. Selden and Hatch

Abut. No. 1, No. 2, & No. 3	—ADT 1965 = 2232
	—ADT 1975 = 4704
Abut. No. 4 & No. 5	—ADT 1958 = 1345
	—ADT 1975 = 4732
Abut. No. 6[1]	—ADT 1958 = 1345
	—ADT 1975 = 4732

Section from Ft. Selden to Hatch Interchange was opened to traffic about June 10, 1965.

Abut. No. 1—Station 1212+59

Subgrade

Maximum Dry Density:	128.1 pcf
Range of Compaction:	97-108%
Range of Moisture:	10.0-13.0%

[1]Authors' Note: ADT values given are believed to be traffic going under the overpass at Abutment No. 6. Actual ADT values are believed to be much lower.

6-In. Cement-Treated Base Course

Maximum Dry Density: 136.2 pcf
Compaction: 104%
Moisture: 6.5%
Gradation:

Sieve	1 In.	¾ In.	No. 4	No. 10	No. 200
% Pass	100	99	63	54	10

4-In. Untreated Base Course

Maximum Dry Density: 129.2 pcf
Compaction: 100%
Moisture: 4.6%
Gradation:

Sieve	1 In.	¾ In.	No. 4	No. 10	No. 200
% Pass	100	94	55	43	9

2½-In. Asphalt Binder Course

Lab Density: 2.199 = 137.2 pcf
Compaction: 101%
Gradation:

Sieve	1 In.	¾ In.	½ In.	⅜ In.	No. 4	No. 10	No. 40	No. 80	No. 200
% Pass	100	93	74	60	46	36	23	11	5

1½-In. Asphalt Surface Course

Lab Density: 2.403 = 149.9 pcf
Compaction: 97%
Gradation:

Sieve	¾ In.	½ In.	⅜ In.	No. 4	No. 10	No. 40	No. 80	No. 200
% Pass	100	87	74	54	40	25	10	4

Abut. No. 2—Station 1348+00

Subgrade

Maximum Dry Density: 129.8 pcf
Range of Compaction: 90% to 97%
Range of Moisture: 8.3% to 11.5%

No. 4 Subbase

Maximum Dry Density: 144.3 pcf
Compaction: 100%
Moisture: 2.4%
Gradation:

Sieve	2 In.	1 In.	No. 4	No. 10	No. 200	LL	PI
% Pass	100	100	49	37	11	Sandy	UP

4-In. Asphalt-Treated Base Course

Lab Density: 2.384 = 148.8 pcf
Compaction: 98%
Gradation:

Sieve	1 In.	¾ In.	No. 4	No. 10	No. 200
% Pass	100	100	51	39	7

2½-In. Asphalt Concrete Binder Course

Lab Density: 2.409 = 150.3 pcf
Compaction: 97%
Gradation:

Sieve	1 In.	¾ In.	½ In.	⅜ In.	No. 4	No. 10	No. 40	No. 80	No. 200
% Pass	100	97	76	62	44	33	23	11	6

1½-In. Asphalt Concrete Surface Course

Lab Density: 2.391 = 149.2
Compaction: 100%
Gradation:

Sieve	¾ In.	½ In.	⅜ In.	No. 4	No. 10	No. 40	No. 80	No. 200
% Pass	100	87	72	53	40	25	11	6

Abut. No. 3—Station 1518+00

Subgrade

Maximum Dry Density: 125.5 pcf
Range of Compaction: 90% to 97%
Range of Moisture: 9.2% to 15.3%

4-In. Subbase

Maximum Dry Density: 144.2 pcf
Compaction: 105%
Moisture: 1.9%
Gradation:

Sieve	2 In.	1 In.	No. 4	No. 10	No. 200	LL	PI
% Pass	100	100	48	35	9	Sandy	NP

4-In. Asphalt-Treated Base Course

Lab Density: 2.333 = 145.6 pcf
Compaction: 97%
Gradation:

Sieve	1 In.	¾ In.	No. 4	No. 10	No. 200
% Pass	100	95	54	45	6

2½-In. Asphalt Concrete Binder Course

Lab Density: 2.431 = 151.7 pcf
Compaction: 96%
Gradation:

Sieve	1 In.	¾ In.	½ In.	⅜ In.	No. 4	No. 10	No. 40	No. 80	No. 200
% Pass	100	95	80	67	44	38	23	11	5

1½-In. Asphalt Concrete Surface Course

Lab Density: 2.392 = 149.3 pcf
Compaction: 98%
Gradation:

Sieve	¾ In.	½ In.	⅜ In.	No. 4	No. 10	No. 40	No. 80	No. 200
% Pass	100	91	77	57	43	27	12	5

Abut. No. 4—Station 184+27

Subgrade

Maximum Dry Density: 129.3 pcf
Range of Compaction: 90% to 104%
Range of Moisture: 5.1% to 10.0%

4-In. Subbase

Maximum Dry Density: 144.2 pcf
Compaction: 103%
Moisture: 3.3%
Gradation:

Sieve	2 In.	1 In.	No. 4	No. 10	No. 200	LL	PI
% Pass	100	100	53	40	10	Sandy	NP

4-In. Asphalt-Treated Base Course

Lab Density: 2.344 = 146.3 pcf
Compaction: 97%
Gradation:

Sieve	1 In.	¾ In.	No. 4	No. 10	No. 200
% Pass	100	96	52	38	6

2½-In. Asphalt Concrete Binder Course

Lab Density: 2.410 = 150.4 pcf
Compaction: 97%
Gradation:

Sieve	1 In.	¾ In.	½ In.	⅜ In.	No. 4	No. 10	No. 40	No. 80	No. 200
% Pass	100	95	77	63	43	32	18	8	4

1½-In. Asphalt Concrete Surface Course

Lab Density: 2.405 = 150.1 pcf
Compaction: 97%
Gradation:

Sieve	¾ In.	½ In.	⅜ In.	No. 4	No. 10	No. 40	No. 80	No. 200
% Pass	100	89	76	54	40	25	13	7

Abut. No. 5—Station 202+00

Subgrade

Maximum Dry Density: 130.1 pcf
Range of Compaction: 90% to 100%
Range of Moisture: 5.2% to 10.3%

4-In. Subbase

Maximum Dry Density: 144.2 pcf
Compaction: 99%
Moisture: 2.6%
Gradation:

Sieve	2 In.	1 In.	No. 4	No. 10	No. 200	LL	PI
% Pass	100	100	37	27	7	Sandy	NP

4-In. Asphalt-Treated Base Course

Lab Density: 2.376 = 148.3 pcf
Compaction: 99%
Gradation:

Sieve	1 In.	¾ In.	No. 4	No. 10	No. 200
% Pass	100	92	50	38	6

2½-In. Asphalt Concrete Binder Course

Lab Density: 2.432 = 151.8 pcf
Compaction: 96%
Gradation:

Sieve	1 In.	¾ In.	½ In.	⅜ In.	No. 4	No. 10	No. 40	No. 80	No. 200
% Pass	100	97	79	67	48	36	21	10	5

1½-In. Asphalt Concrete Surface Course

Lab Density: 2.401 = 149.8 pcf
Compaction: 98%
Gradation:

Sieve	¾ In.	½ In.	⅜ In.	No. 4	No. 10	No. 40	No. 80	No. 200
% Pass	100	86	73	55	41	26	12	6

Abut. No. 6—Station 503+50

Subgrade

Maximum Dry Density: 134.5 pcf
Range of Compaction: 91% to 96%
Range of Moisture: 4.2% to 10.8%

4-In. Subbase

Maximum Dry Density: 140.2 pcf
Compaction: 99%
Moisture: 6.0%
Gradation:

Sieve	2 In.	1 In.	No. 4	No. 10	No. 200	LL	PI
% Pass	100	98	44	34	7	Sandy	NP

4-In. Asphalt-Treated Base Course

Lab Density: 2.273 = 141.8 pcf
Compaction: 98%
Gradation:

Sieve	1 In.	¾ In.	No. 4	No. 10	No. 200
% Pass	100	93	44	33	5

2½-In. Asphalt Concrete Binder Course

Lab Density: 2.338 = 145.9 pcf
Compaction: 98%
Gradation:

Sieve	1 In.	¾ In.	½ In.	⅜ In.	No. 4	No. 10	No. 40	No. 80	No. 200
% Pass	100	98	72	62	48	35	21	12	7

1½-In. Asphalt Concrete Surface Course

Lab Density: 2.336 = 145.8 pcf
Compaction: 99%
Gradation:

Sieve	¾ In.	½ In.	⅜ In.	No. 4	No. 10	No. 40	No. 80	No. 200
% Pass	100	88	74	56	41	24	14	5

Design Charts for Coefficients of Active Earth Pressure of Cohesionless Soils— A Rapid Method

FRED C. BENSON, EIT, Production Department, Humble Oil and Refining Company, New Orleans, La.

•THE Coulomb theory of active earth pressures of cohesionless soils against retaining walls is widely used in engineering practice. The Culmann graphical method is based on Coulomb's theory and is often employed to find the active earth pressure when values of angle of internal friction of the soil ϕ, angle of the wall face to the vertical α, angle of the embankment slope with the horizontal ω and the angle of wall friction δ, are either known, estimated, or substituted on a trial basis (3, p. 154). The Culmann method for finding active earth pressure can be a very time-consuming process when a number of trial solutions need be made in order to arrive at an optimum or desirable set of the variables ϕ, α, ω, and δ. The Culmann method also has the disadvantage that it does not show the relations that exist between these variables and the values of active earth pressure.

A more useful design tool would be a set of information that shows the relationship between active earth pressure and the variables ϕ, α, ω, and δ, and gives ranges of values for them that would cover situations that arise in the field. Such a set of information would be a series of design charts from which active earth pressure could be obtained for any combination of the variables.

PURPOSE

The purpose of this report was to develop a set of design curves for computing active earth pressures of cohesionless soils against retaining walls based on Coulomb's theory. The curves were to be of such a nature as to: (a) allow the designer to see the relationships between active earth pressure and the variables ϕ, α, ω, and δ, as some variables were held constant while others were allowed to vary; (b) allow the designer to arrive quickly at values of active earth pressure for a determined combination of variables; (c) encompass a wide range of possible values for each variable to allow the designer wide latitude; and (d) readily lend themselves to interpolation on the part of the designer.

THEORETICAL CONSIDERATIONS AND ASSUMPTIONS

The Coulomb theory of active earth pressures of cohesionless soils is based on important assumptions and considerations. These must always be recognized and taken into account in any design problem.

One important assumption made by Coulomb was that the surface of failure for a backfill of cohesionless soil was a plane surface, or in a two-dimensional drawing, a straight line, which extended from the toe of the wall to intercept the backfill surface or the embankment slope. The actual failure surface has some curvature near the toe, but Coulomb ignored the curvature. According to Terzaghi and Peck, the error resulting from neglecting the curvatures is very small (3, p. 153).

Other important assumptions were made by Coulomb concerning the relative movement between the retaining wall and the soil mass required for the active earth pressure

Paper sponsored by Committee on Mechanics of Earth Masses and Layered Systems.

conditions to exist. Coulomb actually defines two states in which active pressures may exist (3, pp. 151, 152): (a) the state where the angle of wall friction, δ, is considered positive, and (b) the state where δ is considered negative. This report is concerned solely with the situation where δ can be considered positive.

For the active case where δ is considered positive to hold, the soil mass must move downward with respect to the wall. According to Terzaghi and Peck (3, p. 151), "The downward movement of the sand with reference to the wall develops frictional forces that cause the resultant active earth pressure to be inclined at an angle δ to the normal to the wall. This angle is known as the angle of wall friction."

PROCEDURE

Coulomb's equation for active earth pressure and use of the IBM 7094 computer made possible collection of the data required to develop the design curves. Coulomb's

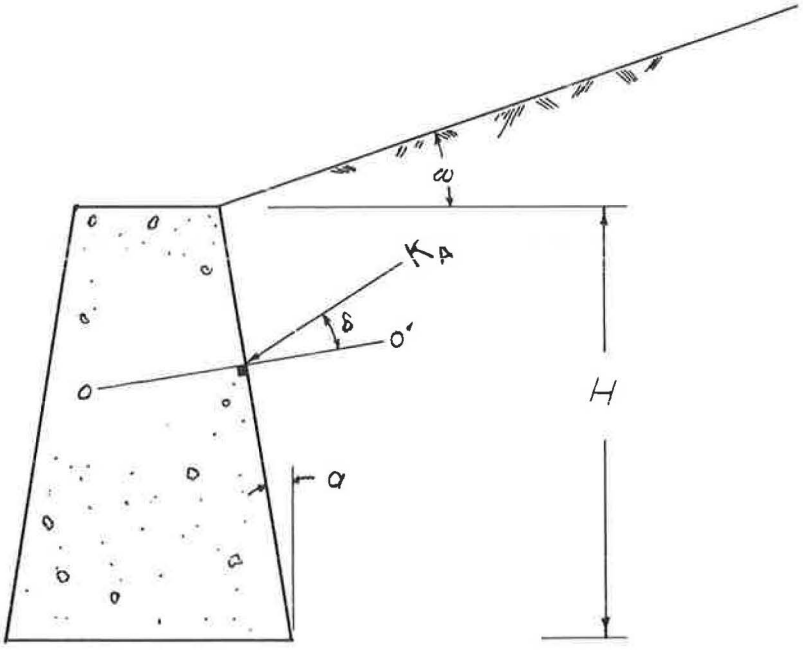

All dimensions and variables represent positive values.

K_A is the coefficient of active earth pressure P_A.

ω is the angle the embankment slope makes with the horizontal.

α is the angle between the wall face and a vertical to the wall toe.

δ is the angle of wall friction or the angle between the reaction of active earth pressure P_A, and a normal to the wall, line segment 0-0'.

ϕ is the angle of internal friction of the soil.

H is the depth of the backfill, in ft, measured at the wall.

γ is the unit weight of the soil in pcf.

Figure 1.

equation for active earth pressure with positive wall friction (δ considered positive) is as follows (2, p. 496):

$$P_A = \tfrac{1}{2}\gamma H^2 \left(\frac{\cos^2(\phi - \alpha)}{\cos^2\alpha \cos(\alpha + \delta)\left[1.0 + \sqrt{\frac{\sin(\phi + \delta)\sin(\phi - \omega)}{\cos(\alpha + \delta)\cos(\alpha - \omega)}}\right]^2} \right)$$

The expression within the parentheses is designated K_A, the coefficient of active earth pressure, and the following relations may be obtained:

$$P_A = \tfrac{1}{2}\gamma H^2 K_A,$$

where

$$K_A = \left(\frac{\cos^2(\phi - \alpha)}{\cos^2\alpha \cos(\alpha + \delta)\left[1.0 + \sqrt{\frac{\sin(\phi + \delta)\sin(\phi - \omega)}{\cos(\alpha + \delta)\cos(\alpha - \omega)}}\right]^2} \right)$$

Figure 1 shows the significance of the variables and explains what each variable represents.

Values of K_A for many combinations of the variables ϕ, α, ω, and δ were obtained. In the several computer programs that were used, the variable ω was allowed to range from 0 to 25°, α was assigned values from 0° to a magnitude of 2ω, ϕ ranged from 15 to 40°, and δ was assigned values ranging from 0° to ϕ. It was believed that these ranges give the designer wide freedom of choice.

Several methods of presenting the relationships between values of K_A and the several variables were investigated. It was decided that a good method of presenting these relationships would be a series of graphs that would give the horizontal and vertical components, K_H and K_V, of the coefficient of active earth pressure, K_A, for various combinations of the variables ϕ, α, ω, and δ. The expression of K_A in terms of the components K_H and K_V would readily enable estimation of expected overturning forces and vertical forces to be encountered.

In several instances checks were made on values of K_A obtained from the computer programs by means of the Culmann graphical method. The checks were necessary to ensure that the Coulomb equation was being used correctly in the computer programs.

RESULTS

The design charts (Figs. 2-34, Appendix) represent the results of the efforts to provide the designer with a means whereby he may determine rapidly the active earth pressure for a combination of the variables ϕ, α, ω, and δ. These charts give the designer flexibility in his choice of a combination of variables and allow him to see the relationships that exist between the variables and the values of active earth pressure. They also allow him the opportunity for interpolation when necessary.

Each chart represents a situation where ϕ and ω are held constant. Values for α and δ are allowed to vary through a substantial range. The designer determines the horizontal and vertical components of K_A directly from the chart for an appropriate combination of ϕ, α, ω, and δ. With K_H or K_V known, the designer can easily determine K_A and P_A.

Example

Required:

Determine the active earth pressure P_A and the horizontal and vertical components of P_A.

Given:

$H = 30$ ft.
$\gamma = 110$ lb per cubic ft
$\omega = 15°$
$\phi = 35°$
$\alpha = 15°$
$\delta = 0°$

Solution:

1. From the design chart, $K_H = 0.450$ and $K_V = 0.121$.
2. The horizontal component of $P_A = K_H \frac{1}{2} \gamma H^2 = (0.450) \frac{1}{2} (110) (30)^2 =$ 22,300 lb/lineal ft of wall length.
3. The vertical component of $P_A = K_V \frac{1}{2} \gamma H^2 = (0.121) \frac{1}{2} (110) (30)^2 = 5,990$ lb/lineal ft of wall length.
4. The total active earth pressure, P_A, can be found from either component. From the horizontal component, $P_A = \frac{22,300}{\cos (\alpha + \delta)} = \frac{22,300}{\cos (15°)} = 23,100$ lb/lineal ft of wall length.

DISCUSSION OF OBSERVED PHENOMENA

During the course of the reduction and presentation of the data, several interesting and important situations were observed.

Cases Where ϕ Is Less Than or Equal to ω

In cases where the Culmann graphical method was used to check values of K_A for values of ϕ less than ω, it was not possible to get a solution. The Coulomb equation was not applicable for values of ϕ less than ω.

The physical interpretation for this failure to produce a solution on the part of both the Culmann method and the Coulomb equation is that a cohesionless soil cannot stand on a slope greater than its angle of internal friction. In reality, a cohesionless soil will not stand on a slope greater than its angle of repose, where the angle of repose represents the minimum angle of internal friction or the ϕ of the soil in its loosest state.

For instances in which ϕ is equal to ω the Culmann method does not appear to provide a solution. It is possible that the Culmann method would approach a solution for K_A as trial failure wedges approached infinitely large areas. The Coulomb equation appears to provide valid values when ϕ equals ω, although it is not probable that cohesionless soil would stand long on a slope equal to its angle of internal friction.

Cases Where Wall Friction Is Not Desirable

Although curves giving values of K_A instead of K_H and K_V are not presented in the design charts, these curves were plotted on a trial basis, and they revealed many instances where an increase in wall friction angle δ increased the coefficient of active earth pressure rather than decreasing it. The belief held by many is that an increase in the wall friction will always serve to reduce the value of K_A. Terzaghi and Peck, in discussing Rankine's theory of active earth pressure of cohesionless soils against smooth retaining walls, imply that any friction that is generated by wall roughness works in the designer's favor. These authors state that "It is shown subsequently that the roughness of the back of a wall commonly reduces the active and increases the passive earth pressure." (3, p. 144)

A case of K_A increasing as δ increases is illustrated in the design chart where $\phi = 35°$, $\omega = 15°$, and α is assigned the value of 15°. The value of K_A for $\delta = 0°$ is found to be 0.466, whereas the value of K_A for $\delta = 35°$ is found to be 0.505.

Situation Where the Active Case Ceases To Exist

In the design chart where $\omega = 25°$, $\phi = 40°$, $\delta = 40°$ when α was given a value of 2ω or 50°, the resultant coefficient of active earth pressure, K_A, was found to have a

vertical line of action. Therefore, K_A had no horizontal component, K_H, and it may be concluded that a state of active earth pressure does not exist. The Coulomb equation is not applicable for this combination of the variables, and will not apply in any situation where the sum of the angles α and δ equals 90°. When this occurred, no points were plotted on the design chart.

CONCLUSIONS

The design charts developed in this report are applicable to the design of retaining walls that must resist active earth pressures of cohesionless soils for cases where the angle of wall friction δ will be positive. The assumptions and limitations of the Coulomb theory must always be considered when use is made of the charts.

The major assumptions made by Coulomb were that the surface of failure for a backfill of cohesionless soil was a plane surface, and that the effect of curvature of the actual failure surface could be neglected. The relative movement between the retaining wall and the soil mass must bring about a state of active earth pressure for which the wall friction angle δ is positive. The major limitations include cases where the Coulomb equation and the Culmann graphical method fail to give solutions for K_A. A cohesionless soil cannot stand on slopes greater than its angle of repose. When the line of action of K_A is vertical so there is no horizontal component K_H, the active earth pressure case does not exist.

When used with a full understanding of the Coulomb theory and the limitations to the theory, the design charts offer a means to quickly and accurately calculate earth pressures against retaining walls. They allow the designer to see the relationships between the components K_H and K_V and the variables ϕ, α, ω, and δ, and interpolation is possible.

ACKNOWLEDGMENT

This paper is based on a report submitted in partial fulfillment of the requirements for the degree of Master of Engineering in the College of Engineering of Texas A&M University. Credit is given to Dr. Wayne A. Dunlap and to Professor Bob M. Gallaway for their assistance.

REFERENCES

1. Hansen, Jorgen Brinch. Earth Pressure Calculation. The Danish Technical Press, Copenhagen, 1953.
2. Taylor, Donald W. Fundamentals of Soil Mechanics. John Wiley and Sons, New York, 1948.
3. Terzaghi, Karl, and Peck, Ralph B. Soil Mechanics in Engineering Practice. John Wiley and Sons, New York, 1948.

Appendix

DESIGN CHARTS

The design charts (Figs. 2-34) are presented on the following pages.

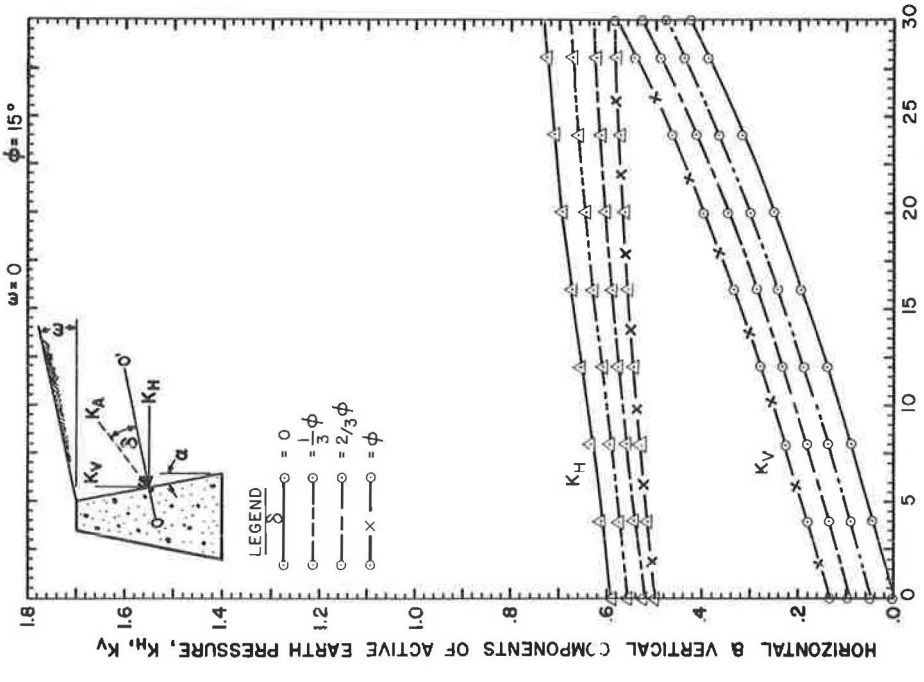

Figure 2.

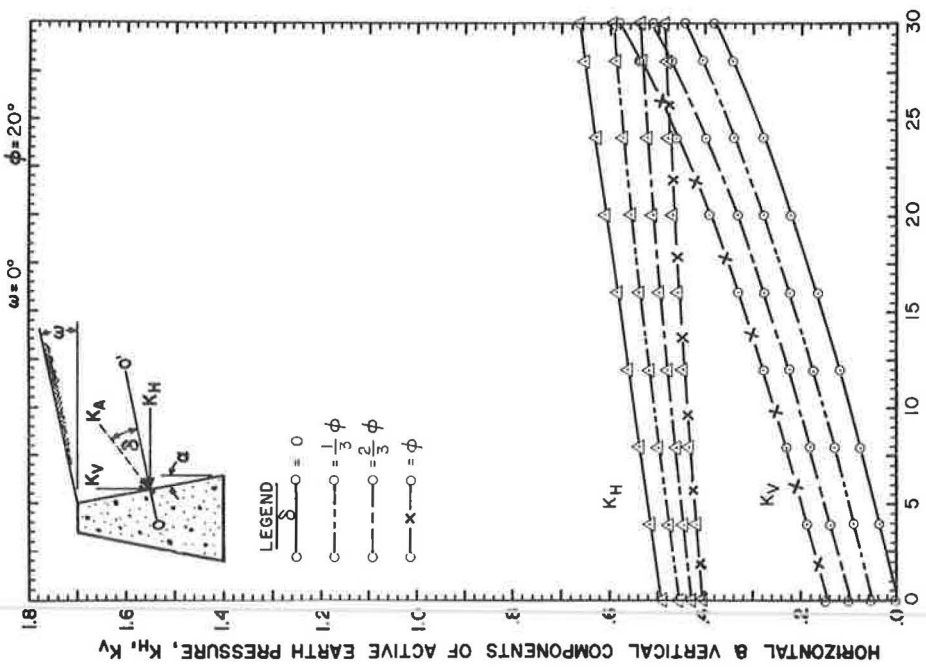

Figure 3.

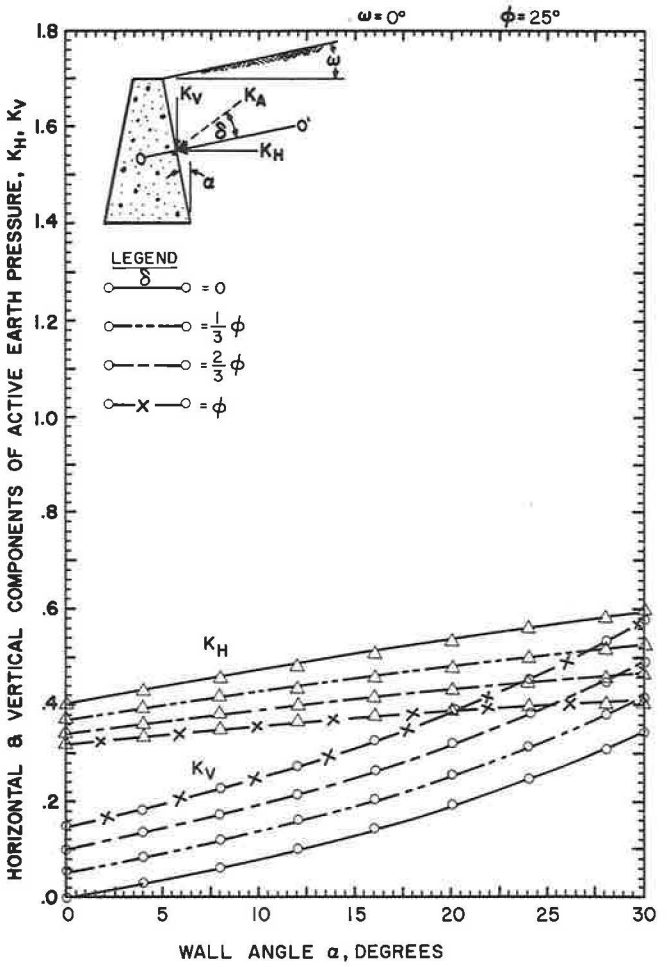

Figure 4.

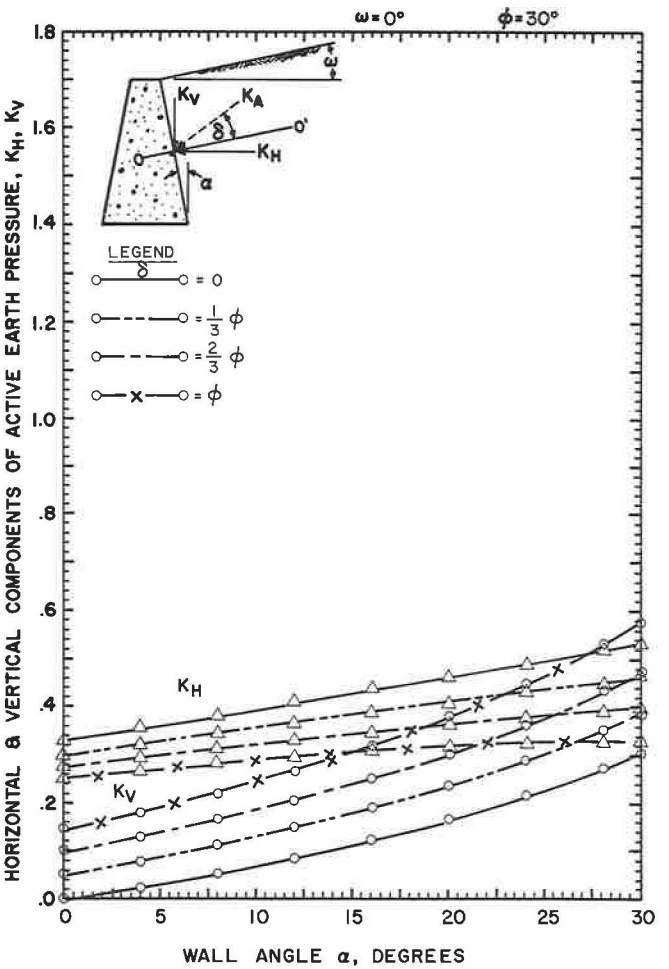

Figure 5.

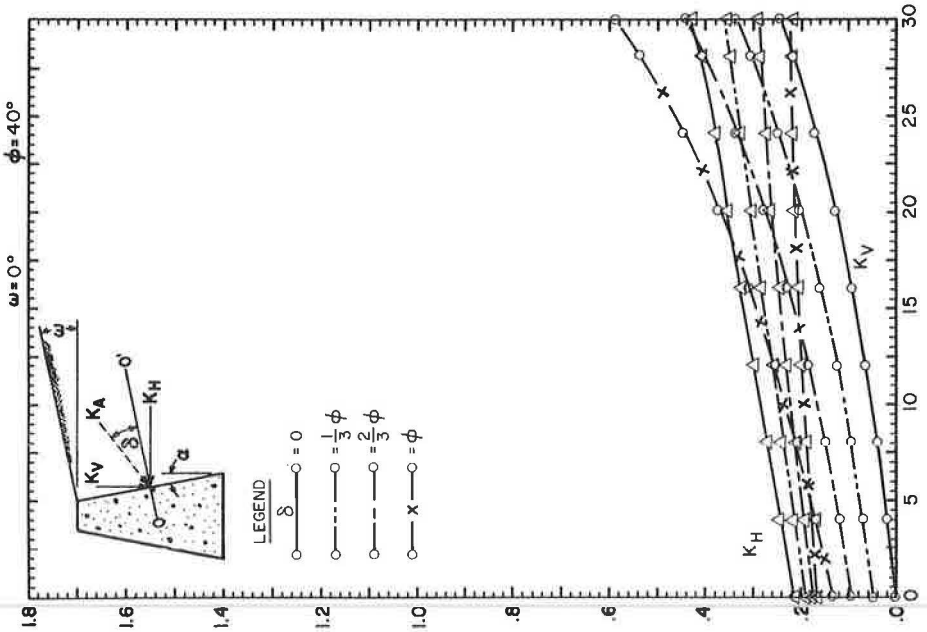

Figure 7.

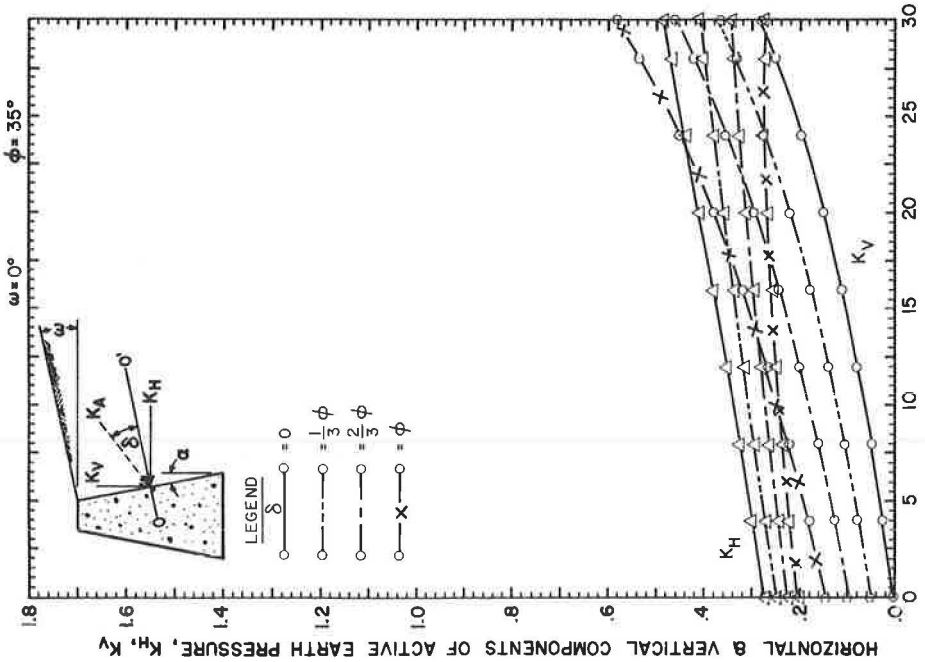

Figure 6.

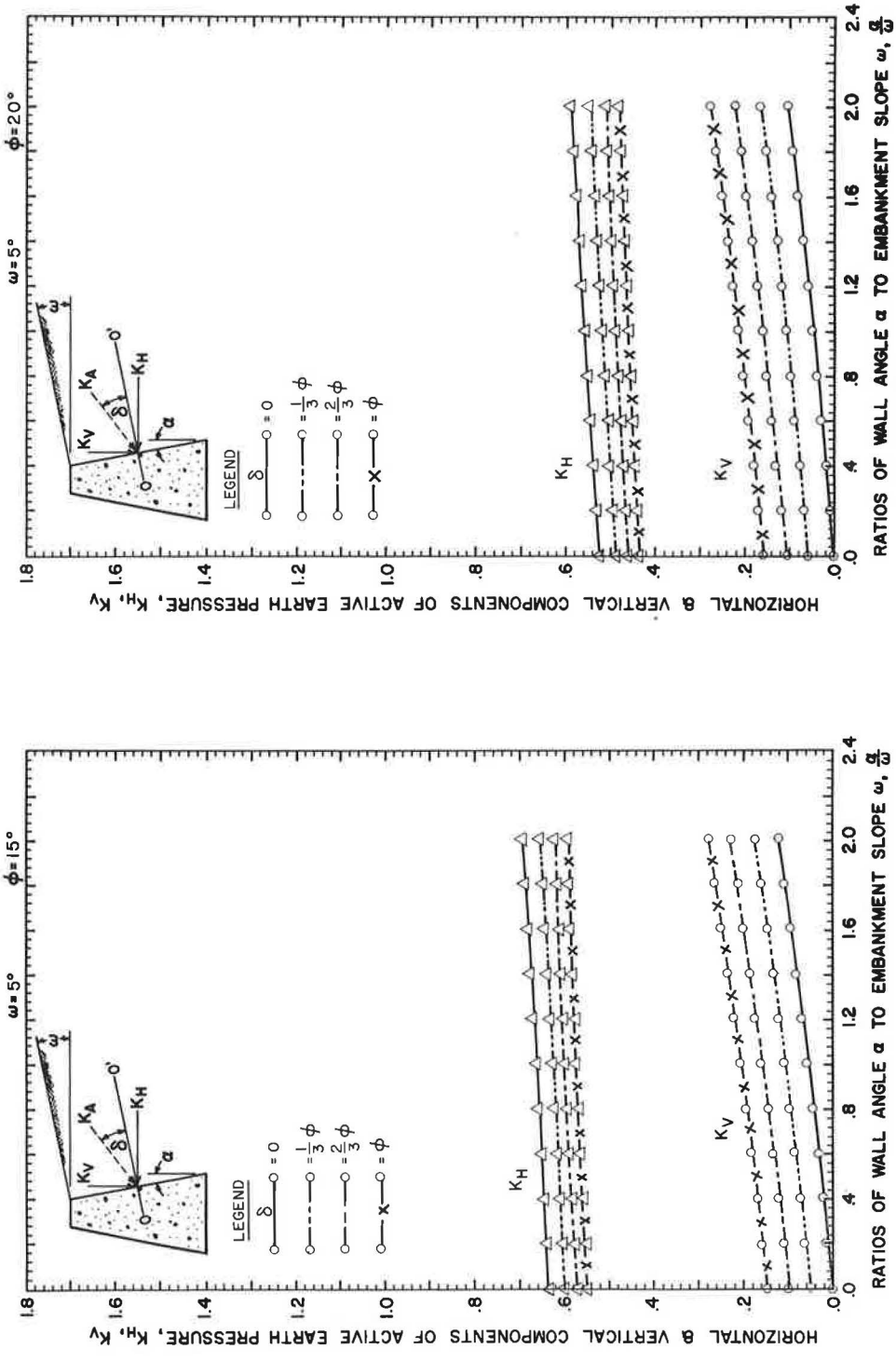

Figure 8.

Figure 9.

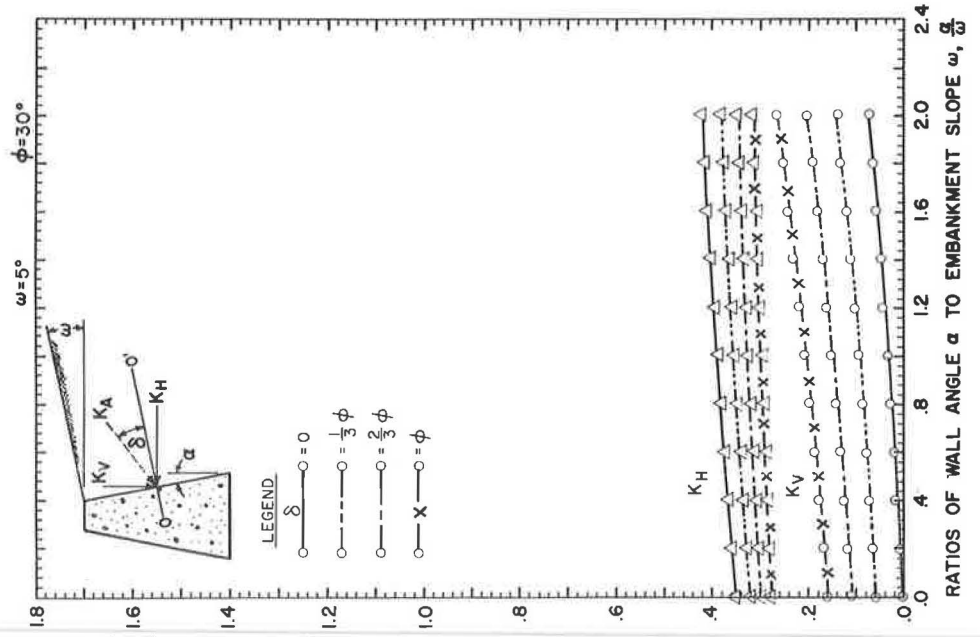

Figure 11.

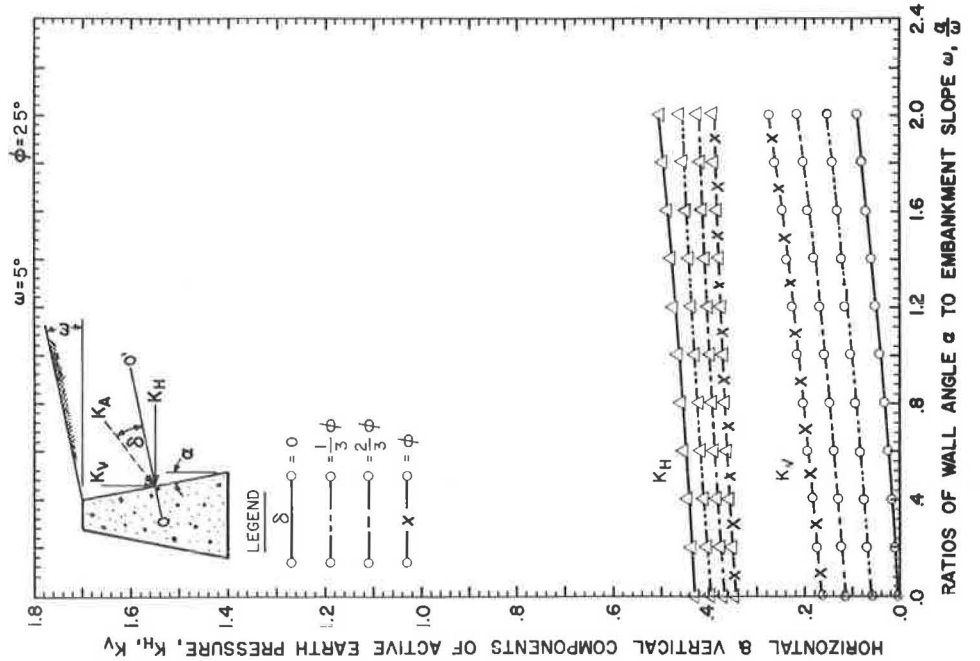

Figure 10.

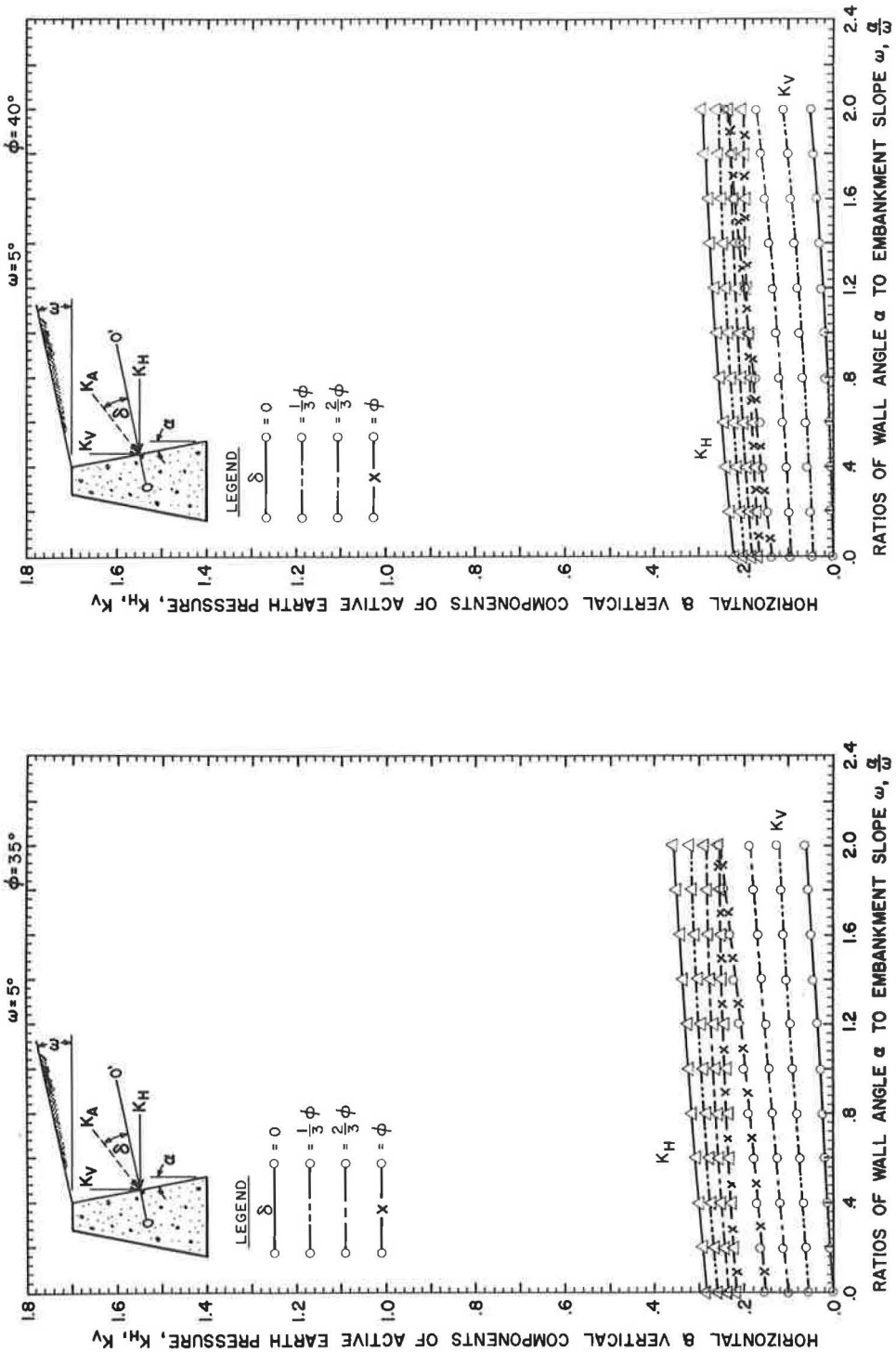

Figure 12.

Figure 13.

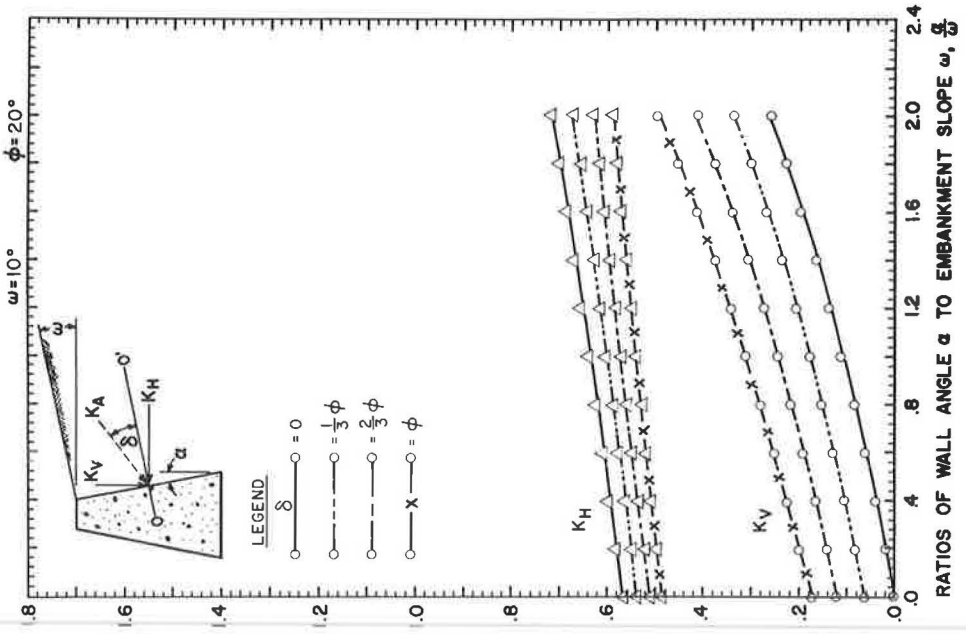

Figure 14.

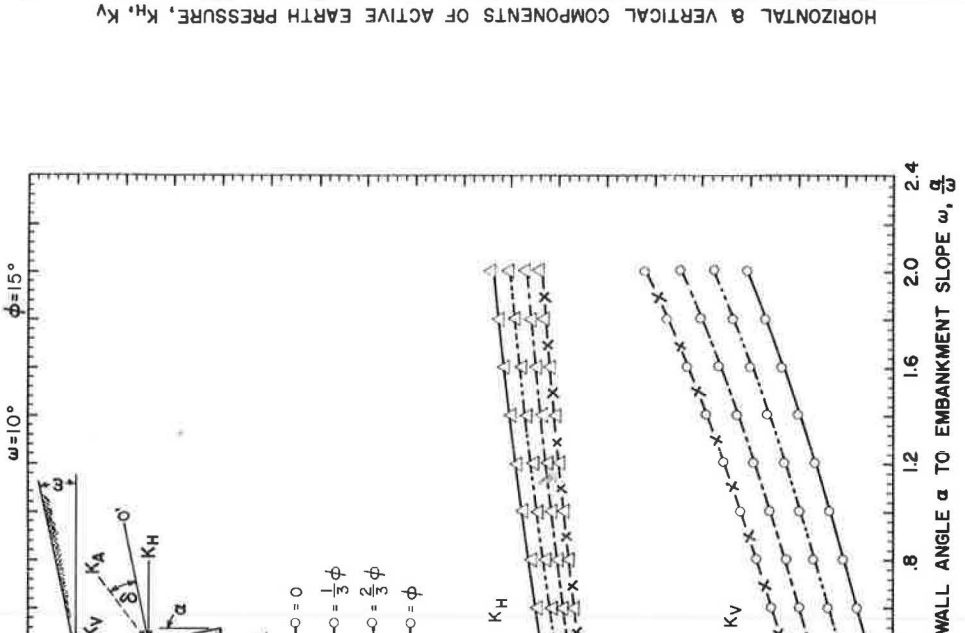

Figure 15.

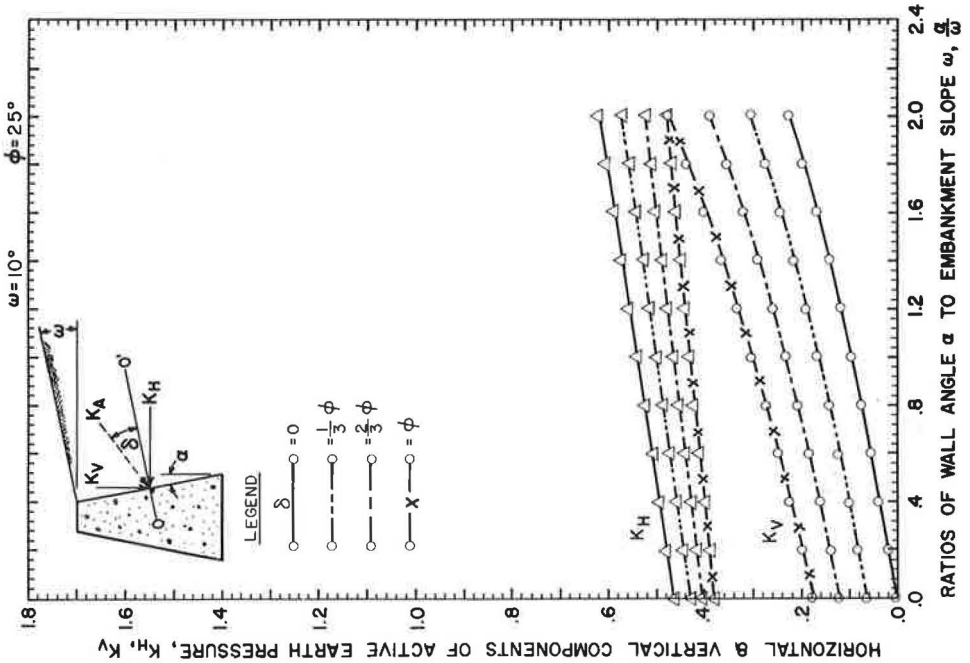

Figure 16.

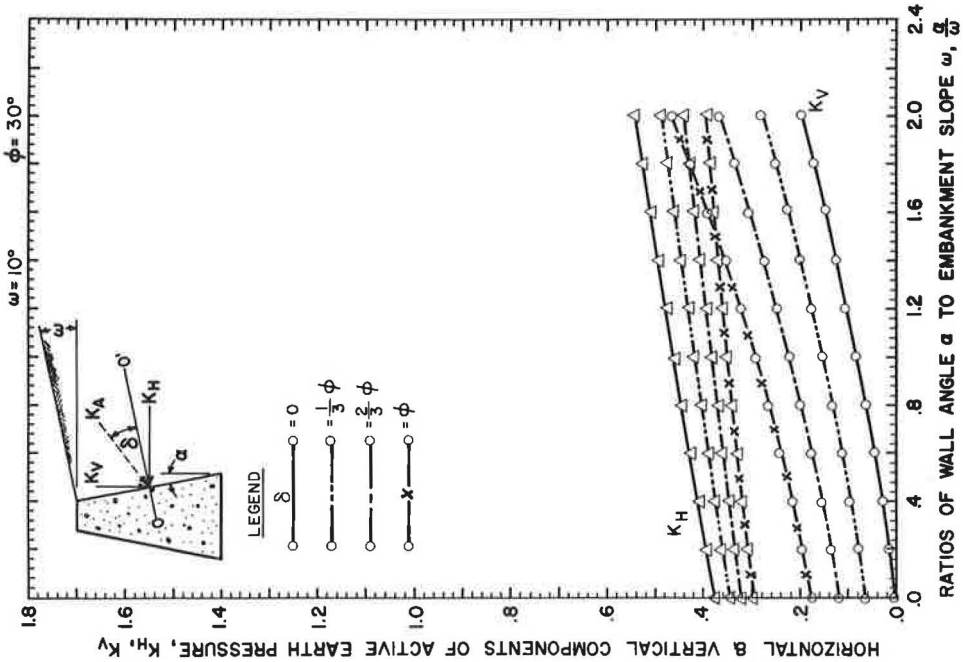

Figure 17.

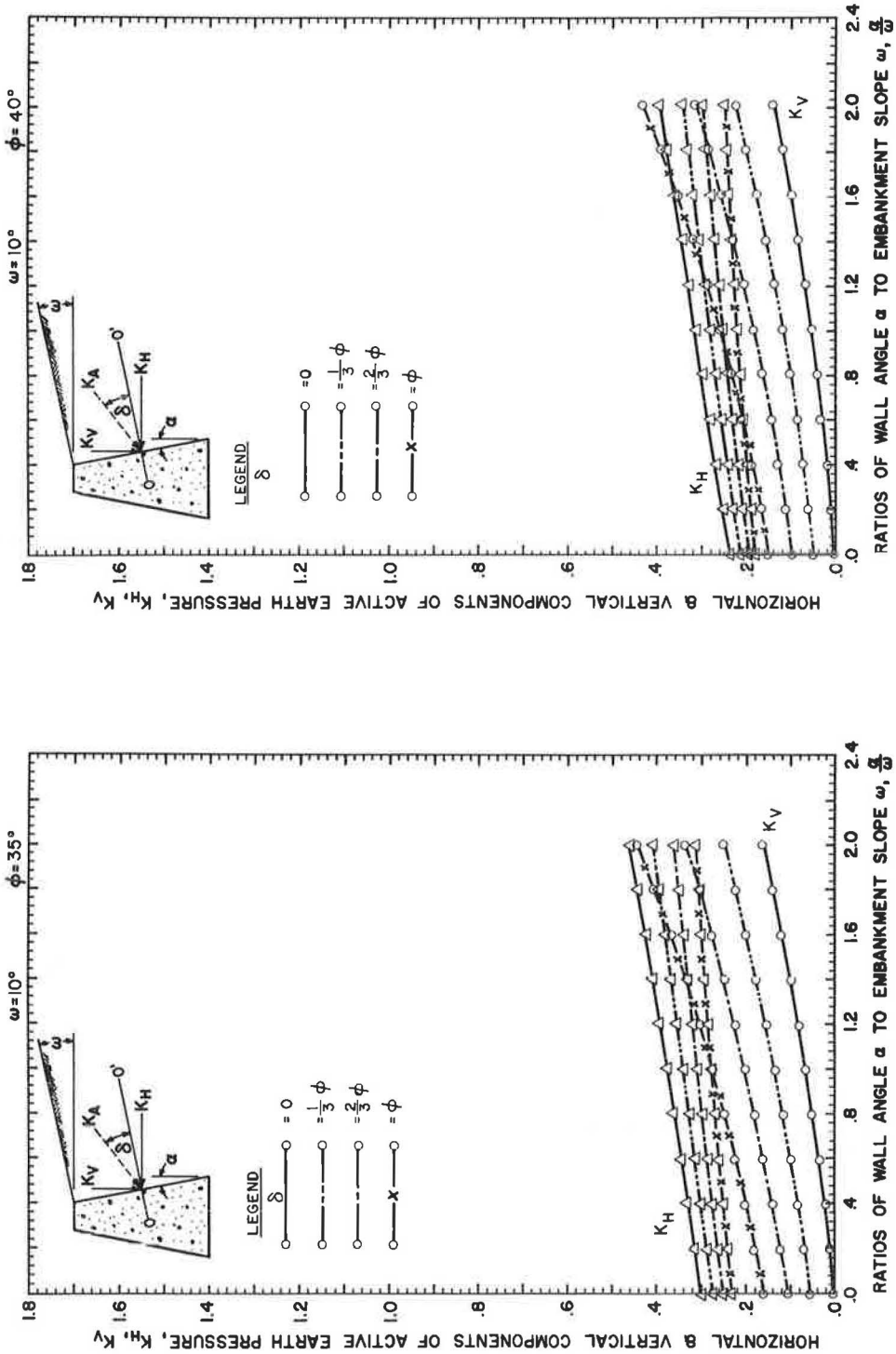

Figure 18.

Figure 19.

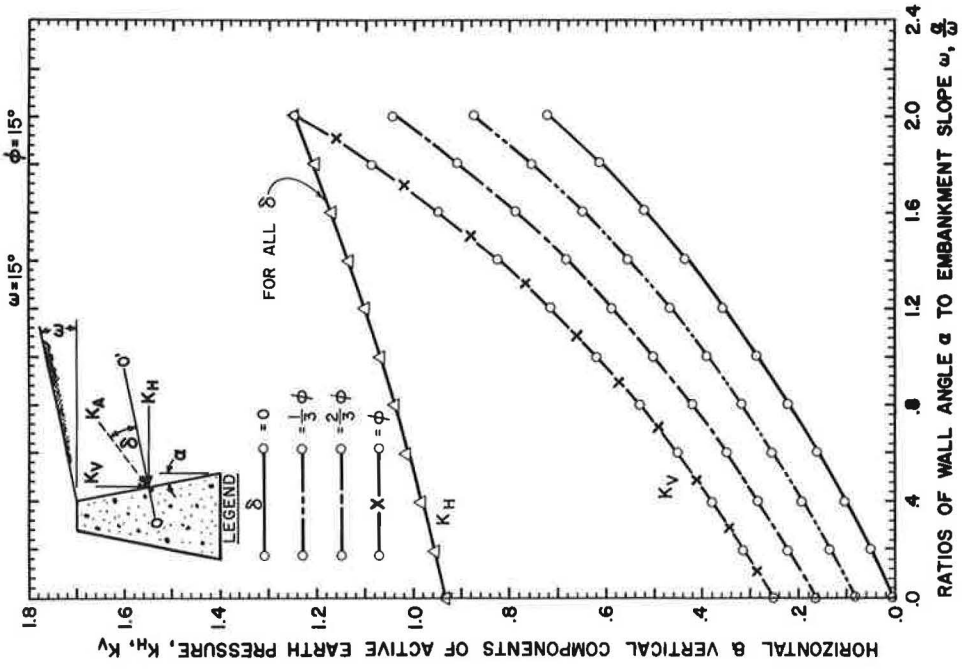

Figure 20.

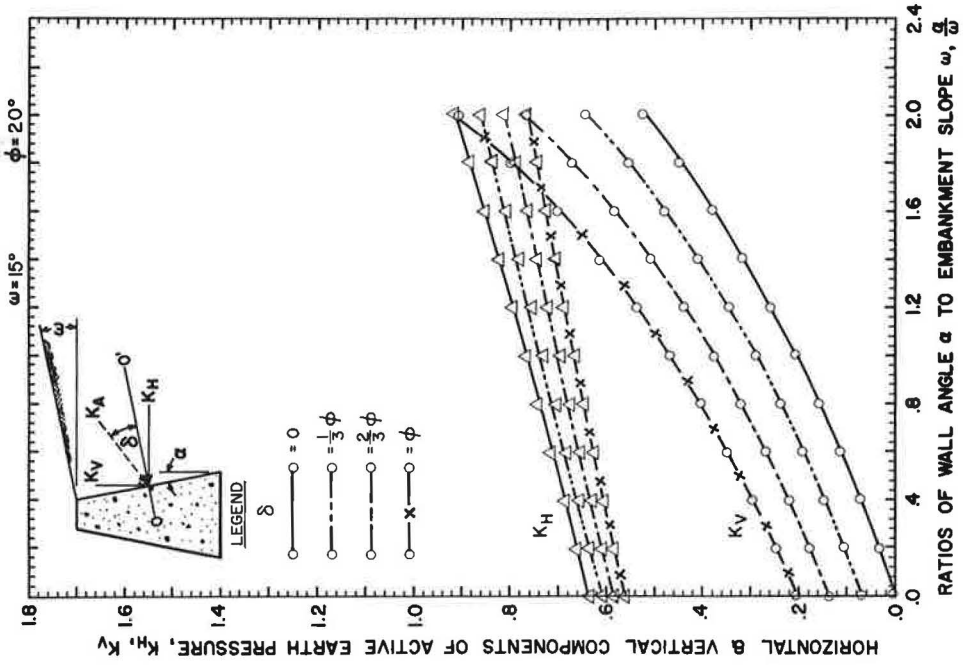

Figure 21.

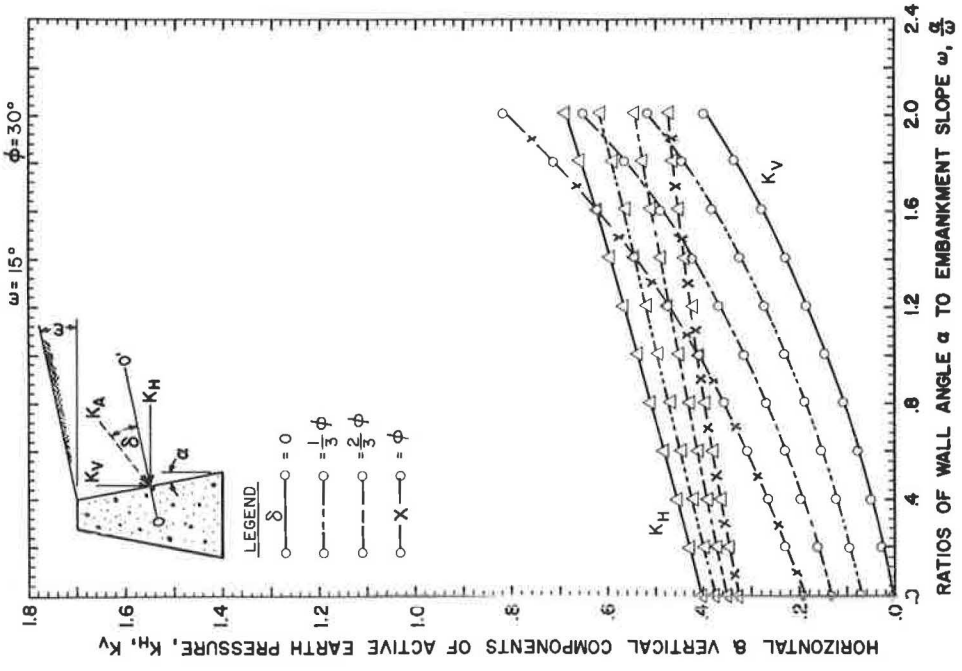

Figure 23.

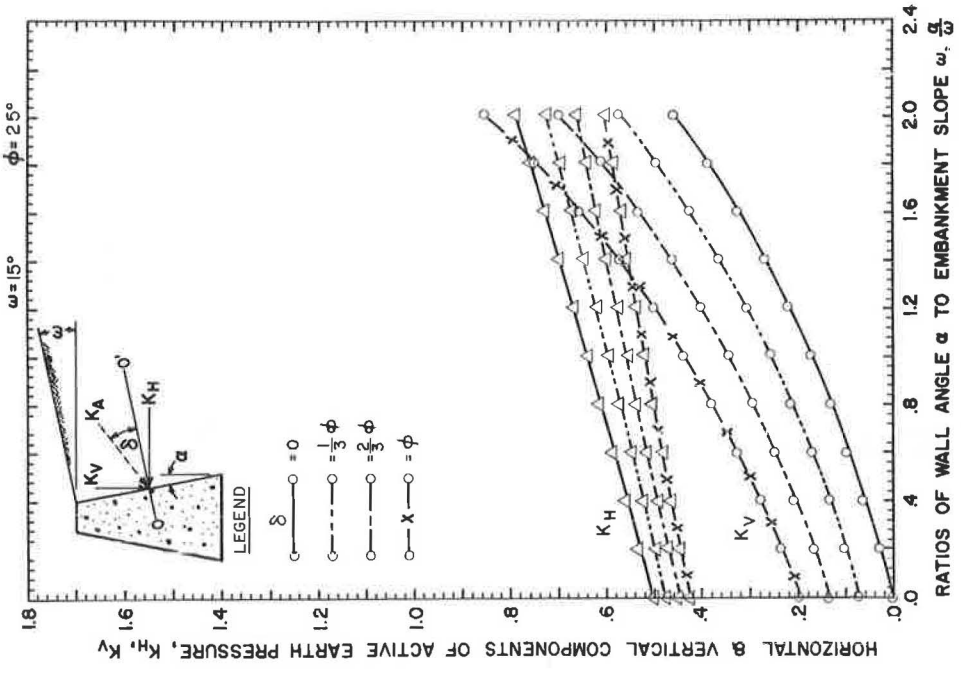

Figure 22.

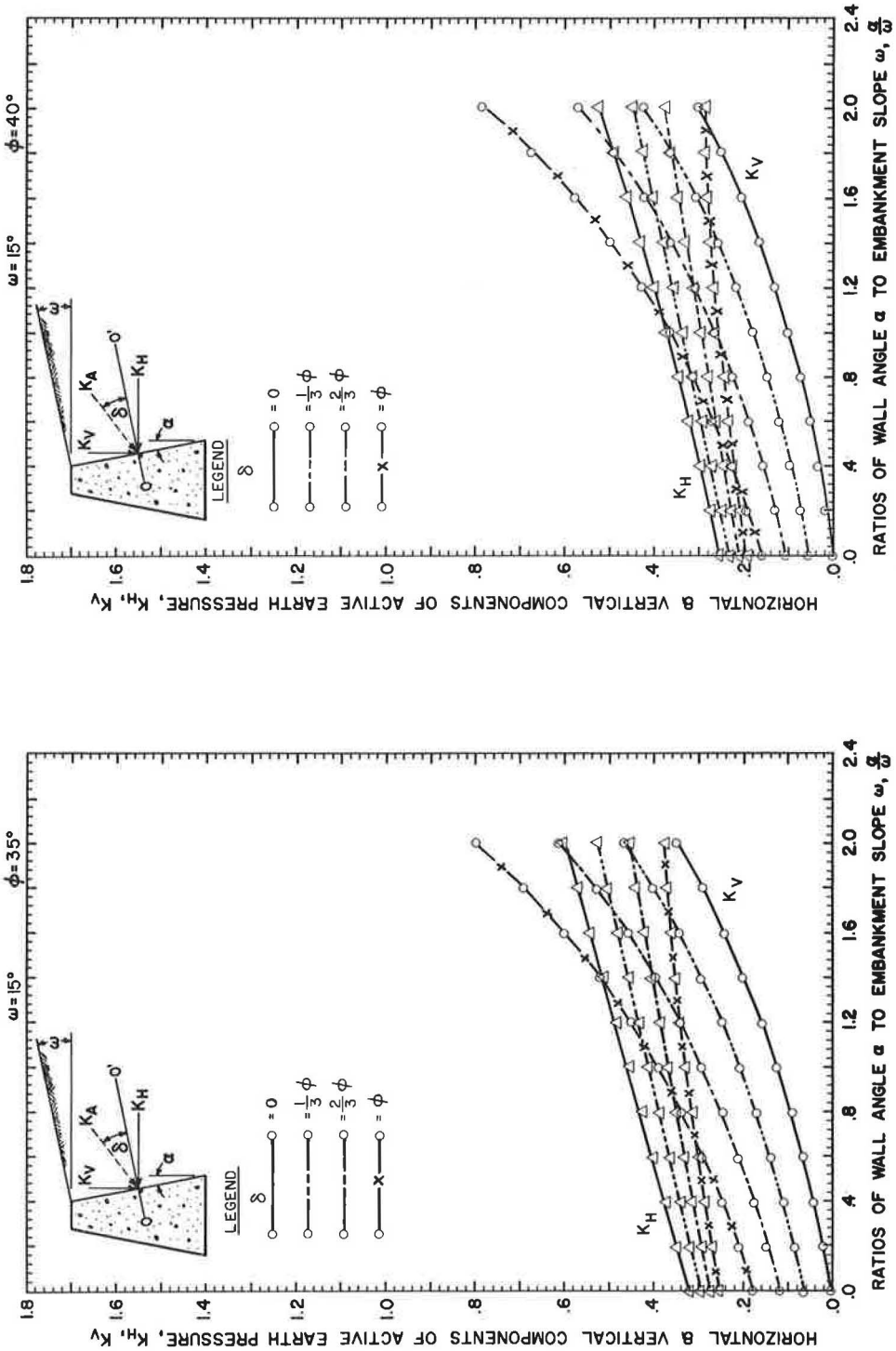

Figure 24.

Figure 25.

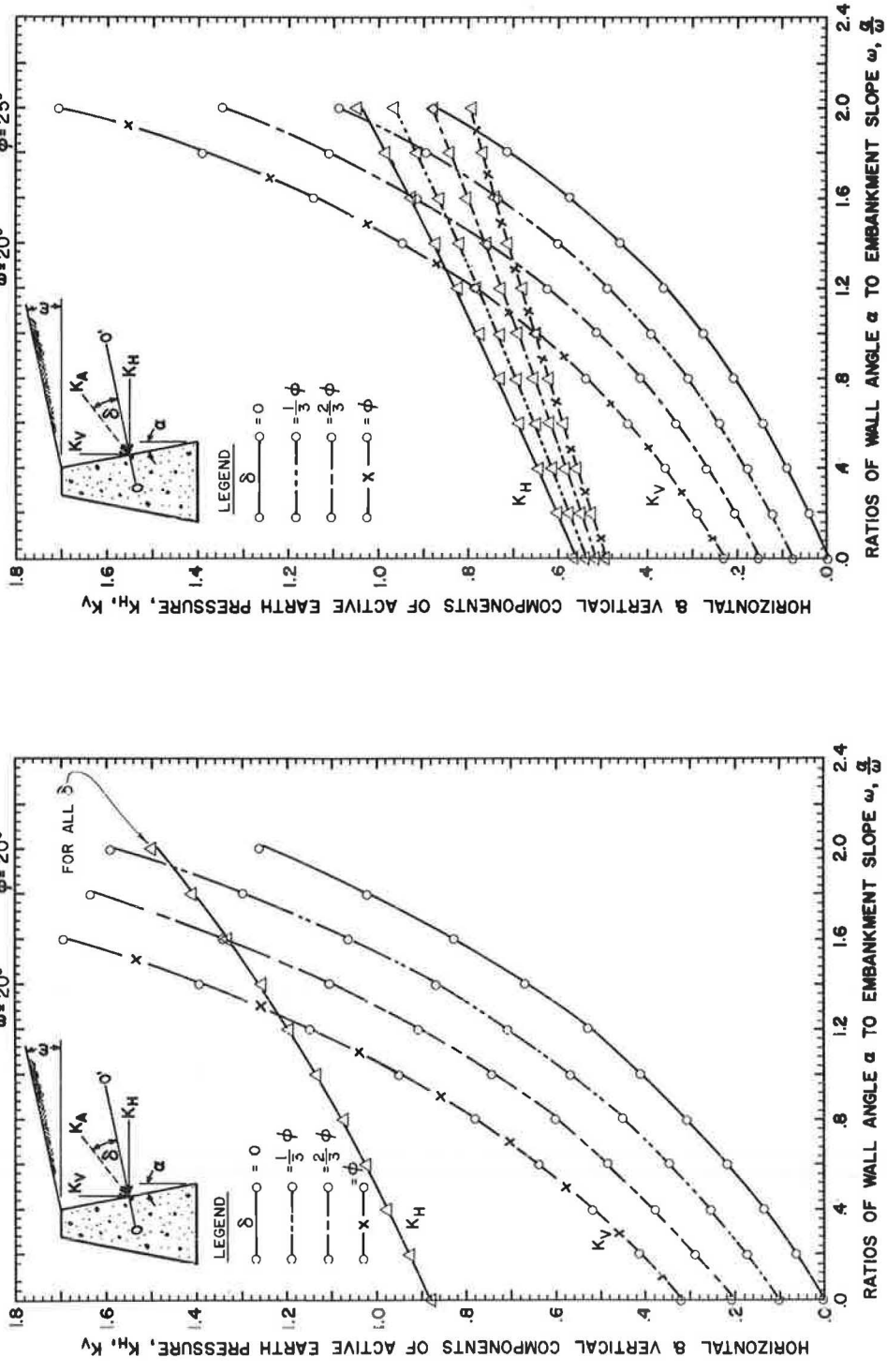

Figure 27.

Figure 26.

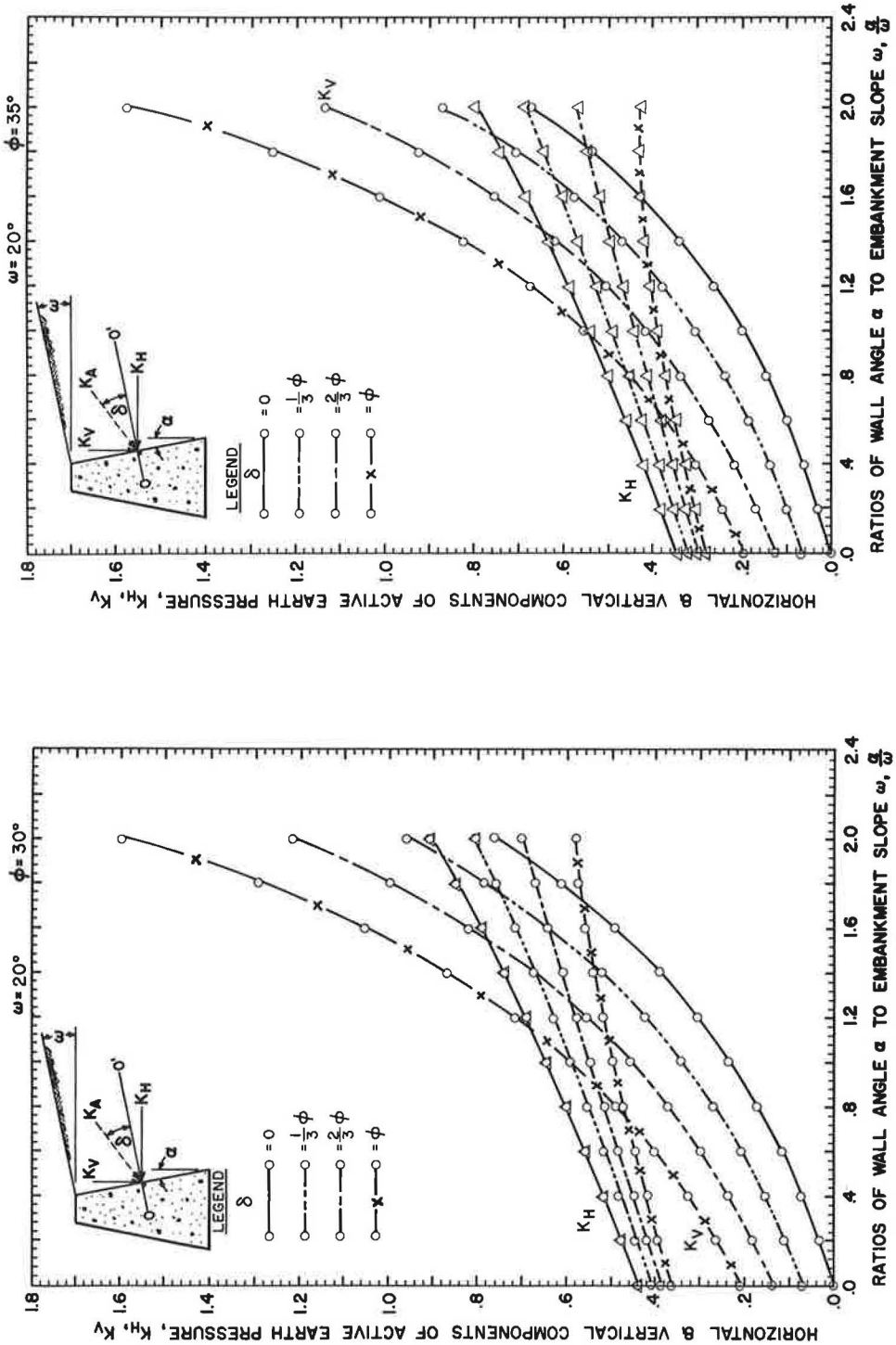

Figure 28.

Figure 29.

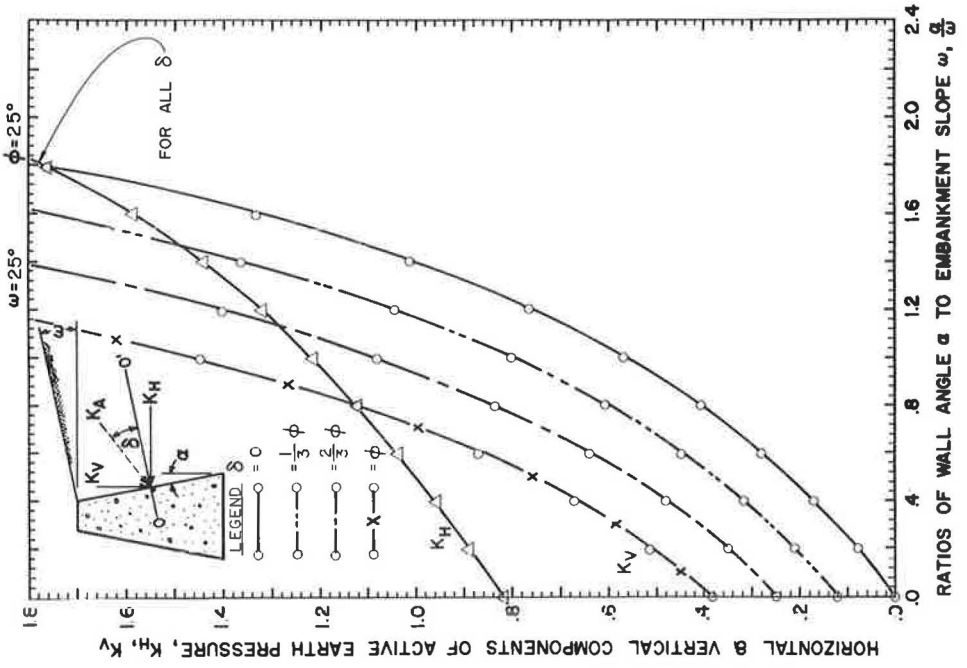

Figure 31.

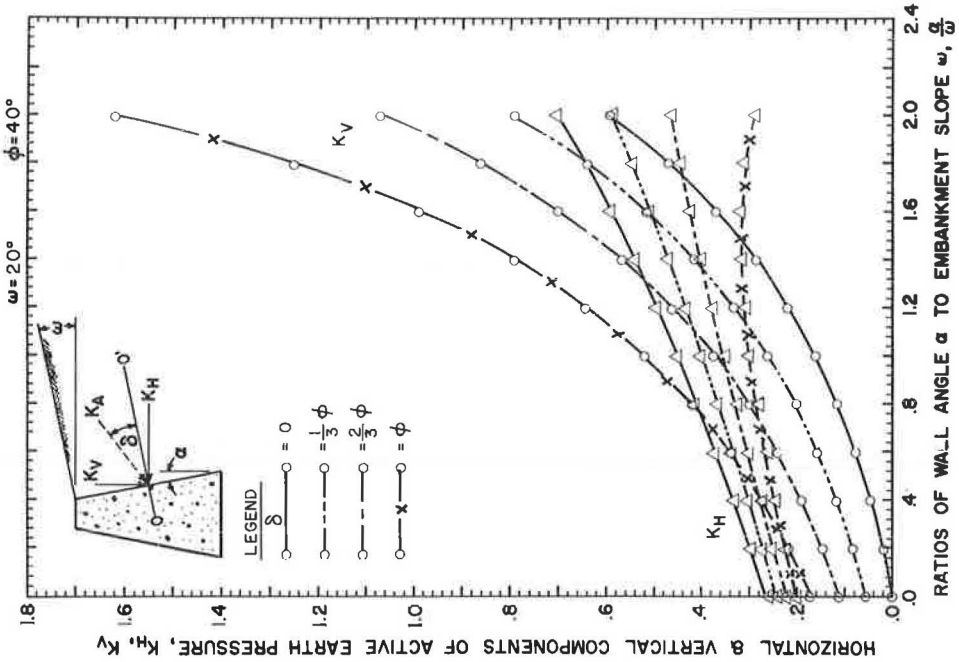

Figure 30.

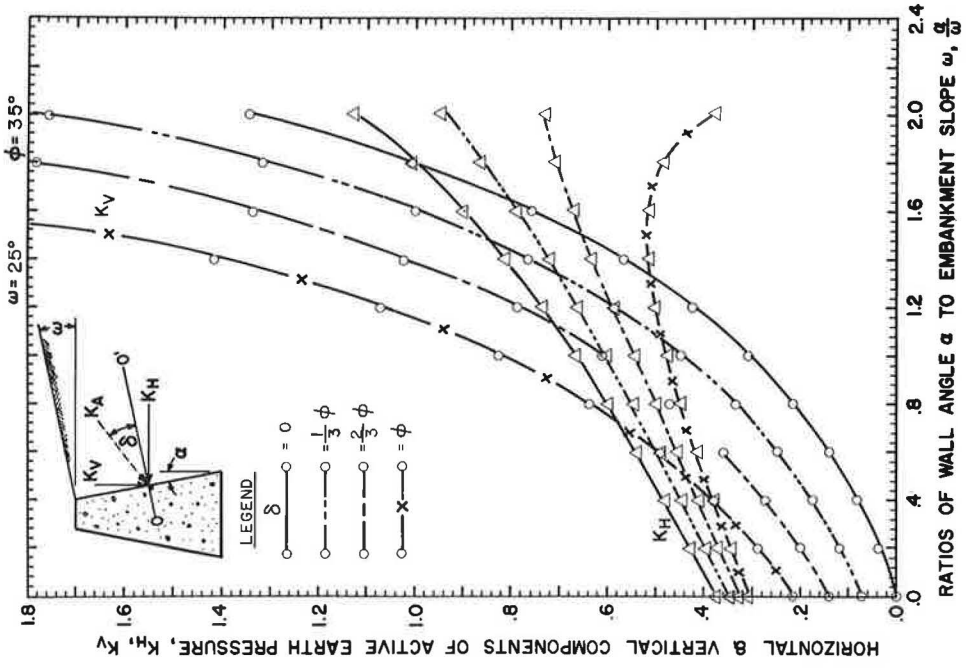

Figure 33.

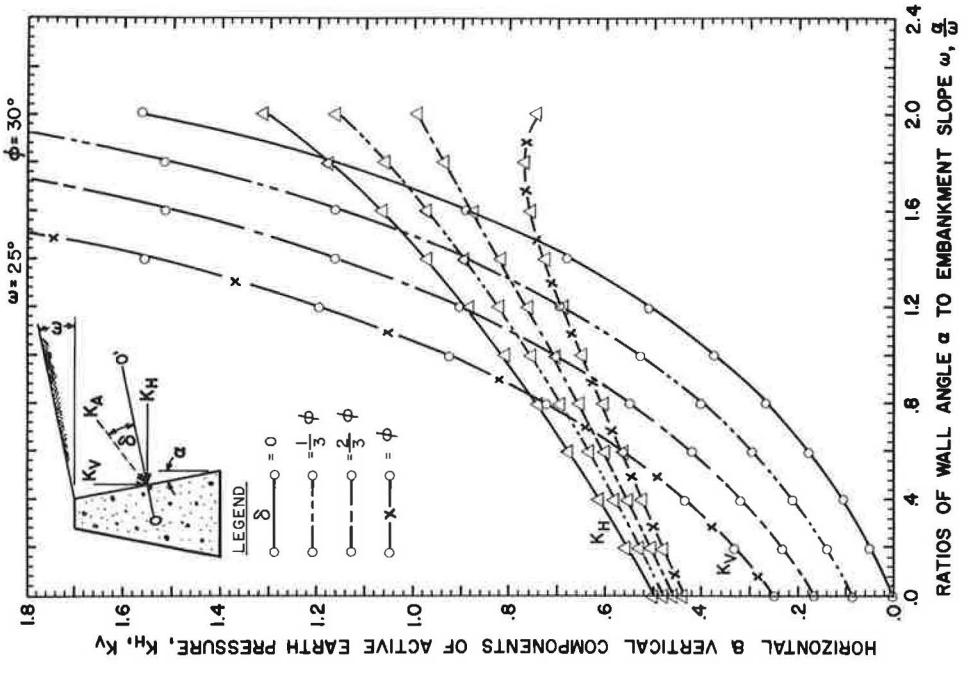

Figure 32.

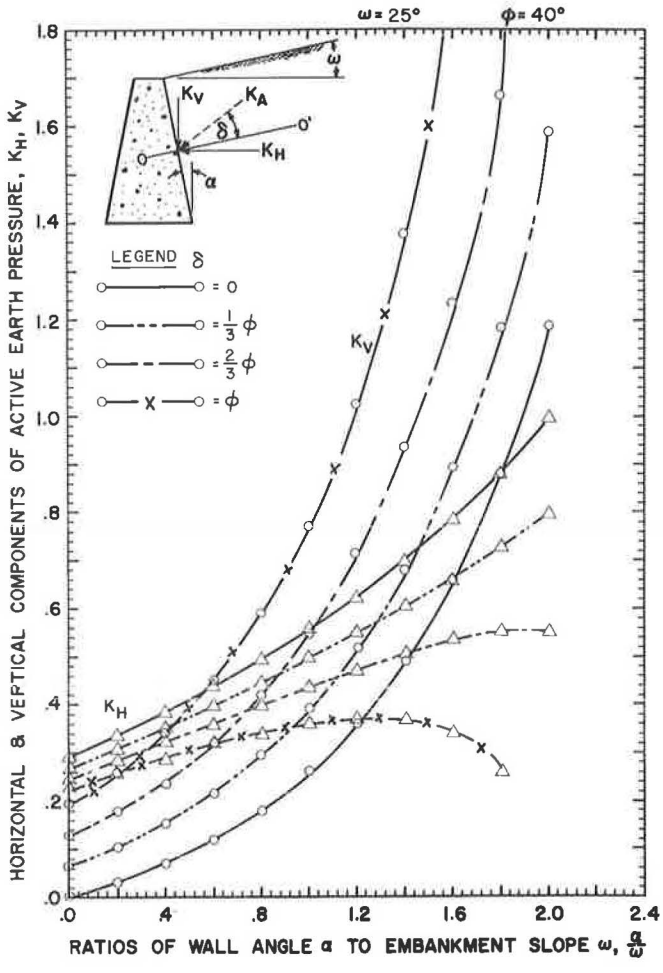
ω= 25°
φ= 40°
HORIZONTAL & VEFTICAL COMPONENTS OF ACTIVE EARTH PRESSURE, K_H, K_V
RATIOS OF WALL ANGLE α TO EMBANKMENT SLOPE ω, α/ω
LEGEND δ
= 0
= 1/3 φ
= 2/3 φ
= φ
K_V
K_A
K_H
δ
α
ω
O
O'
1.8
1.6
1.4
1.2
1.0
.8
.6
.4
.2
.0
.4
.8
1.2
1.6
2.0
2.4

Figure 34.

Use of Insulation To Uniformly Retard Frost Penetration Under a Highway Pavement

ARTHUR L. STRAUB, Professor of Civil Engineering, Clarkson College of Technology; and
WAYNE G. WILLIAMS, Engineer, The Dow Chemical Company

This paper describes the placement of insultation under a 9-in. portland cement concrete highway pavement. Special emphasis was given to the problem of uniformly retarding frost penetration under the entire slab width, i.e., to eliminate uneven penetration at the edge compared with the center. Results showed the definite reduction in frost penetration in the insulated sections, and indicated that the insulation should be extended beyond the pavement edge to obtain the desired uniformly attenuated penetration. Methods utilized to carry out the research included (a) the use of simulation techniques to predict frost penetration patterns and to aid in the design of the test site, and (b) the analysis of temperature measurements to locate the actual depth of frost penetration.

Excessive cost estimates forced attention toward means of shortening the test site length. The problem of duplicating in a short test site the heat transfer conditions found in an actual highway is discussed. Two test sections each 10 ft in length and divided by vertical insulation, were designed, constructed, and monitored over one winter. Results showed that the test sections satisfactorily duplicated the heat transfer conditions required.

Definite usefulness of simulation techniques to predict frost penetration is concluded. A research method is suggested, whereby these techniques could be further refined through successively developed field verification, which shows promise of leading to design applications.

•FROST ACTION in highway pavements has long been recognized as a severe problem in many states and in several countries throughout the world. Solutions to the problem have been attempted through many approaches; for example, by using courses of clean gravel in the base (using material not subject to detrimental heaving), or by using special care to prevent water from having access to certain layers.

Much attention has been directed recently toward the use of insulation under pavements to inhibit the penetration of freezing temperatures into pavement substructure, and several field studies have been reported (3, 5, 7, 8, 9).

From the research cited above several problems needing further study have been suggested. Among them have been (a) the determination of the lateral extent of the frozen zone at the edge of the insulating layer (8) (in order to uniformly attenuate frost penetration under the pavement itself), and (b) "The development of analytical tools to treat the two-dimensional heat flow problem and its experimental verification so that the minimum width of insulation required to prevent undesirable edge effects could be predetermined reliably" (7).

Paper sponsored by Committee on Frost Action and presented at the 46th Annual Meeting.

The research described in this paper evolved from the foregoing suggestions and is based on work completed at Clarkson College of Technology (11). It is directed toward the use of simulation techniques to predict general frost penetration patterns, and the design and construction of a field site to provide experimental verification for the simulation. In current engineering terminology, "simulation" implies any technique in which a real system is replaced by a mathematical or physical model which, in turn, is then manipulated so that the effects of various parameters can be evaluated. A recent paper by Carroll, Schenck, and Williams (2) describes an approach to the use of digital simulation for the prediction of freezing temperatures in soils exposed to an actual climate.

PURPOSE

The purpose of this paper is to: (a) describe the research conducted, (b) present and discuss the results obtained, (c) illustrate the usefulness of simulation techniques, and (d) suggest a research method incorporating repeated cycles of simulated prediction of frost penetration patterns, experimental verification, and revision of the simulated model. The ultimate objective of the phases of research described above is the accurate prediction of frost penetration beneath a highway utilizing an insulating layer.

DESIGN OF EXPERIMENT

General

From the early stages of development it was desired to investigate the "edge effect," i.e., the effect of extending the insulation beyond the pavement edge to obtain uniformly attenuated frost penetration beneath the pavement itself. Several such configurations of insulation were considered which could possibly solve the edge effect problem.

Use of Simulation

Subsequently, the various configurations of insulation were analyzed by means of analog simulation techniques. The simulation was based on a model which had been previously developed by the Mechanical Engineering Department of Clarkson College

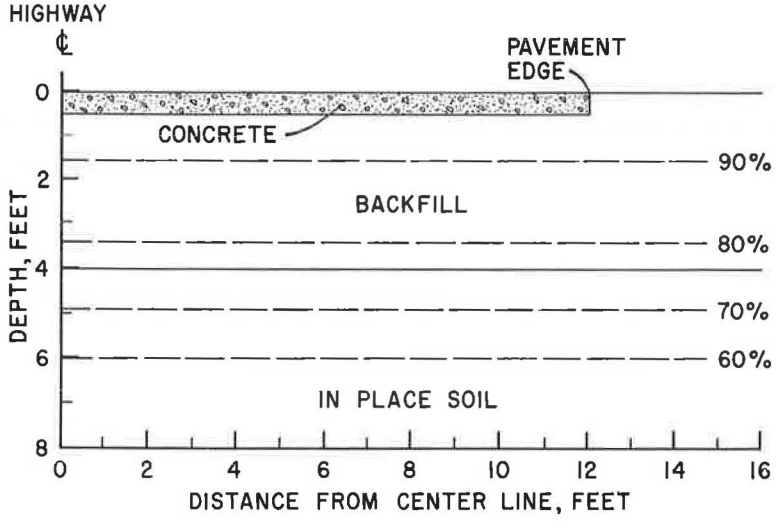

Figure 1. Location of thermally equipotential lines beneath a highway pavement without an insulating layer.

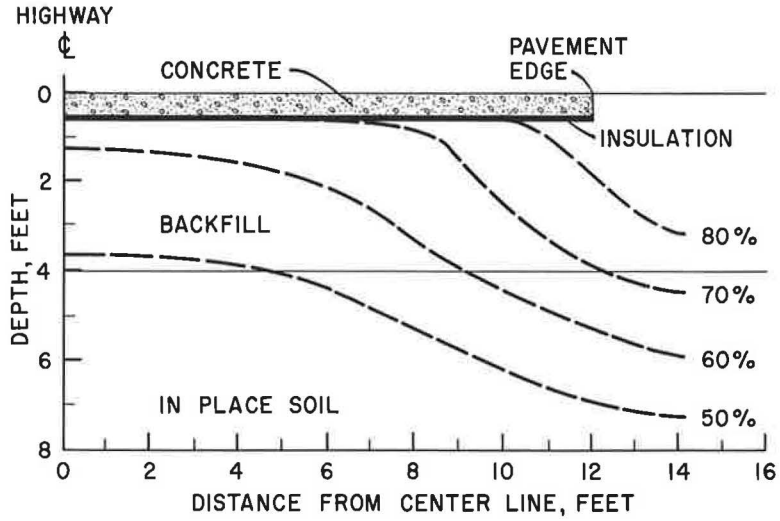

Figure 2. Location of thermally equipotential lines beneath a highway pavement with insulation to the pavement edge.

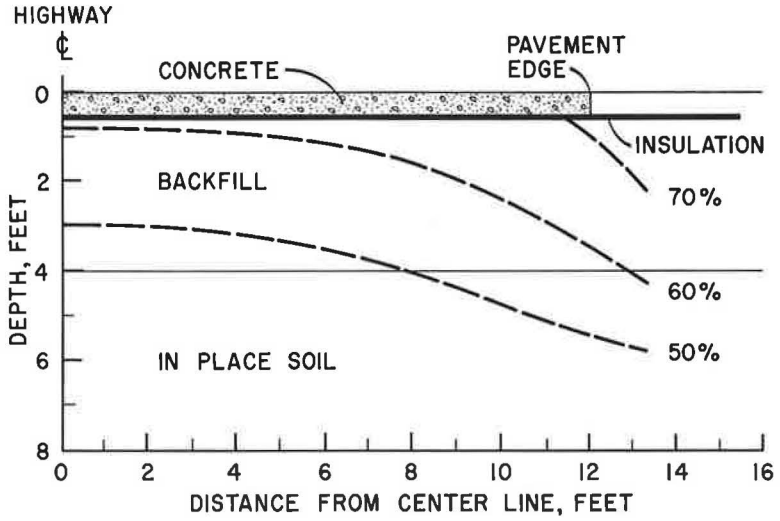

Figure 3. Location of thermally equipotential lines beneath a highway pavement with insulation extended four feet beyond the pavement edge.

of Technology (4). The predicted patterns were based on supplied thermal data and a step input boundary condition with results being shown as equal potential lines representing the percentage of the applied input as shown in Figures 1-4. Figure 1 shows the location of the equipotential lines beneath a highway cross section without an insulating layer. Although the model does not actually predict the expected frost penetration, it does give patterns of equipotential lines which represent percentage of applied input and can be considered synonymous to isotherms. On this basis let us examine Figure 1 and say, for purposes of future comparison, that the depth of frost penetration expected in this geographic area is about 5 ft. From the diagram it can be seen that the 70 percent equipotential line is located at a depth of 5 ft. Therefore, we will say

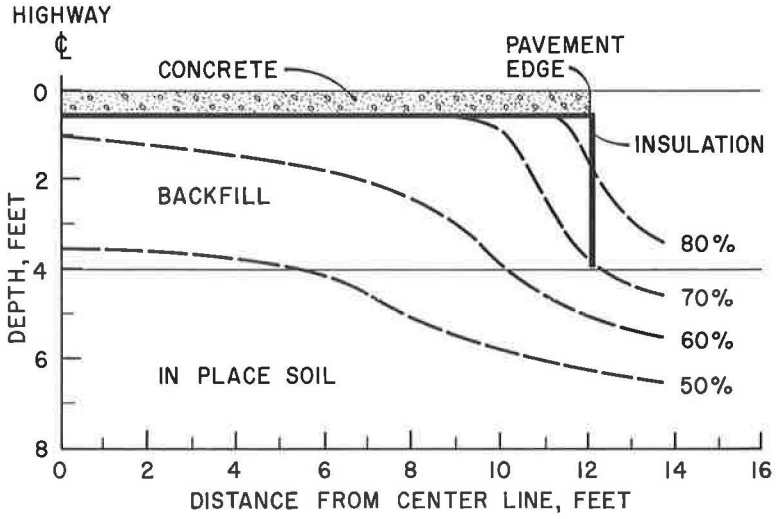

Figure 4. Location of thermally equipotential lines beneath a highway pavement with insulation placed vertically at the pavement edge.

that the 70 percent line represents the maximum frost penetration expected and now proceed to consider its predicted location in the various cross sections utilizing different configurations of insulation. Figures 2, 3, and 4 show the predicted frost penetration using the insulation extended only to the pavement edge, 4 ft beyond the pavement

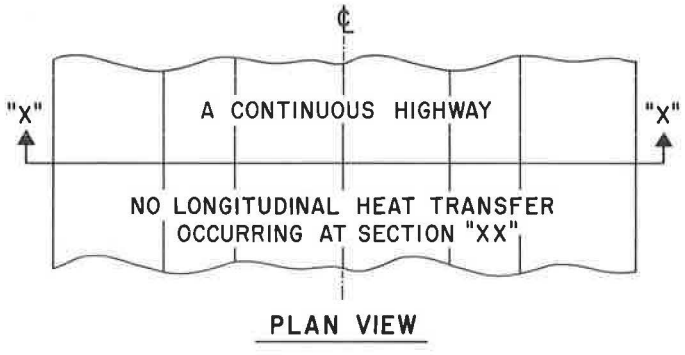

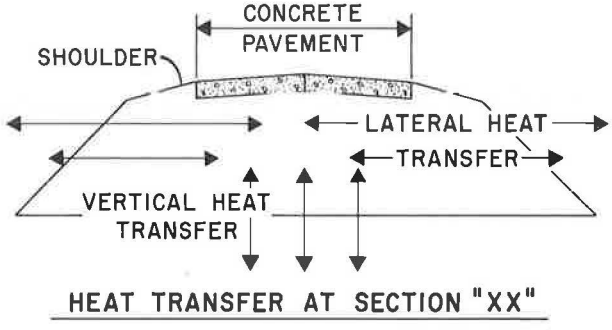

Figure 5. Thermal conditions found in an actual highway.

edge, and vertically at the pavement edge, respectively. As is evident from these diagrams, the horizontal extension of the insulation beyond the pavement edge best satisfies the desired result of uniformly attenuated frost penetration beneath the pavement itself.

Based on the foregoing predictions and limited funds available for test site construction, it was decided to investigate the following full-scale highway cross sections exposed to an actual climate:

1. A control section without insulation but with two different types of shoulder designs.
2. Two edge configurations of insulation: (a) with the insulation under the pavement extended only to the pavement edge, and (b) with the insulation extended under the shoulder at the same slope as the shoulder.

DESIGN OF TEST SITE

Economic Considerations

Preliminary cost estimates on a full-scale highway test site comparable in length to those used in previous studies (3, 5, 7, 8, 9) (approximately 40 to 100 feet/cross section) showed that construction costs would far surpass the funds available for this project. In view of the limited funds available, there were two possible courses of action: (a) to abandon the investigation of some of the cross sections, or (b) to study closely the heat transfer conditions occurring in an actual highway and to determine how short a test section could be used to duplicate these thermal conditions. It was decided to investigate the latter alternate in an effort to obtain the desired information within the limits of the funds available.

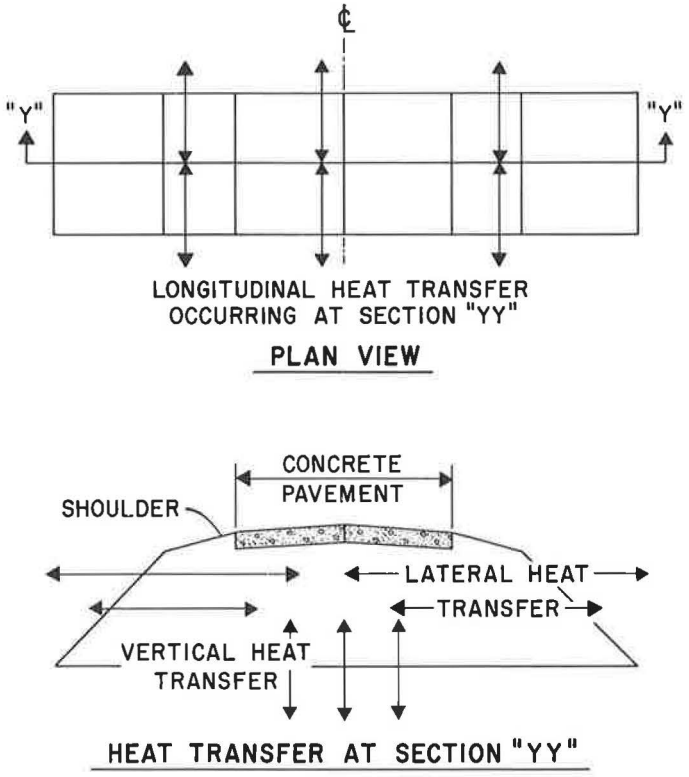

Figure 6. Thermal conditions found in a non-continuous test section (test site too short).

Duplication of Desired Thermal Conditions

The thermal conditions found in an actual highway are shown in Figure 5. It should be noted that the highway is continuous in the longitudinal direction and that only vertical and lateral heat transfer occur at any Section XX along the highway. It is these thermal conditions which must be duplicated in the short test site if valid temperature data are to be obtained. Figure 6 shows a test site which is too short because the longitudinal heat transfer which is occurring is affecting temperatures in Section YY, the plane in which temperatures would be recorded.

Use of Simulation

Again employing the analog simulation model, a value was obtained for the length of test site required to satisfy the two-dimensional heat transfer situation occurring in an actual highway. As shown in Figure 7, the minimum length of site necessary to obtain the desired two-dimensional heat transfer at Section ZZ is approximately 25 ft. Because of cost considerations a further reduction in site length was necessary. It was decided to investigate the possibility of using vertical insulation on the ends of the site to further reduce the length required. From the analog simulation a distance of 10 ft was found to be required, as shown in Figure 8, if 1-in. thick vertical insulation is assumed to be installed at the ends of a test section.

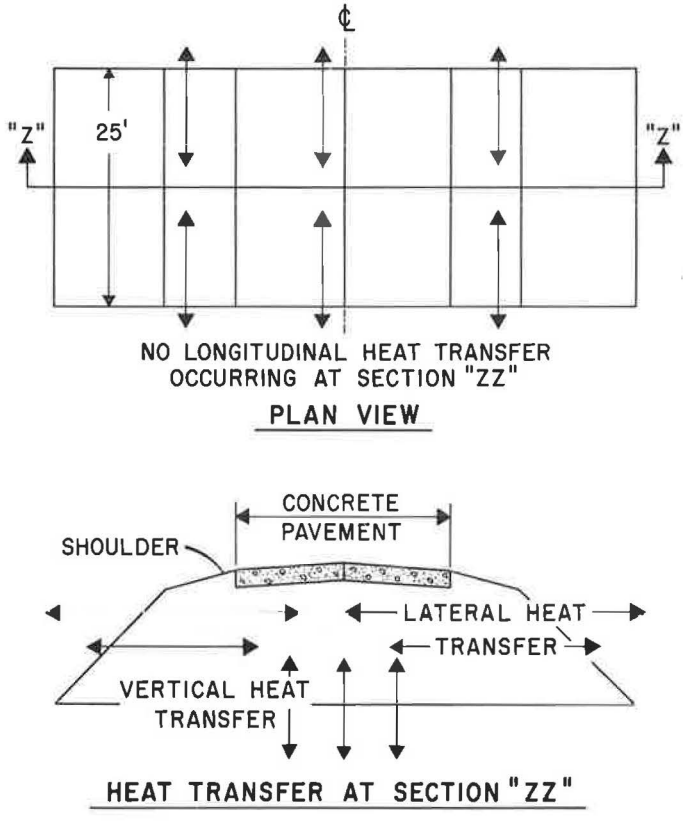

Figure 7. Thermal conditions found in a non-continuous test section (test site just meeting minimum length requirements).

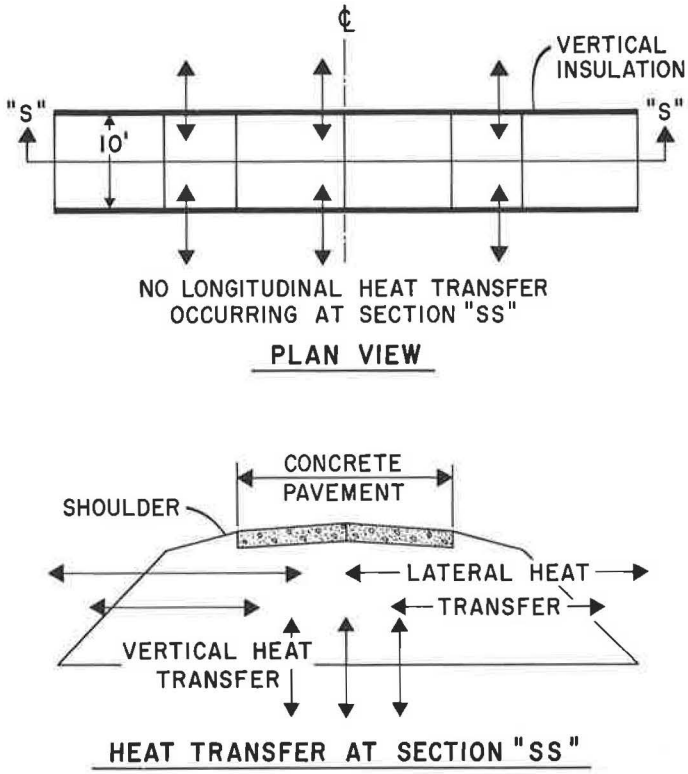

Figure 8. Thermal conditions found in a non-continuous test section using vertical insulation (test site just meeting minimum length requirements).

Selected Design

The cross section of the selected test site (excluding the insulation) followed the design commonly used by the New York State Department of Public Works for a 4-ft high fill section of two lanes of 9-in. thick portland cement concrete pavement with 8-ft wide shoulders. Although it was desired to construct a standard asphalt concrete pavement, construction equipment costs dictated the use of concrete pavement, the forms for which could be built by hand.

On the basis of the results of the simulation runs, the selected test site was designed using 1-in. thick vertical insulation on the ends and between the two sections as shown in Figure 9. The cross sections to be investigated, which were mentioned earlier, are shown in Figure 9 as Sections AA and BB. Hereafter, Section AA shall refer to the control section, and Section BB to the insulated section with two edge configurations of insulation. An oblique view of the test site is shown in Figure 10.

It should be noted that two different types of shoulders were used in Section AA (see Fig. 9). One was constructed of gravel and had a natural, light brown surface color. The other shoulder was constructed of New York State Department of Public Works Item 59 W, a mixture of gravel and an oil-water emulsion designed to reduce the permeability of the shoulder material and to increase the structural integrity of the shoulder (6). Its surface was dark brown in color.

The best locations of the limited number of temperature probes available were determined in part by the prediction of the analog model. The placement of the probes in Section AA and Section BB is shown in Figures 11 and 12 respectively. Two additional temperature probes were located (Fig. 13) to indicate the effect of the longitudinal heat transfer on the temperatures at Sections AA and BB—hereafter referred to as the

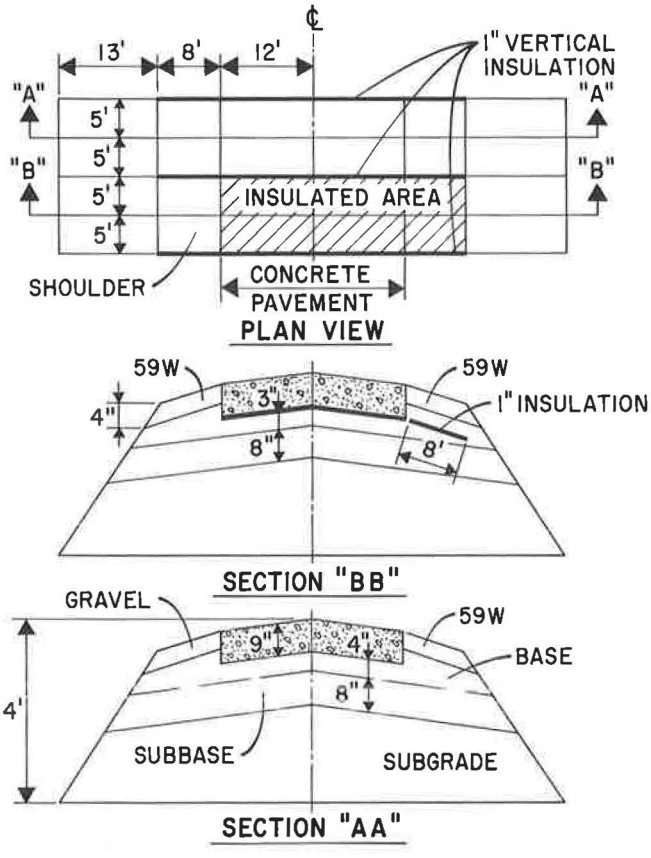

Figure 9. Selected design of test site.

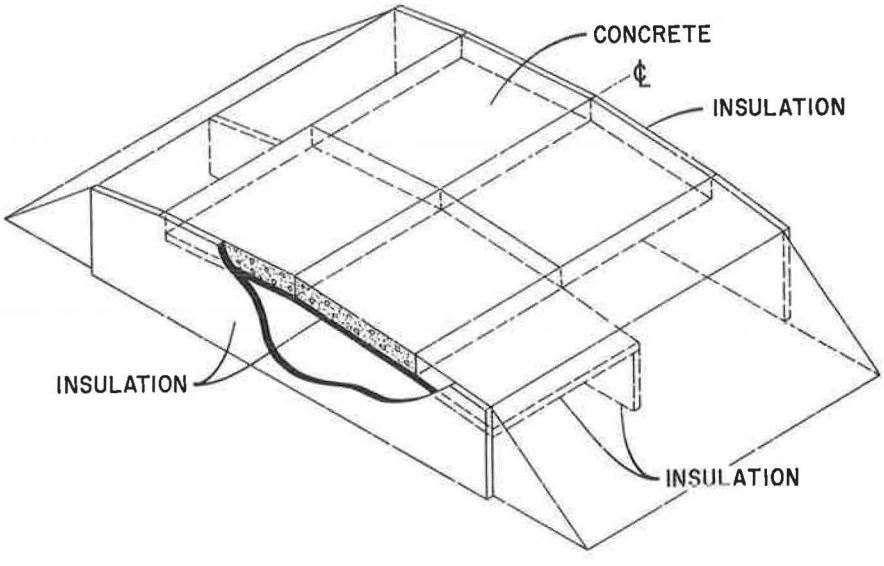

Figure 10. Oblique view of site showing vertical insulation.

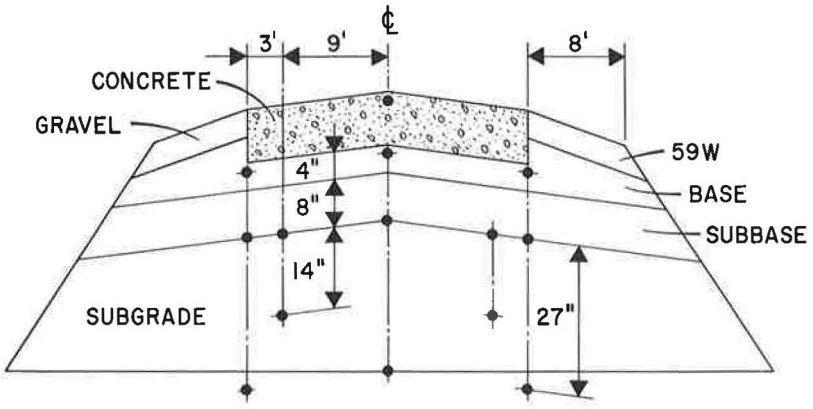

Figure 11. Location of temperature probes in Section AA.

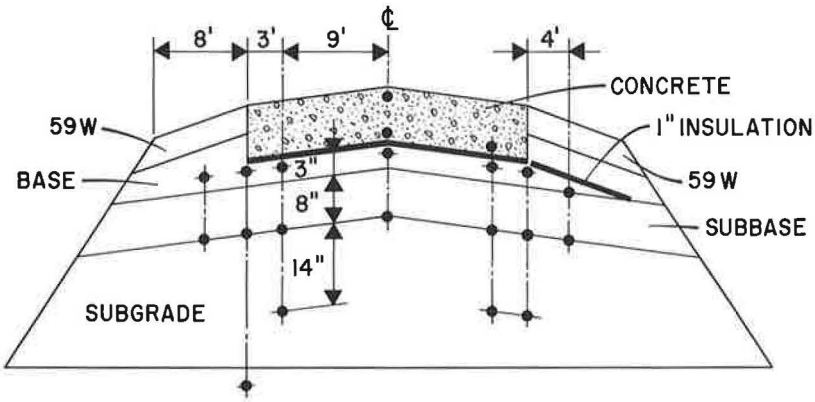

Figure 12. Location of temperature probes in Section BB.

end effect. As shown in Figure 13, the two additional check probes are located at a depth of 21 in. beneath the surface at a distance of 4 ft from the end of the site. It was felt that if the temperatures recorded by the probes at 4 and 5 ft from the end of the site were the same throughout the winter, then the desired situation of having only two-dimensional heat transfer at Sections AA and BB would have been obtained.

INSTRUMENTATION

Frost penetration at the test site was monitored by placement of temperature probes as shown in Figures 11, 12, and 13. Temperature data were obtained by using a Fenwal five-point Model 582 thermistor sensing indicator with 37 matched probes, each having a range of -50 F to +150 F. Calibration of each of the thermistor probes was carried out with all lead wires attached and the resulting accuracy obtainable was considered to be ± 0.5 F. Experience over one freezing period showed that the system operated smoothly and accurately without breakdown.

CONSTRUCTION OF TEST SITE

Construction Specifications

The designed test site was constructed in accordance with New York State Department of Public Works Specifications (6) whenever possible. A summary of the soil properties of the subgrade, subbase, and base materials is given in Table 1.

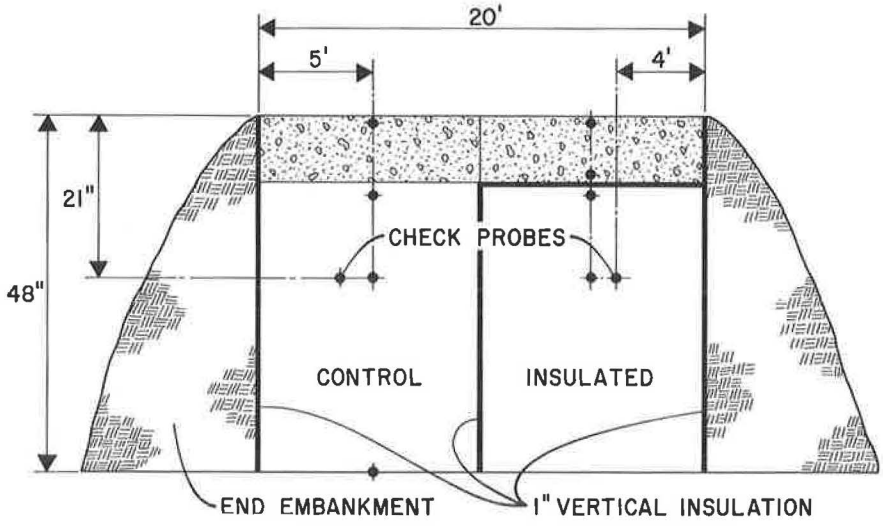

Figure 13. Section of test site at centerline.

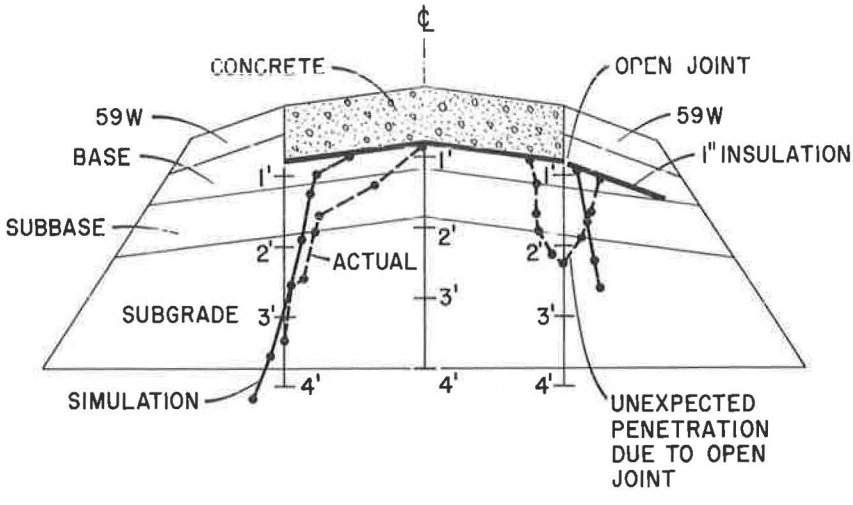

Figure 14. Simulation prediction compared with the actual maximum penetration of the 32 F isotherm.

TABLE 1

PROPERTIES OF SOILS USED IN TEST SITE

Property	Subgrade	Base and Subbase
Plasticity index	N. P.	N. P.
No. 200 U. S. standard sieve (%)	25	8.9
Optimum dry density (standard Proctor, pcf)	132	128
Avg. dry density of compacted material, pcf	118.5	129
Optimum moisture content	7.5	8.0
Avg. moisture content of compacted material	10.5	8.8

Construction Procedure

In general, the construction of the fill followed repeated cycles of (a) placement of material, (b) compaction, and (c) placement of necessary temperature probes. The vertical insulation (shown in Fig. 9) was placed in two lifts by digging narrow trenches and backfilling around the insulation.

Description and Installation of Insulation

All insulation used in this project was an extruded expanded polystyrene plastic foam insulation board manufactured by the Dow Chemical Company. The thermal

conductivity, k, of the insulation used was approximately 0.25 Btu-in./sq ft-hr-F, the same value as used in simulation trials. The installation of the insulation boards (2 by 4 ft by 1 in.) used in this project generally followed the procedure recommended by Oosterbaan (7) and presented no construction problems.

DATA COLLECTION AND PROCESSING

Period of Observation

The data obtained consisted of a continuous record of air temperature and daily to bi-daily observations of temperatures in the cross sections. Data collection began on December 20, 1965 and terminated on April 8, 1966.

Air Temperature and Cross-Section Temperature Data

The air freezing index recorded for the 1965-66 winter was 972 degree-days Fahrenheit. An analysis of climate records for 37 seasons (10) for Canton, New York (located 11 miles away), showed that the air freezing index recorded could be expected to be equaled or exceeded 85 percent of the time. The Corps of Engineers (1) shows the mean freezing index for this area to be about 1350 degree-days Fahrenheit.

Analysis of the cross-section temperature data included interpolation to determine the location of the 32 F isotherm (taken as the location of the depth of frost penetration). The overall accuracy obtained in the location of the 32 F line was probably on the order of $\pm 1\frac{1}{2}$ in. of the value reported.

Winter Maintenance Practices

Although there was no traffic on the test section, snow removal practice followed by New York State was maintained. This included complete removal of snow from the pavement and shoulders to the side slopes, immediately following any significant snowfall.

RESULTS AND DISCUSSION

Validity of Test Site

The analysis of the data obtained from the end effect probes (see Fig. 13) showed very little, if any, effect due to longitudinal heat transfer. On the average, the temperatures recorded 5 ft from the end of the site were less than 0.25 F cooler than those recorded at a distance of 4 ft. Since the accuracy to which temperature measurements could be recorded was 0.5 F, the difference observed was not considered significant. Therefore, on the basis of the end effect data, the constructed test site was considered adequate for obtaining the desired heat transfer conditions and resulting temperatures which would be found in an actual highway.

Simulation Compared With Actual Location of 32 F Isotherm

The maximum frost penetration recorded in the control section, with the same type of shoulder as found in the insulated sections, was 50 in. Referring to Figure 1, it can be seen that 50 in. of frost penetration corresponds to the 75 percent equal potential line. The 75 percent lines for the insulated sections are shown in Figure 14, together with the actual maximum penetration recorded in these sections. From the figure it can be seen that the simulated predicted pattern of frost penetration closely corresponds to the actual penetration recorded where the insulation was placed only beneath the pavement.

The disagreement between the predicted and recorded frost penetration, in the section with the insulation extended beneath the shoulder, can be attributed to the following factors:

1. The recorded values show frost penetration locally concentrated beneath an improperly constructed joint in the insulation. The progression of the 32 F isotherm at this point is shown in the bottom right portion of Figures 15, 16, and 17. This penetration

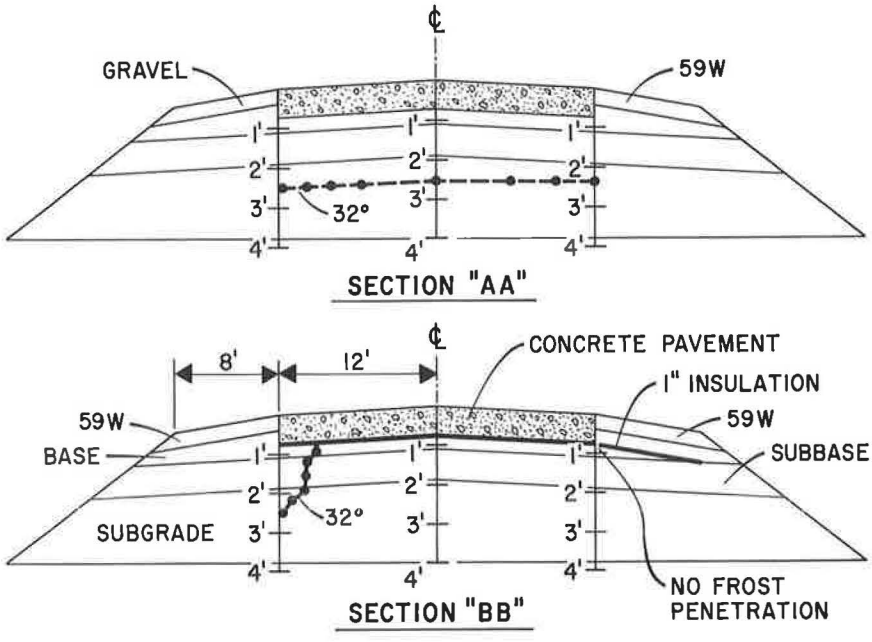

Figure 15. Location of the 32 F isotherm for the insulated and uninsulated sections on January 17, 1966.

was caused by joint leakage and not by penetration from the edge of shoulder insulation. This is apparent by the pattern of development of the 32 F isotherm as shown in the above figures.

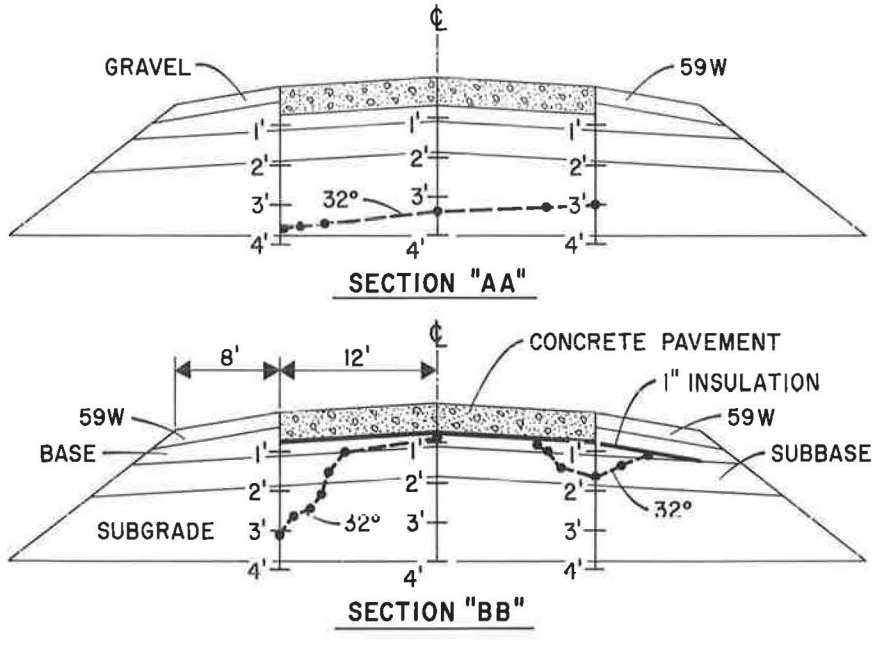

Figure 16. Location of the 32 F isotherm for the insulated and uninsulated sections on Feb. 7, 1966.

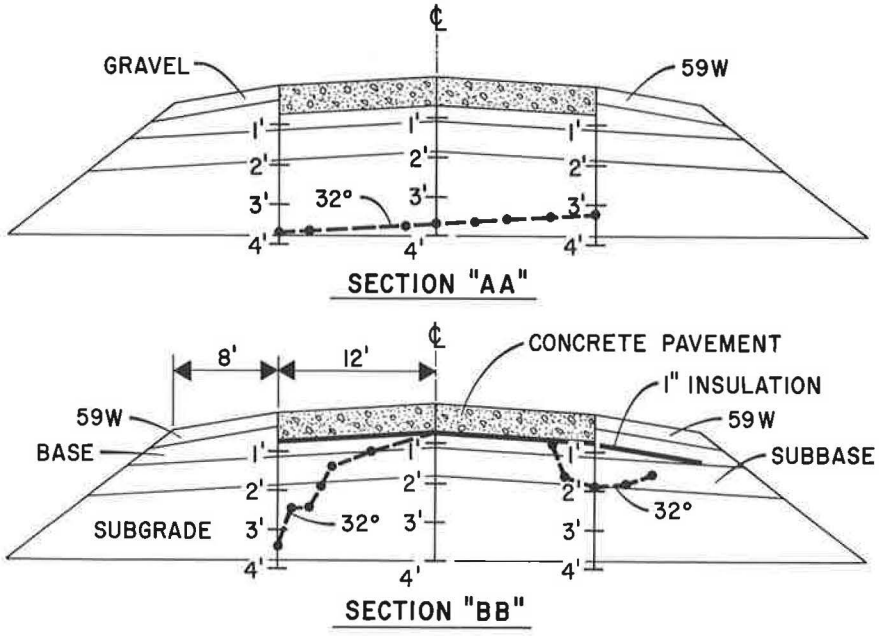

Figure 17. Location of the 32 F isotherm for the insulated and uninsulated sections on February 21, 1966.

2. The simulated prediction is based on an assumed 4-ft extension of the insulation beneath the shoulder instead of the 8 ft actually used to insure uniformly retarded frost penetration.

Comparison of Insulated and Uninsulated Sections

The frost penetration observed beneath the centerline of the insulated and uninsulated sections (Sections BB and AA, respectively) is shown in Figure 18. Examination of this figure shows the retardation of the frost penetration throughout the winter in the insulated section (Section BB). The maximum frost penetration recorded in Section AA was 50 in. and 10 in. in Section BB (which is the depth at which the insulation was placed).

An overall representation of the recorded frost penetration is also shown in Figures 15, 16, and 17. In these figures are shown the frost penetrations in Sections AA and BB for three selected days during the freezing period. Important points to be noted in the diagrams include: (a) much greater frost penetration in the uninsulated section; (b) more uniformly attenuated frost penetration in the insulated section where the insulation is extended beyond the pavement edge; and (c) slightly less frost penetration beneath the Item 59 W shoulder (dark in color) than beneath the gravel shoulder in Section AA.

Edge Effects

As previously mentioned, it was desired to obtain uniformly attenuated frost penetration beneath the pavement—that is, to have the reduced frost penetration at the pavement edge be the same as that recorded at the centerline. Figure 19 shows a comparison of the frost penetration (location of the 32 F isotherm) beneath the pavement edge for each test section. Examination of the gravel and Item 59 W shoulder plots for Section AA shows similar unretarded frost penetration beneath the pavement edge. Comparison of these plots with the Section AA centerline plot (see Fig. 18) shows similar unretarded frost penetration at the edge and centerline of the pavement.

Examination of the frost penetration at the pavement edge for the two insulated sections (see Fig. 19) shows the definite effect of extending the insulation beyond the

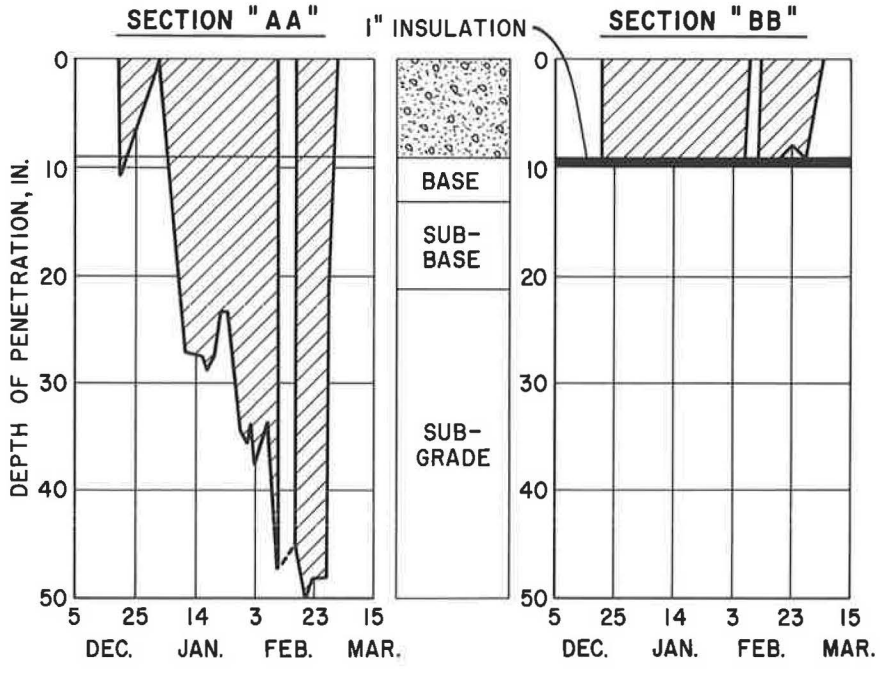

Figure 18. Depth of the 32 F isotherm at the centerline with and without insulation.

pavement edge. Again, reference to Figure 18 shows the necessity of extending the insulation into the shoulder in order to obtain uniformly attenuated frost penetration beneath the entire pavement width.

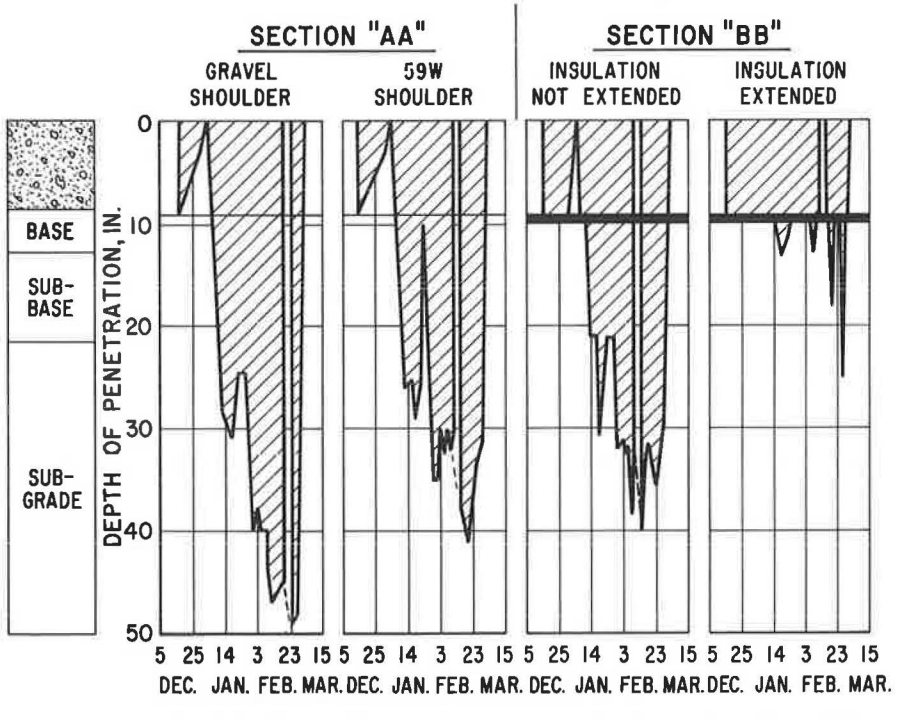

Figure 19. Depth of the 32 F isotherm at the pavement edge in sections AA and BB.

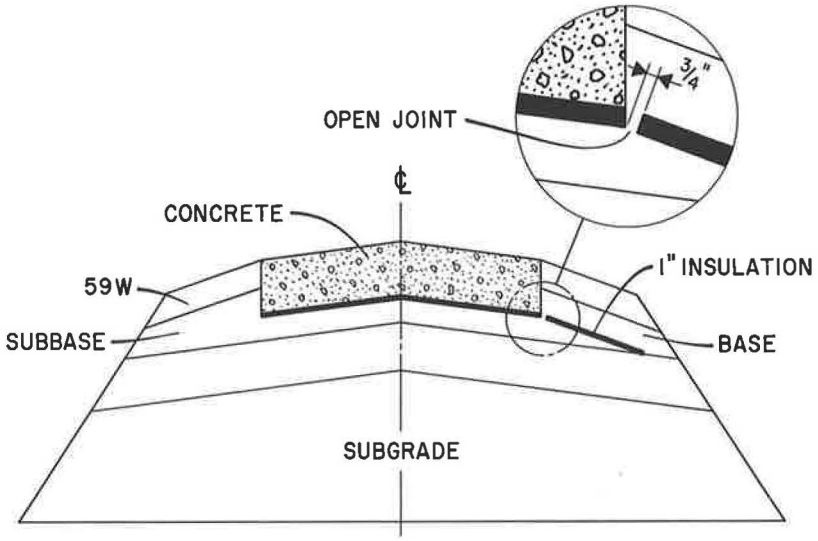

Figure 20. Detail of open joint at slope change which permitted some local frost penetration.

Additional Points for Discussion

The sudden "thaw" shown to occur in Figures 18 and 19 (Section AA) from February 9-15 is of special interest. Following an extended period of freezing, the average daily air temperature for these days rose to approximately 40 F, and all of the temperature probes in Section AA rapidly rose to 33-35 F (distinctly above 32 F), therefore suggesting that a complete thaw in the entire section had occurred. In the succeeding few days, February 19-21, the average daily air temperature fell to below 0 F, and the 32 F isotherm returned very rapidly to its former depth of 40 in. or more. No complete explanation of this observation can be given although several theories have been considered. It is felt that this anomaly in the data was not due to instrumental error but there is not sufficient information to substantiate another explanation. Therefore, while the period under question is shown as unfrozen in Figures 18 and 19, the dashed lines show the suspected depth of frost penetration.

In general, over the winter, the average temperatures observed in the slab above the insulation were less than those in the uninsulated slab. A few times during the winter ice was observed on the surface of the insulated sections while only water existed on the uninsulated sections. Although this ice formation was noted, no definite conclusion can be drawn as to its severity because the pavement was not exposed to any traffic or abrasive surface treatment, such as sanding commonly used on actual highways.

As shown in Figures 16, 17, and 19, the frost penetration recorded beneath the pavement edge, in Section BB where the insulation is extended into the shoulder, is greater beneath the joint in the insulation at that point. As shown in Figure 20, the joint referred to above is not a true butt joint. Upon careful excavation, it was found that the actual gap at the top of this joint was approximately $\frac{3}{4}$ in. in width which exceeds the permissible value of $\frac{1}{4}$ in. derived by Oosterbaan (7) for a thermally efficient butt joint. It would be no problem to bevel one of the boards and to make a better joint at this location. It is the opinion of the authors that this would retard the frost penetration observed beneath this joint.

CONCLUSIONS

The following conclusions can be drawn from the data obtained in this project:

1. A short test site duplicating thermal conditions found in an actual highway can be

designed and constructed, thus greatly reducing material and construction costs.

2. Comparison of the insulated and uninsulated sections showed the definite favorable effect of the insulation in reducing frost penetration.

3. Simulation techniques are useful not only in predicting frost penetration patterns, but also in the design of a test installation.

4. In order to uniformly attenuate frost penetration beneath the pavement, the insulation must be extended some distance into the shoulder. The 8 ft of extension used in this project was more than sufficient to uniformly retard the frost penetration beneath the pavement for the winter observed.

5. Data were obtained which can be the basis for the continuation of the study program, such as refinement of simulation techniques.

6. From the experience gained, it is concluded that reasonable care in joint construction at slope changes is needed to construct a continuous insulating layer.

SUGGESTED FUTURE RESEARCH AND APPLICATIONS

Since the operation of the test installation described above is to be continued for several seasons, a few internal suggestions have been made (e.g., fixing the joint in the insulation at the pavement edge).

The thermal data secured from the test site (together with climate records and site moisture measurements which were obtained) can now be used to refine the simulation model. Further use of the refined model can aid in developing an efficient research program, which in turn can be used to develop further the simulated model. The aim of such an approach would be to develop simulation techniques to a point where they could provide a needed and useful tool in engineering design. With such an analytical tool, frost penetration patterns which would result from using various configurations of insulation could be predetermined accurately. The development of such an analytical tool would enable the engineer to select the design which would be most suitable to the conditions and degree of protection desired for his particular situation.

ACKNOWLEDGMENTS

The authors wish to express grateful acknowledgment to the many organizations and individuals who willingly contributed to this project.

The Division of Research and the Civil Engineering Department of Clarkson College of Technology provided funds supporting this project, and the Department of Buildings and Grounds gave assistance in test site construction.

The Dow Chemical Company donated the Styrofoam HI brand expanded polystyrene insulation used.

Prof. H. N. Schenck of the Mechanical Engineering Department and several of his graduate students, including Raymond W. Lingenfelter, provided helpful suggestions and simulation results. William Carman, civil engineering graduate student, was an active participant in site design, construction, and operation. Undergraduate students Raymond Powers, David Cornish, and Frank Przybycien completed a substantial amount of the analysis of data and plotting.

In addition, several other individuals gave assistance in many ways, all of which is deeply appreciated.

REFERENCES

1. Corps of Engineers, U. S. Army. Engineering and Design, Pavement Design for Frost Condition. EM 1110-345-306, May 1962.
2. Carroll, C., Schenck, H., Jr., and Williams, W. Digital Simulation of Heat Flow in Soils. Jour. of Soil Mech. and Found. Div., ASCE, Vol. 92, No. SM4, Proc. Paper 4865, July 1966.
3. Subgrade Insulation to Prevent Soil Freezing. Iowa Highway Research Board, Project HR-87, Iowa State Highway Commission, 1965.
4. Lingenfelter, Raymond W. Simplified Construction and Operation of a Two-Dimensional Fast-Time Analog. MSCE thesis, Clarkson College of Technology, 1965.

5. Maine State Highway Commission. Investigation of Insulating Effect of Material on Subgrade, Construction and Instrumentation Report. 1965.
6. New York State Department of Public Works. Public Works Specifications, State of New York, 1962.
7. Oosterbaan, Marvin D. Investigation of Foamed Plastic as an Insulating Layer in Highway Pavements. MSCE thesis, Purdue Univ., 1963.
8. Oosterbaan, M. D., and Leonards, G. A. Use of Insulating Layer to Attenuate Frost Action in Highway Pavements. Highway Research Record 101, pp. 11-27, 1965.
9. Penner, E., Oosterbaan, M. D., and Rodman, R. W. Performance of City Pavement Structures Containing Foamed Plastic Insulation. Highway Research Record 128, pp. 1-12, 1962.
10. Straub, A. L., and Wegmann, F. J. Determination of Freezing Index Values. Highway Research Record 68, pp. 17-30, 1965.
11. Williams, W. G. The Use of Insulation to Uniformly Retard Frost Penetration Under a Highway Pavement. MSCE thesis, Clarkson College of Technology, 1967.